MID-INFRARED SPECTROSCOPY OF EQUINE SYNOVIAL FLUID FROM NORMAL AND DISEASED JOINTS

A Thesis

Submitted to the Graduate Faculty

in Partial Fulfilment of the Requirements

for the Degree of

Doctor of Philosophy

in the Department of Health Management

Atlantic Veterinary College

University of Prince Edward Island

Monchanok Vijarnsorn

Charlottetown, Prince Edward Island, Canada

October, 2006

Your file Votre référence
ISBN: 978-0-494-22843-2
Our file Notre référence
ISBN: 978-0-494-22843-2

CONDITION OF USE OF THE THESIS

The author has agreed that the Library, University of Prince Edward Island, may make this thesis freely available for inspection. Moreover, the author has agreed that permission for extensive copying of this thesis for scholarly purposes may be granted by the professor or professors who supervised the thesis work recorded herein or, in their absence, by the Chair of the Department or the Dean of the Faculty in which the thesis work was done. It is understood that due recognition will be given to the author of this thesis and to the University of Prince Edward Island in any use of the material in this thesis. Copying or publication or any other use of the thesis for financial gain without approval by the University of Prince Edward Island and the author's written permission is prohibited.

Requests for permission to copy or to make any other use of material in this thesis in whole or in part should be addressed to:

Chair of the Department of Health Management

Atlantic Veterinary College

University of Prince Edward Island

Charlottetown, P. E. I.

Canada C1A 4P3

SIGNATURE

PAGE(S)

(iii)

REMOVED

SIGNATURE

PAGE(S)

(iv)

REMOVED

ABSTRACT

Infrared (IR) absorption patterns of equine synovial fluid (SF) were studied. The objectives were to: 1) develop and optimize laboratory protocols suitable for mid-infrared (MIR) spectroscopic analysis of equine SF, 2) identify significant differences among MIR spectra of SF from anatomically different types of equine joints, and 3) determine the feasibility of using MIR spectroscopy and classification algorithms for the differentiation of SF samples from diseased and control joints.

The technique of MIR spectroscopy of dried films was optimized for equine SF. Suitable MIR spectra of equine SF were obtained from the 8 μL aliquots of 3:1 SF to aqueous potassium thiocyanate solution deposited onto a silicon microplate by using an optimal spectral acquisition protocol. The overall MIR absorption pattern of equine SF is similar to the MIR absorption pattern of human SF reported in literature. The laboratory methods used in the current research for collecting the MIR spectra are technically straightforward and economical.

Inter-articular variability among 3 clinically normal high motion joints (antebrachiocarpal (AC), midcarpal (MC) and tarsocrural (TC)) was investigated. Statistical comparisons of MIR absorption patterns of SF from study joints were made. Samples from the contralateral pairs were likely to yield a similar MIR absorption pattern. Differences in spectral features between ipsilateral AC and MC were detected, and comparisons between the spectra of the carpal and TC joints revealed more widespread discriminatory absorption bands. The results suggested that inter-articular variation should be considered when using this technique.

The feasibility of the use of IR spectroscopy combined with statistical classification algorithms was assessed by using SF samples from joints with traumatic arthritis (TA) and control joints. The MIR absorption patterns of SF from joints with TA differed significantly from corresponding patterns for controls. A classification model was developed based on characteristics of 3 optimal MIR regions, and yielded an overall accuracy of 97% (sensitivity 93%; specificity 100%) in the calibration dataset. The same model with cost-adjusted prior probability of 0.60:0.40 produced an overall accuracy of 89% (sensitivity 83%; specificity 100%) for a validation dataset, and 100% correct classification for a second validation set of normal control SF.

The feasibility of this technique was further confirmed by comparing SF samples from tarsocrural joints with osteochondrosis (OC) and control joints. Disease-associated characteristics within MIR spectra of SF were identified by the use of statistical modeling. The classification model developed was based on the characteristics of 6 optimal MIR regions, and yielded an overall accuracy of 77% (73% sensitivity; 81% specificity).

The feasibility of IR and statistical classification algorithms for the differentiation of spectra derived from samples of diseased and control joints were demonstrated in this current research project. These findings favor the further development of this method for diagnosis of equine joint disease. Further recruitment of samples from both diseased and normal equine populations is required to evaluate the clinical usefulness of IR spectroscopy in diagnosis of equine joint diseases.

ACKNOWLEDGEMENTS

This dissertation is a fruition of collaborative efforts from many generous and inspiring people. Without their guidance and technical helps, this dissertation would not have been completed.

Firstly, I wish to express my deep appreciation to my supervisor, Dr. Chris Riley for his valuable advice, knowledge and immense support. His enthusiastic attitude towards orthopedic research has contributed to my development as a veterinary surgeon and researcher. I would like to thank Dr. Liz Spangler, my co-supervisor. Without her practical advice and perceptiveness, this dissertation would not have been finished.

Special thanks go to my committee members, Drs. Laurie McDuffee and Nola Etkin for their encouraging words, thoughtful criticism and careful reviews of this dissertation even in the busiest time of the semester. I wish to express my sincere gratitude to Dr. Dan Ryan for giving me an opportunity to learn statistics by real-world examples with insightful guidance. I appreciate him as a true intellectual person and one of the most active committee members in my graduate program. I am beyond grateful to Dr. Anthony Shaw for introducing me into spectroscopic world, and teaching me how to apply this technique to my orthopedic world. His expertise and hospitality have supported and encouraged me throughout my study program.

My heartfelt thanks also go to my dear friends, Drs. Tammy Muirhead, Simone Stahel, Jonathan Spears and Marcos Lores as well as technical staff in large animal clinic, radiology and post mortem units in the AVC Veterinary Teaching Hospital who provided me with specialized assistance. I would like to extend my gratitude to Dr. Patricia Rose for her skillful recommendation in radiology. Special thank to Dr. Wayne McIlwraith for his collaboration. My dearest thanks go to all horses and horse owners particularly, Yogi Fell who participated in this research project. Without the support from these people this research project would not have been possible.

I owe a huge debt to my best friend Dr. Narudee Kashemsant for her never-failing friendship and for sharing sorrows and joys in my academic life. My hearty thank-you goes to my dear friends in AVC graduate student community who made my graduate study life in Canada full of love, laugh and joy.

Finally I would like to thank my parents for their tireless encouragement and understanding.

This dissertation is dedicated to my parents, Nan and Nitch

TABLE OF CONTENTS

LIST OF TABLES

LIST OF FIGURES

LIST OF ABBREVIATIONS

Abbreviations	Terms
234 CEQ	Collagenase-generated neoepitope of type-II collagen fragment
AC	Antebrachiocarpal
ANN	Artificial neural network
BSE	Bovine spongiform encephalopathy
C	Carbon
CLL	Chronic lymphocytic leukemia
cm^{-1}	Reciprocal centimeter or the number of wave cycles in one centimeter or wavenumber
COL2-3/4C_{short}	Collagenase-generated neoepitope of type-I and type-II collagen fragment
CPII	Carboxy propeptide of type II procollagen
CS-846	Chondroitin sulfate epitope 846
CT	Computer Tomography
CTx1	Cross-linked telopeptide degradation fragment of type-I collagen
DA	Discriminant analysis
DNA	Deoxyribonucleic acid
DPR	Disease pattern recognition
ELISA	Enzyme-Linked Immunosorbent Assay
FIR	Far-infrared
FT-IR	Fourier transform infrared spectroscopy
H	Hydrogen
Hb	Deoxyhaemoglobin
HbO2	Haemoglobin
IR	Infrared
KS	Keratan sulphate

KSCN	Potassium thiocyanate
LDA	Linear discriminant analysis
MC	Midcarpal
MIR	Mid-infrared
MRI	Magnetic resonance image
N	Nitrogen
NIR	Near-infrared
NMR	Nuclear magnetic resonance
O	Oxygen
OA	Osteoarthritis
OC	Osteochondrosis
PLS	Partial least square
QDA	Quadratic discriminant analysis
RA	Rheumatoid arthritis
RNA	Ribonucleic acid
SCC	Somatic cell count
SD	Standard deviation
SF	Synovial fluid
TC	Tarsocrural
TSE's	Transmissible spongiform encephalopathies
UV	Ultraviolet

CHAPTER 1

POTENTIAL AND CURRENT ROLES OF BIOMEDICAL INFRARED SPECTROSCOPY AS AN ADVANCED DIAGNOSTIC TOOL IN VETERINARY CLINICAL SCIENCE

1.1 Introduction

Clinical diagnosis is a process of information gathering with intention of clarifying the character of patient's condition that will further lead to an accurate prediction of prognosis and an appropriate treatment regimen (1). Generally, clinical diagnoses can be made by means of an evaluation of a patient's history and physical examination, laboratory examination of body fluids, cell and tissue specimens and diagnostic imaging (2). The art of clinical diagnosis links a knowledge of basic science with clinical medicine and the nature of the disease mechanism, including the biochemical and morphological alterations of the body in the response to disease (3). Various diagnostic technologies have been developed and introduced to assist with clinical diagnosis in the past few decades. Alterations in the biochemistry and morphology of organs, tissues, and cells have been probed by electron microscopy, immunological assays, novel molecular biology techniques and biophysical techniques, including spectroscopy (4-9). These have provided physicians and veterinarians revolutionary and powerful technologies with which to detect or screen for disease, determine the severity or extent of a disease, monitor the pathologic progression and response to treatment, predict the response to treatment, and formulate a prognosis.

Fourier-transform infrared (FT-IR) spectroscopy remains one of the most important tools in analytical chemistry, on par with nuclear magnetic resonance (NMR), ultraviolet (UV) spectroscopy and mass spectrometry (10). The innovation of high quality FT-IR spectrometers, incorporating developments both in the interferometer and in digital data acquisition, as well as computational processing have revolutionized the breadth of applications for infrared technology (11-13). These advances have contributed enormously to the enhancement of accuracy, reproducibility and signal to noise ratio (11, 12). Today infrared spectroscopy is generally accepted as one of the most versatile of analytical techniques (11, 12). The application of this emerging technology has been extended from the analytical chemistry community to other scientific communities, such as the biomedical sciences where this innovation has been utilized to diagnose clinical problems and to gain insights into pathogenesis (12, 14).

1.2 Theory of infrared spectroscopy

The fundamental theory underpinning infrared (IR) spectroscopy relies on absorption characteristics of the molecules within a sample when exposed to broadband IR radiation (15). Infrared radiation spans the electromagnetic region between the red end of the visible region and the microwave region (0.78-1000 μm) (16). The IR region has traditionally been subdivided into near-infrared (0.78-2.5 μm, NIR), mid-infrared (2.5-50 μm, MIR) and far-infrared (50-1000 μm, FIR) regions (16). The absorption of IR radiation occurs when the frequency of the incident IR

radiation is matched with the frequency of a characteristic molecular vibration (15-17). The position and intensity of each absorption depends upon the atoms displaced during the vibrational cycle, i.e. the nature of the bond(s) involved, the type of vibration (e.g. stretching or bending), and the inter- and intramolecular interactions that may modify the atomic motions defining otherwise free vibrations (15, 17). Some vibrational modes are localized to such an extent that they may be viewed as vibrations of particular bonds or bond types. For example, the "C-H stretching region" encompassing the wavenumber range 2800-3100 cm^{-1} includes a variety of absorptions that can be traced to the stretching motions of C-H bonds. For such absorptions, within a compound, the intensity of a given IR absorption band is roughly proportional to the concentration of molecular bonds (e.g. C-H bonds) or functional groups within the molecule being probed (18, 19).

The IR absorption spectrum is typically displayed as a plot of absorbance versus wavenumber within the IR range (16). The absorbance is defined as $-\log(I(\nu)/I_0(\nu))$, i.e. the negative logarithm of the ratio of measured intensities for single-beam spectra with the sample in the IR beam ($I(\nu)$) and with no sample in place ($I_0(\nu)$); the "background" spectrum (20). For mid-infrared (MIR) spectra, the absorption position is universally reported as wavenumber or the number of waves per unit of length - simply the inverse of the wavelength (in centimeters) (16). This unit of inverse centimeters (cm^{-1}) is convenient since it is proportional to the frequency and the energy of IR radiation (16). The wavenumber range of the MIR region (2.5-50 μm) is therefore 400 to 4000 cm^{-1}.

1.3 Advantages of IR spectroscopy

An important limitation of IR spectroscopic analysis is that biochemical information can be obtained only from IR active molecules (17). Infrared active molecules are those molecules that react to IR radiation by changing the net dipole moment, thus their IR absorption can be measured (16, 17). Despite this limitation, IR spectroscopy still offers several advantages in biomedical applications because most organic molecules absorb IR radiation (16, 17, 19).

This analytical technique can be performed on any state of the sample (gas, liquid, or solid) giving a variety of possibilities for biological samples (body fluids, cells and tissue etc.) to become candidates for IR measurement (15, 16). The IR active components in a sample give rise to IR absorption bands without any need for chemical or immunological modification (18). No reagents are required for most biomedical IR measurements, making IR spectroscopy a cost effective technique for batch analysis of samples (18). By using computer-assisted spectral analysis and modern bioinformatics techniques, an enormous amount of information on chemical composition and structure can be gained from IR measurement of biological samples (11, 12).

The aforementioned advantages make IR spectroscopy suitable for both ex vivo analyses (where a spectroscopic measurement is performed on living cells or tissue specimens or biological fluids taken from the patients) and in vivo assessments (where the spectroscopic measurement is performed directly on the patient's body).

Infrared analyses of the exfoliated cells, biopsy tissue and biological fluids constituted the ex vivo infrared applications in IR clinical chemistry and pathology (21-26). The in vivo analysis by use of near-infrared (NIR) spectroscopy allowed the real-time monitoring of tissue perfusion and oxygenation (27). In addition, non-invasive screening tests for human diseases such as rheumatoid arthritis (28) and skin lesions (29, 30) have been developed using the NIR fiber optic probe. The details of these applications will be described in the following sections.

1.4 The molecular basis of infrared spectral interpretation

Using a high performance IR spectrometer, the spectra may be produced with good reproducibility. The pattern of absorptions (both their positions and intensities) making up the spectrum of a particular substance is highly specific to that substance, and may be considered analogous to the fingerprint of a person (10). The unique characteristics of the infrared absorption pattern have been used for structural elucidation and identification of compounds for many decades (10, 31). For complex mixtures of large molecules such as biological samples, IR spectra become correspondingly more complex, with bands inevitably overlapped to such an extent that explicit assignment of individual bands to individual molecules is difficult or impossible (11). However in spite of this complexity, IR spectra of biological samples such as body fluids, cells and tissue provide biochemically relevant information regarding the chemical structure(s) and their relative abundances of the constituents (11).

Traditional spectral interpretation in organic chemistry according to empirical rules has been documented elsewhere (31, 32). These manual interpretative strategies are used by spectroscopists for compound identification and structural elucidation. The concept of vibrational group frequency is one of the useful guidelines for spectral interpretation (12, 19, 20). According to this approach, the MIR region may be subdivided into 4 subregions according to the nature of group frequencies that give rise to the absorption bands. The subregions are as follows: 1) the X-H stretching region at 4000-2500 cm^{-1} (where X = oxygen, carbon, or nitrogen atoms); 2) the triple bond region at 2500-2000 cm^{-1}; 3) the double bond region at 2000-1500 cm^{-1}; and 4) the fingerprint region at 1500-600 cm^{-1} (19, 20). These rules and guidelines have been used to assist spectroscopists and other trained persons in diagnostic assessment of an IR spectrum. Digital spectral libraries and various computer-assist spectral interpretation systems (so called expert systems) are available for chemical structure elucidation (33). The establishment of spectral library databases not only for the systems for IR spectra, and multi-dimensional systems that incorporate spectroscopic information acquired from other types of spectroscopy and spectrometry such as NMR and mass spectrometry, have revolutionized scientific and medical progress (33).

Guidelines to assign the major MIR bands in tissues and cells have also been documented (6). For instance, protein IR signatures include characteristic absorptions whose maxima are located at 3290, 3050, 1655, 1545, and 1280 cm^{-1} for amide A (N-H stretch), amide B (N-H bending first overtone), amide I (C=O stretch), amide II (N-

H bending) and amide III of collagen, respectively (6). Carbohydrates typically contribute strong absorptions in the 1000-1200 cm^{-1} range, corresponding to C-O stretching vibrations (6). The CH_3 and CH_2 groups of lipids and proteins give rise to the peaks at 3000-2800 cm^{-1}, while peaks at 1220, 1240 and 1080 cm^{-1} are typically assigned as the asymmetric and symmetric stretch of nucleic acid and lipid phosphate (PO_2) groups (6). These guidelines are very useful for spectral interpretation and analysis of cells and tissues.

1.5 Biomedical infrared spectroscopy

The proper selection of spectroscopic measurement technique (NIR versus MIR) is crucial in IR spectroscopic measurement (6, 34). The selection of an IR spectroscopic method depends on the disease being studied, the tissues affected, the nature of the chemical species of interest, and whether the measurement is to be carried out in-vivo or ex-vivo. Both MIR and NIR spectroscopy have been widely exploited in clinical and diagnostic research (6, 18, 35-38). The MIR region (400-4000 cm^{-1}) is the most information rich region since it contains the absorption bands corresponding to the fundamental vibrations of most organic species (18). The abundance of chemical information from MIR spectroscopic measurement makes MIR spectroscopy the method of choice for ex vivo analytical and diagnostic works (18).

Near infrared spectroscopy generally provides spectra that are simpler than MIR spectra. The NIR spectra typically arise from overtone and combination

absorptions of C-H, O-H and N-H groups (6). In some circumstances, the absence of absorption from other confounding bonds or other functional groups facilitates the identification of the species of interest when using NIR spectroscopy. However, the NIR is not as rich in information when compared to MIR, due to the absence of information other functional groups such as carbonyl and phosphate groups (6). The main attractions of NIR spectroscopy lie in the availability of inexpensive optical fibers that permit the easy implementation of NIR spectroscopy for in vivo applications, and in the depth of penetration by near-infrared radiation into tissue (27). The penetration depth of NIR radiation into a sample can vary from 0.01 millimeter to several centimeters (37). In biological fluids and tissues, the ability of 0.2 mm to 5 mm depth penetration for NIR radiation has been reported, enhancing its in vivo utility (37). The depth of penetration is insufficient to fully penetrate most whole organs or the entire body of most species, but information from the surface of the organ and surrounding tissues can be acquired with NIR spectroscopy, and may be sufficient for the diagnosis of some conditions (27, 35, 37). This capability has lead to the development of non-invasive monitoring and diagnostic tools incorporating either fiber optic technology or spectroscopic imaging systems (27, 35, 37).

1.6 Biological sample preparation and IR spectroscopic measurements

Infrared spectroscopy can be used to analyze a wide range of samples of biological origin. For example, spectroscopic analyses have been performed on the

simplest biological fluids such as serum, synovial fluid, and amniotic fluid (38). More complex samples such as white blood cells, cells collected directly from patients via fine needle biopsy, or impression smears, have also been investigated (6). A remarkable advancement in IR technology is the development of IR microscopy, which couples a reflecting microscope to IR spectroscopy to obtain spectra from small, defined areas (typically 30x30 microns) within biopsy tissue sections (6). To obtain IR spectra from a variety of sample types, care should be taken to use sample preparation techniques which minimally perturb the nature and stability of the samples, and avoid introduction of artifacts (6). The very strong water absorptions centered at ~1640 cm^{-1} and 3300 cm^{-1} (the O-H bending and stretching vibrational modes) dictate that MIR spectroscopy of aqueous specimens requires very short optical path lengths (in simple terms the thickness of the sample), on the order of 6 to 10 microns (18, 38). This is very inconvenient in practice, requiring specialized cells that are inconvenient to use even for the specialist, and certainly not appropriate for implementation in routine clinical or diagnostic use. Furthermore, water contributes the same very strong absorptions to aqueous biological samples, dominating and obscuring the absorptions of the solutes of interest and hindering the meaningful analysis of such samples (18, 38).

Special apparatus and techniques, such as attenuated total reflectance (ATR) spectroscopy, are designed to overcome this problem and to allow the measurement of specimens in their native aqueous state (18, 38). However, the spectroscopic information above the IR region 3000 cm^{-1} is still inaccessible in the ATR spectrum

because the region is dominated by the strongest (OH stretching) water absorption (38). The most effective and simplest way to eliminate water absorption bands lies in the preparation of dried films from fresh specimens (38), which provides the further advantage of inactivating degradative enzymes (6). It is easily accomplished by applying approximately 5 - 50 μL of aqueous specimens onto an appropriate optical material and allowing it to dry before the acquisition of IR spectra (18, 38). While the NIR spectroscopic approach offers a more convenient method for handling aqueous samples because NIR spectral acquisition can be achieved by using optical path length of 0.5 mm or greater (18, 38), the NIR spectrum of an aqueous sample lacks information that is present in the counterpart MIR spectrum of a film dried from the same sample.

In microscopic tissue sample preparation, the best guideline is to keep the sample preparation simple and to a minimum (6, 39). The introduction of stains or the application of some tissue preparation solutions may induce artifacts and systematic variation in the spectroscopic data. This may further lead to bias in data interpretation and statistical analyses (6). The goal of IR microscopy is to obtain the spatially resolved spectroscopic information within the tissue section. To that end, the IR beam is focused on a small area of the sectioned tissue approximately 30 x 30 μm (6). Automated IR measurements may be acquired by the IR microscope, using a high precision computer controlled raster-scanning stage. The spectrum obtained from each small area (pixel) is combined to generate an IR spectroscopic map of the tissue (6). The data from IR mapping/imaging systems can be manipulated, reproduced, and

displayed in several meaningful ways. One of these methods is intensity-functional group mapping (6). An intensity-functional group map is produced by plotting the intensity of an absorption band of interest as a function of 2-dimensional position (area within the tissue section) (6). Such plots can be very useful, for example, to visualize the distribution of lipids, protein and DNA within the study tissue (6).

1.7 From IR spectroscopic data to IR-based diagnosis

The most challenging and rewarding part of IR biomedical spectroscopy is the development of algorithms that convert IR data into clinically useful tools. The purpose of this step is to discover and make use of significant information within the IR spectra to serve the diagnostic objectives of the clinician or researcher (13). An IR spectrum of a biological sample consists of the superimposition of all IR active components within the sample. Their relative intensities are weighted with respect to the concentration. A large volume of data is contained in the biomedical spectrum from a single measurement (11, 12). The central hypothesis underlying the diagnostic interpretation of IR spectra is that the factor of interest (e.g. disease) produces characteristic, significant alterations in the sample composition (which may be related to many of the chemical constituents within the sample) and that these alterations in turn promote characteristic, significant alterations in the corresponding IR spectrum of that sample. Such composition alterations due to disease or dysfunction may lead to changes in one or several characteristics of the IR absorption pattern, including changes in peak height, band width, and peak position (36). The key elements in the

development of infrared-based diagnostic tests are the extraction and recognition of spectroscopic patterns which are highly correlated to the presence or absence of disease or the concentration of the analytes of interest (11). Advanced computational techniques and operations associated with the mathematical manipulation and interpretation of IR derived chemical data (chemometrics) have been employed to fulfill this need (12, 13, 18, 36, 38, 40-42).

1.8 Ex vivo analyses by IR spectroscopy in biomedical science

1.8.1 Infrared clinical chemistry

Diagnostic information can be sought through the quantification of specific analytes of interest (26, 43-47). Quantitative analysis of IR spectra relies on Beer's Law, which describes the relationship between the absorbance and concentration of a particular component within non-scattering samples (18, 48). For a mixture, Beer's law is (18, 48);

$$\mathbf{A}(\nu) = \Sigma\, \varepsilon_i(\nu)\, c_i\, \mathbf{L}$$

where $\mathbf{A}(\nu)$ is the absorbance as a function of wavenumber, $\varepsilon_i(\nu)$ is the molar absorptivity of the $\mathbf{i}^{th}$ constituent as a function of wavenumber, c_i is concentration of the $\mathbf{i}^{th}$ constituent and $\mathbf{L}$ is the optical path length (18, 48).

Conversion of spectroscopic data into meaningful analytical information requires an unbiased study population that yields high quality samples, a spectroscopic measurement that yields good quality spectra, levels for the analyte(s) of interest as determined by standard reference analytical methods and the

development of a mathematical algorithm to recover the analyte concentration(s) from spectroscopic features (38). The usual procedure begins with the collection of samples that have had their analyte levels of interest determined by standard assay, with concentrations that span the range expected in the target population (23, 26, 43-47). One half to two-thirds of the spectra of these samples are randomly assigned into a calibration set and the rest is designated as the validation set (18). The calibration model is developed using the spectra in the calibration set. The most common modeling method reported in the literature is partial least squares (PLS) (23, 26, 43-47). As a secondary analytical method, PLS calibration models are built upon statistical correlations relating spectroscopic features to analyte levels (as determined by accepted analytical methods). Model development is iterative; several possible models are explored and refined to derive the best predictors or PLS factors that minimize the standard error of the calibrated concentration based on IR spectroscopy when compared to the reference analytical assay. Finally the model is validated by an independent validation set to ensure the performance and the general applicability of the developed model (18, 38).

Using the approach described above, the concentrations of several analytes have been successfully recovered from IR spectra using MIR spectral analysis of dried films. For example, serum analytes including albumin, cholesterol, glucose, total protein, triglycerides and urea have been quantified by IR spectroscopy and chemometric methods (PLS), with minimal standard errors of prediction (26). A serum cholesterol panel can be measured in single IR spectroscopic measurement to

simultaneously quantify the concentration of high-density lipoprotein cholesterol and low-density lipoprotein cholesterol, total cholesterol and triglycerides (43). The quantification of glucose and urea concentration in whole blood samples has also been reported (44). Other types of biological fluid samples such as urine, saliva and amniotic fluid have also been study using dried film spectroscopic techniques (23, 47, 49). The successful spectroscopic analyses of multiple analytes in urine such as urea, creatinine, and total protein, suggests that the IR-based analytical technique is accurate enough to serve as a routine clinical laboratory method for urea and creatinine analysis (47). In another study, an IR-based assay for the assessment of fetal lung maturity has been developed (23). Partial least square models have been used to predict the surfactant/albumin ratio based on IR spectra of amniotic fluid, and their corresponding levels by standard quantification methods. An excellent correlation was reported between the level of surfactant/albumin ratio predicted by reagent free IR-based analysis and standard TDx FLM II assay (23).

In most of these studies, the IR spectroscopic measurement has been carried out by spreading the biological sample on a barium fluoride substrate, chosen because this salt is transparent to IR radiation (to a low wavenumber limit of ~800 cm^{-1}). The high cost of these windows is justified by their compatibility with aqueous samples, since barium fluoride is not water soluble (50). A glass substrate has also been tested for use in MIR spectroscopy (45). However, glass is opaque at wavenumbers below 2000 cm^{-1}, therefore, spectroscopic information below 2000 cm^{-1} is inaccessible (45, 46). Interesting enough, by using glass as optical material, the serum concentration of

albumin, glucose, protein, urea, cholesterol and triglyceride can be accurately predicted using only the spectroscopic data between wavenumbers 2800 and 3500 cm^{-1} (46). This research offers alternative, reproducible, reliable and inexpensive method for clinicopathological analysis using MIR spectral analysis of dried film.

1.8.2 Infrared pathology

All forms of disturbances and injuries of organs in the body begin with molecular or structural alterations within the basic unit of life, namely the cell (3). Cells are chemically and structurally sophisticated units since they contain about 1000 different molecules such as variety of amino acids, carbohydrates, fatty acids (39). These are the basic molecules that are assembled into more complex molecules including protein, nucleic acids, DNA and RNA (39). Alterations in the structure or concentration of these cellular constituents lead to the morphological and functional changes in organ level or higher clinical manifestations (3). Infrared spectroscopy of the cell, tissue and biological fluids may provide an effective and reliable means for detecting and staging such changes in response to disease processes, whether they be clinical or preclinical (6, 36, 39). Moreover, spectroscopic methods may become useful to evaluate treatment responses, leading to improvement of therapeutic regimens (51, 52). The ultimate goal of IR pathology is to provide rapid, reliable and economical means for preclinical diagnosis so that clinical care and therapy can be prescribed in a timely manner (11).

The aim of employing IR for pathological evaluation is to obtain spectroscopic data that are faithfully related to the pathological changes which have

occurred either in concert with or in response to the presence of disease, and not from artifactual elements that may be present in the biological samples. In biological samples, some compositional changes in the spectrum may arise through other unrelated biological sources of variation, which may not be part of the pathological process (11). Potential sources given rise to such variations were described elsewhere in molecular epidemiology literatures (53-55). The biological samples may possess some inherent variability. Intra-subject and inter-subject variability may be associated with physiological, genetic, or environmental factors such as age, race (breed), sex, activity, occupation, and circadian rhythm etc. (55). Other components of variability found in biologically based measurements including IR spectra of biological samples may be attributable to procedures involving sample collection, processing, and storage, and laboratory analysis (53, 54). As generally accepted, in the development of a diagnostic test, an appropriate study design and a proper selection of "diseased" and "normal" individuals are crucial for the validity of the study (53, 56). Infrared-based diagnostic test development must therefore be carried out with a large number of spectra to avoid the detection of subtle differences that may be associated with other sources of variation and to ensure the general applicability of the diagnostic test in the target population (11).

Care should be taken in choosing the spectroscopic method and sample preparation technique to ensure that the quality of the spectra is acceptable (6, 39). After the appropriate sample preparation technique is chosen and the spectroscopic measurements completed, then the next step in the process is to seek significant

diagnostic information, for example using feature selection and extraction methodologies (57). This process has 3 purposes: to eliminate the irrelevant spectroscopic information; to enhance some of the weak features that are believed to be important for disease diagnosis; and to transform the data into a form that is suitable for further analysis (57). Prior to executing the feature selection process, spectral preprocessing can be extremely beneficial as a means to minimize extraneous spectral features and amplify the genuine spectral information of potential diagnostic utility. Preprocessing commonly includes mathematical manipulation methods such as spectral differentiation and smoothing, spectral normalization, and spectral integration (22, 36, 40, 42, 57-61). Once the spectral pre-processing is completed, a statistical and computational procedure called multivariate diseased pattern recognition (DPR) can be used to identify spectral subregions that form the basis of an optimal diagnostic test and to remove subjectivity from spectral analysis (22, 36, 40, 42, 57-61). Infrared spectroscopic features, defined by the particular combination of variables from the spectra (integrated intensity within the set of spectral subregions, peak amplitude, band width, area under the peak, slope of the band etc.), are then used as an input to a classification model (34, 36).

Two major approaches of pattern recognition have been utilized and yield successful outcomes in many different kinds of research (14, 22, 24, 40, 42, 58-62). Unsupervised pattern recognition is a method that recognizes patterns common to subgroups of spectra and classifies the spectra into classes (subgroups) with no prior knowledge about the number of classes and pattern characteristics of the classes (6,

34, 36). The most popular unsupervised pattern recognition technique is hierarchical cluster analysis (14, 59, 60). The essence of cluster analysis is to calculate some measures of the similarity between the spectra in the data set. Then the spectra are grouped based on their degree of similarity (34, 36). While cluster analysis based on these features can occasionally result in a final grouping of spectra that corresponds to disease status (24), it is often the case that the spectra cluster according to criteria that are unrelated to the disease of interest. In the latter case, supervised classification methods can be effective.

The second type of pattern recognition, namely supervised pattern recognition is a method whereby the spectra are classified based on prior knowledge of class identity or class membership (e.g. disease present versus disease absent) (18, 34, 36). Discriminant analysis (DA), either linear (LDA) or quadratic (QDA), has been commonly used for this purpose (21, 22, 25, 40, 42, 61, 62). The spectroscopic features that are believed to contain diagnostic information based on a set of spectra (this set is often referred to as the calibration set or training set of samples) are used to calibrate the classification model (6, 18, 34, 36). The robustness of classification and the general applicability are then tested by a new set of spectra (the test or validation data set) (6, 18, 34, 36). The validation process is challenging when the sample size of the data set is small. Some studies have exploited alternative resampling methods for validating the classification model. Two such methods are the leave-one-out resampling and bootstrapping (6, 34, 36). The leave-one-out resampling generates the classification model based on **N**-1 spectra of the data set

containing **N** spectra. Then the model is used to predict the class membership of the remaining spectrum. The resampling procedure is repeated until all the spectra in the data set take a turn to become the validation spectrum (6, 36). Boot strapping is a simulation based on multiple iterations of resampling with replacement (6, 22, 36). The number of spectra (e.g. **N**/2) is randomly selected as a training set for generating a classification model and then the remaining spectra are used for model validation (6, 22, 36). By utilizing one of these two resampling methods, the average performance of classification can be evaluated by averaging sensitivity and specificity of the classification model developed from each of these independent steps (41). The strategies as described are for training the discriminant analysis model to differentiate between the patterns of disease and non-diseased in the spectra. Once the final classification model is developed and refined to achieve a satisfactory classification result (i.e. the model can discriminate the spectra with a high degree of accuracy in both sets), the same model can then be applied to the spectrum of unknown sample to predict the disease status (34).

Sophisticated but highly efficient methods based on artificial intelligence have recently been developed and successfully used to characterize diagnostic features of sample spectra and to generate diagnostic algorithms for IR spectroscopic analysis of the biological samples (12). These artificial intelligence approaches include genetic algorithms for spectral features selection and artificial neural networks (ANN) (6, 12). A genetic optimal region selection algorithm has been successfully employed by many researchers (21, 63-65). This algorithm is programmed to seek a set of spectral

subregions that can provide a basis for classification. The input data are the features of the spectra in the dataset and their actual class designation (21, 63-65). The artificial neural network classification is a machine learning system based on self-adjustment internal control parameters. The system consists of layers of processing elements primarily used for solving pattern recognition problems (66-68).

1.8.2.1 Infrared spectroscopic applications in arthrology

The differentiation of sera and synovial fluid samples of normal individuals from patients with various types of arthritis has been reported using IR spectroscopy combined with DPR methods (21, 42, 61). Mid-infrared and NIR spectroscopic techniques have been exploited to categorize rheumatoid arthritis (RA), osteoarthritis (OA), and spondyloarthropathy (SA) synovial fluid samples in humans (21, 61). Despite the difference in IR spectroscopic measurement, an excellent and equivalent accuracy of class prediction of 95% was reported by both spectroscopic techniques. Diagnostic features from C-H moieties (combination bands) in the NIR region and C-H stretching band in the MIR region were believed to contribute to the success achieved in both studies (21, 61). The synovial fluid from temporomandibular joints of patients with OA, RA and control samples was also studied by the MIR spectroscopic technique (69). The intensity differences among the study groups appear to be most discriminatory at 2300 cm^{-1}, which corresponds to carbon dioxide absorption peak (69). However, no classification model was developed because of the limited number of spectra in the dataset.

Infrared based disease pattern recognition testing for rheumatoid arthritis has been investigated using serum as a specimen for analysis (42). Discriminant analysis with a complex optimization procedure was exploited, and a sensitivity and specificity of 84% and 88% reported from a dataset of 97 healthy and 94 rheumatic patients (42). Disease pattern recognition, a complex optimization procedure including a combination of disease marker values (the levels of rheumatoid factor, antinuclear antibodies, and C-reactive protein), and the IR spectroscopic DPR score (the score represents the probability of belonging to the healthy class) have been utilized in some IR-based diagnostic studies (40-42, 67). The multivariate DPR may provide the means to relate the actual disease status to the spectroscopic data even in the situation where the information concerning the underlying molecular components and processes is partially or completely unavailable (41).

The degree of cartilage degradation has been determined by using MIR fiber optic probe directly placed on articular cartilage of tibial plateau specimens (51). An encouraging result from a recently published work with MIR spectroscopy and a chemometric method (PLS) demonstrated correlation between the IR spectroscopic data and the grossly visual and histopathological grading system for assessment of cartilage degradation. The partial least squares model yielded a correlation between the actual and IR predicted grossly visual grade with $\mathbf{R^2}$ = 0.82 and 0.84 for a histopathological grading system (51). This promising methodology may lead to the development of minimally invasive and objective assessment of cartilage degradation that may be performed in conjunction with arthroscopy in the future.

1.8.2.2 Infrared spectroscopic applications in oncology

A classical example of IR-based diagnosis in oncology is the study of chronic lymphocytic leukemia cells by IR spectroscopy (24). In this study the isolated mononuclear cells from patients diagnosed with chronic lymphocytic leukemia (CLL) and normal individuals were collected, and the MIR spectra of cell suspensions were obtained using the dried film technique. The spectral were pre-processed using normalization, differentiation, and smoothing techniques (24). Then hierarchical cluster analysis was applied to partition the spectra into clusters. This unsupervised approach was able to separate the CLL cells from normal mononuclear cells based on the IR regions that originate from DNA and lipid in the cell (24).

The study of CLL cells using IR-spectroscopy has been extended to determine the drug resistant status of these cells (52). In vitro resistance to two therapeutic agents, chlorambucil and cladribuine, was studied by exposing isolated CLL cells to the agents. The viability of the cells was determined by a cytotoxicity assay, identifying the inhibitory concentration sufficient to cause 50% loss in viability (IC50) (52). The chemosensitivity of the cells was determined by establishing a cut-off value based on the mean of the IC50. The actual chemosensitive status, drug-sensitivity or drug-resistance, was determined and assigning the cells to one category or the other based on the IC50 cut-off value. The predicted status based on IR spectroscopic data was determined using LDA. The analyses for 2 chemotherapeutic agents were performed separately (52). The accuracy of the class prediction of the training (calibration) sets was 100% for both agents. However, the accuracy of test

(validation) sets dropped to 83% and 70% for cladribuine and chlorambucil respectively (52). It was suggested that alteration in DNA and membrane lipid associated with the development of resistance may have been reflected in changes in spectroscopic features used in the classification algorithm (52).

The use of MIR spectroscopic analysis has demonstrated its potential to discriminate malignant gastric tissue from normal control specimen collected from the same patients (62). The significant differences between cancerous and normal tissues were identified by t-test, yielding one p-value per wavenumber. Subregions that demonstrated p-value < 0.05 were used as inputs for classification model. These subregions were subjected to discriminant analysis. An accuracy of detection of neoplastic tissue of 88.6% (sensitivity of 96% and specificity of 75%) was reported by this method (62). The discrimination was believed to be based on the changes in amount of nucleic acids, collagen, and some amino acids of the tissue that may associate with the presence of gastric cancer (62).

Infrared spectroscopy combined with multivariate DPR techniques can be used for staging of breast tumors based on spectroscopic features derived mainly from the nucleic acids (22). The reliable classifier proposed in this study was achieved by LDA with bootstrapping cross-validation. The Nottingham standard scale for grading breast tumor (low, intermediate and high grades) was correlated to spectroscopic features. An accuracy of 87% for tumor grade prediction by the algorithm was reported (22). The breast tumor spectra were also classified according to the presence of estrogen and progesterone receptors. The classification model yielded an accuracy

of prediction 93.9% and 89.9% for the presence of estrogen and progesterone receptors respectively (22).

1.9 In vivo analyses by IR spectroscopy in biomedical science

Tissue spectra are the primary outcome derived from in vivo NIR reflectance spectroscopic methods. The technique is based on absorption and reflection properties of the target tissue when exposed to NIR radiation. If the sample is thick, as commonly encountered in vivo, a fraction of light that is "injected" by optic fibers at a certain point is scattered to such a degree that it re-emerges through the same surface; NIR radiation can be detected around the location where IR radiation enters the sample (27, 37). The term "interactance" is often preferred to "reflectance" spectra for this measurement geometry, since the direct probe-surface contact eliminates the air/surface reflective interface (27, 37). Both absorbance and light scattering properties are the factors determining the penetration depth of NIR into the target tissue.

Focal changes in tissue haemodynamics can be assessed by using a NIR reflectance or interactance fiber optic probe (27, 37). A more sophisticated NIR camera system equipped with an array detector, the IR-sensitive silicon-based charged coupled device (CCD), and a variable-wavelength tunable filter allows for the imaging of spatially resolved oxygenation changes in the target tissue. For example, NIR images of regional oxygenation variations on the heart or skin surface may be generated by this technique (27, 37). The reflected NIR light is gathered

either at the collector probe (in the case of fiber optic measurements) or by the array detector in case of NIR imaging. A pseudo-absorbance spectrum (intensity as a function of wavelength) may be calculated for the interactance spectrum by using the ratio between intensity of the radiation gathered from sample ($\mathbf{I_s}$) to the intensity of the reflected radiation derived from a neutral reflector sheet at the same wavelength ($\mathbf{I_r}$) (27). The pseudo-absorbance is calculated according to equation (27, 37):

$$\mathbf{A_\lambda} = -\log (\mathbf{I_s} / \mathbf{I_r})$$

The equation is analogous to absorbance in IR transmission spectroscopy (27, 37).

1.9.1 Assessment of tissue perfusion and oxygenation using NIR spectroscopy

Non-invasive NIR reflectance spectroscopy and imaging have been utilized in various proof-of-concept studies in different tissue types including brain (70, 71), cardiac (72), muscle (73, 74) and skin tissues (75, 76). The NIR absorption bands of interest originate from the NIR absorption characteristics of oxyhaemoglobin (HbO_2), deoxyhaemoglobin (Hb), and water in tissue (27, 37). The distinct maxima of NIR absorption by these chromophores and water content have been well documented (27, 37). A distinctive Hb absorption can be detected at 760 nm while HbO_2 has a characteristic absorption peak at 920 nm. The intensity of these peaks may be monitored in relation to the isosbestic point for the spectra of Hb and HbO_2, at 800 nm (37, 76). The hydration status of the tissue may be tracked via the intensity of water absorptions at 970 and 1450 nm (75).

An algorithm to quantify chromophores (Hb, HbO_2, and water) in tissue was developed using the relationship between their absorptivity spectra, and their tissue

concentrations (72, 75, 77, 78). According to the Lambert-Beer law, the intensity (A_λ) as a function of wavelength attributable to each chromophore is proportional to the concentration of that chromophore, its molar absorptivity (as a function of wavelength), the optical pathlength, and a path length factor that accounts for tissue scattering properties (72, 77, 78). Some authors also suggest an additional term that accounts for the measurement geometry (77, 78). The method is not without problems. For example, the position of the focal length change relative to the illumination source and detector, and the wavelength dependent optical properties of the tissue are possible sources of systematic error when objectively assessing focal changes in target tissues by NIR spectroscopy (77, 78).

Numerous proof-of-concept studies confirm the capability of NIR spectroscopy for non-invasive assessment and monitoring of changes in tissue perfusion and oxygenation (70-76). The non-invasive NIR fiber optic probe and imaging system has been used to monitor oxygen saturation and water contents in the pedicle skin flap of rats (75-76). The NIR imaging system has been utilized to measure oxygen saturation in skeletal muscle. The oxygen saturation of gastrocnemius muscle was assessed in human subjects during exercise (74). The regional differences in oxygen saturation within the muscle were detected with exercise suggesting the potential of NIR imaging system in monitoring muscle tissue metabolism (74). The NIR spectroscopic imaging system was used to generate maps of regional cardiac oxygenation in an open-chest porcine model (27, 72). The coronary artery was ligated to produce regional ischemia on cardiac tissue (72). The

images based on the regional distribution of deoxy- and oxyhemoglobin clearly demonstrated the ischemic area (72). Non-invasive NIR fiber optic optodes have been developed for monitoring cerebral oxygenation and metabolism of the brain in infant. For this purpose, the newborn piglets have been chosen as an animal model (70). The development of non-invasive NIR spectroscopy for oxygenation assessment of brain tissue has faced many challenges. The contribution of extracerebral component such as skin, skull and cerebrospinal fluid to the signal is one of the problematic issues (71). The confounding interference attributable to the extracerebral components may be minimized and the signal of the cerebral tissue may be maximized, with careful setup of the measurement by placing the light delivery optode very close to the signal receiving optode (27, 71). The method of NIR spectroscopy and imaging are still in the early phase of application development (71).

1.9.2 Non-invasive in vivo diagnosis of rheumatoid arthritis

Non-invasive fiber optic NIR spectroscopy has been utilized to pass IR light through the joints of patients with rheumatoid arthritis (RA) to objectively evaluate the tissue properties within the joints (28). The NIR spectra were obtained from multiple joints of both RA and normal control patients. The spectroscopic data within the NIR range were examined and spectral subregions were statistically selected based on univariate t-tests on individual wavelengths and principal component analysis (28). The validation of the model indicated that NIR spectroscopy combined with a statistical pattern recognition method was successful in differentiating joints with RA from unaffected joints. The correct classification rates of early stage and late

stage of RA (when combined data from all joints) were 77.3% and 71.2% respectively (28). The selected IR subregions are associated with the absorption features of water, cytochromes and heamoglobin suggesting that the method may rely on the oxidative status of joint tissue (28).

1.9.3 Non-invasive screening methods for skin lesions

The feasibility of in vivo diagnostic analysis using NIR fiber optic spectroscopy has been demonstrated by the differentiation of 6 common skin lesions in humans: actinic keratoses, basal cell carcinoma, actinic lentigo, dysplastic nevi, benign nevi, and seborrheic keratoses (29, 30). The results of this exploratory study demonstrated significant differences in several regions between the spectra from skin lesions and normal control skin using paired t-tests applied at each individual wavelength (30). The difference spectra (diseased-normal) were subjected to analyses of covariance to confirm the significance of differences between skin lesion groups. The alterations in the spectroscopic data may be associated with the changes in heamoglobin species, water content and absorption of protein N-H vibrational mode (30). The data set was further explored using optimal region selection genetic algorithm to identify discriminatory spectral regions (29). The classifier, based on LDA with leave-one-out cross-validation, classified the spectra according to skin lesion groups with accuracy of 70-98% (29).

1.10 Current applications of IR spectroscopy in veterinary medicine

The applications of IR spectroscopy developed for biomedical sciences can be utilized to solve clinical problems in veterinary medicine; successful proof-of-principle research in the biomedical field has inspired the development of applications specifically oriented towards veterinary medicine. The aforementioned advantages of small sample requirements (5-50 μL), reagent free analysis, and the potential for automation at very low cost have all served to enhance its appeal in animal health (15, 16, 18). These advantages suggest the possibility of developing IR-based analyses of biological fluids such as serum, milk, and synovial fluid that may assist the evaluation of health status at the herd level and in disease screening for the animal population at large (66, 67, 79-82).

1.10.1 Infrared spectroscopy applications in veterinary urology

An example of the straightforward clinical utilization of IR spectroscopy is the identification and structure elucidation of urinary calculi or urolithiasis. The prevention and treatment of urolithiasis is facilitated by a knowledge of the composition and chemical structure of the calculi (83), and to that end urinary calculi in canid, felid and equid species have been studied by infrared spectroscopy (83-86). These analyses rely on the strong and distinctive absorption bands that characterize and differentiate the various chemical compositions of these calculi. For example, calcium oxalate uroliths may be recognized by the presence of characteristic bands at 1320 cm^{-1}, whereas struvite uroliths may be recognized by the presence of typical absorption bands at 1010 and 572 cm^{-1} (83, 85, 86). Information from IR spectroscopy as well as scanning electron microscopy has contributed to further the

understanding of the chemical nature of these uroliths, etiology and risk factors contributing to the formation of such calculi, and assist in recommending the proper prevention and appropriate therapeutic regimens, such as dietary management (83).

1.10.2 Infrared spectroscopy applications in herd health management

Dairy herd management systems may benefit from certain IR spectroscopic methods. For example, FT-IR multi-component milk analysis is an important and reagent-free tool that measures fat, protein, lactose, and urea in milk with a low cost per sample, at a speed of up to 500 samples per hour (79, 80). Infrared analysis of milk urea was reported to have excellent reliability and repeatability when compared to a standard enzymatic test using urease enzyme to convert urea to ammonia (Eurochem CL10) (79). The development of a screening test for ketosis in dairy cows is a good example of an IR-based screening test for metabolic disease (80). Ketosis results in lower milk production and lower fertility performance (80). Milk acetone content is considered the best indicator of ketosis in cows (80, 81). A feasibility study of IR spectroscopy that combined principal component analysis (data reduction process) and partial least squares calibration (model development), resulted in an accurate test for detecting subclinical ketosis with 95-100% sensitivity, and 96-100% specificity, assuming a prevalence of subclinical ketosis of 10-30% (81).

Another example of IR spectroscopy applied to dairy herd management is somatic cell count (SCC) determination in milk by NIR spectroscopy (82). Somatic cell counts in milk are considered to be the most important indicators of infection and inflammation of mammary gland or mastitis, and are commonly evaluated both at the

bulk tank and at the individual cow level. Calibration of SCC was performed using a PLS model that correlated NIR spectroscopic data to logarithm transformed SCC values. The standard errors of calibration and prediction were 0.36% and 0.38% respectively (82). The prediction of SCC by NIR spectroscopy was thought to be associated with alterations in lactose content, ionic concentration and the protein fraction in milk. The results of this study confirmed the possibility of this test for accurately screening for mastitis (82).

1.10.3 Infrared spectroscopy applications in the detection and screening of infectious diseases

The application of IR spectroscopy has been extended to the detection and screening of infectious diseases. Transmissible spongiform encephalopathies (TSE's) in the forms of scrapie in sheep and bovine spongiform encephalopathy (BSE) in cattle are life threatening neurodegenerative disorders that raise significant concerns for human health (87). Infrared spectroscopic analyses of tissue and serum from infected animals have been performed recently (66, 67, 87-90). The technique of FT-IR microscopy has been used to study the molecular alterations associated with the scrapie infection in sections of hamster brain tissue and homogenized brain tissue samples (88, 89). IR spectra of different areas in brain tissues revealed compositional changes in proteins, lipids, carbohydrates, and the phosphate backbone of nucleic acids from the membrane constituents (88, 89). The changes in IR spectra were used to differentiate scrapie-infected tissues from the non-infected ones by means of both cluster analysis and artificial neural networks (ANN) (88, 89).

A feasibility study has been reported for scrapie diagnosis based upon MIR spectroscopy of serum in scapie-innoculated hamsters, with the aim of developing and antemortem screening test (90). A spectral classifier based on covariance and ANN analyses was able to discriminate serum spectra of infected animals from normal control spectra with a test sensitivity and specificity of 97% and 100% respectively (90). While the test works in a practical sense, i.e. a disease-specific signature was recovered from MIR spectra of serum by means of multivariate classification algorithms, the biomolecular basis of the spectral signal underlying the successful diagnosis of scrapie could not be readily explained by the authors; the individual serum constituents contributing to the infrared signature remain unknown (90).

Not long after the reported success of IR-based antemortem test in laboratory animals, the antemortem identification of a BSE-associated signature in MIR spectra of bovine serum was investigated (66, 67). Various computational and classification algorithms have been explored to seek a reliable assignment of spectra to the infectious or noninfectious categories (67). The classification results from 4 classification approaches including principle component analysis plus LDA, robust LDA, ANN, support vector machine were combined and mathematically transformed into a DPR scoring system (67). The numerical scoring system ranges from 0 to 1, indicating the likelihood of a serum spectrum belonging to either disease or control classes (40, 42, 67). Interestingly, the combination of 4 classifiers yielded a sensitivity > 85% and a specificity > 90% at a confidence level of 95% (67). The

results from these studies support the hypothesis that the presence of disease is accompanied by characteristic constituent and structural changes in serum composition.

1.10.4 Infrared spectroscopic application in veterinary arthrology

The potential of IR spectroscopy to solve diagnostic challenges in musculoskeletal disease has been investigated. For example, the spectra of synovial fluid derived from horses with osteochondrosis and normal controls were reported (91). Based on a limited number of the samples, it was suggested that differences in intensities at wavenumber 1000, 1035, 1115 and 1245 cm^{-1} may be associated with the presence of osteochondrosis (91). However, a classification algorithm that discriminated between the osteochondrosis and control spectra was not described.

Synovial fluid spectra from horses with traumatic arthritis have recently been subject to multivariate analysis (92). A set of spectroscopic features differentiating the synovial fluid samples associated with traumatic arthritis from the spectra of control samples were extracted. A preliminary classification model based on this set of features was calibrated by means of LDA and was validated with two independent sets of samples (92). The accuracy of calibration set and the validation sets were 97% (93 % sensitivity and 100 % specificity) and 89 % (83% sensitivity and 100% specificity) respectively (92). The second independent set of the samples from clinically normal horses was classified with 100% accuracy (92). These results confirmed the feasibility of IR spectroscopy, combined with multivariate statistical analysis, for the diagnosis of equine joint disease.

1.10.5 Assessment of tissue perfusion and oxygenation using NIR spectroscopy: veterinary applications

In veterinary clinical science, the potential of using NIR spectroscopy in real time monitoring tissue perfusion and tissue oxygenation saturation has also been explored in equine and porcine models (93-96). The technique has been used to study haemodynamics and oxygenation status of tissue in the hoof wall of horses (93), in muscular tissue (95), and intestinal tissue (94).

A noninvasive NIR spectroscopy technique was use to evaluate pedal haemodynamics and oxygenation in normal and laminitic horses (93). Both NIR emitter and detector sensors were placed on the dorsal surface of the hoof wall of one front foot in order to assess the vascular function within the hoof (93). Vascular occlusion models e.g. cuff inflation and manual occlusions of digital vessels were used to induce mechanical changes within the pedal microvessels. The responses to ischemic and reperfusion were gauged by alterations in HbO_2 and Hb absorption bands around 900 and 760 nm respectively (93). A weak absorption band between 780-870 nm was ascribed to oxidised cytocrome aa3, a terminal enzyme in mitrochodrial electron transport chain (93). This enzyme is an indicator of intracellular aerobic metabolism of the cells when oxygen is available. The decrease in HbO_2 and increase in Hb as well as reduction in cytochrome aa3 had been observed in sedated horses subjected to digital vessel occlusion (93). When the vascular occlusion was released, the return-toward-baseline of HbO_2 and Hb were observed in NIR spectra indicating the reperfusion of oxygenated blood and washout

of deoxygenated blood. The initial reduction of cytochrome aa3, when the digital vessels were occluded, may be consistent with low oxygen availability. The rates of response in laminitic horses were different from normal horses (93). The change in cytochrome aa3 in laminitic horses was more rapid than those found in normal horses. The rapid change may be associated with the lower oxygen storage within compromised perfusion tissue of the laminitic hoof. The results from the study suggested the potential role of NIR spectroscopy in diagnosis of laminitis and prediction of pre-laminitic condition in horses (93).

The assessment of muscle oxygenation by use of NIR spectroscopy was investigated in horses by use of tourniquet occlusion and induction of systemic hypoxaemia under general anesthesia and unanesthetized condition (95). The NIR absorption bands of oxygen dependent chromophores including heamoglobin, myoglobin and cytochrome aa3 have also been probed by the use of noninvasive NIR spectroscopy. In the muscle, the NIR spectrum of myoglobin can not be distinguished from heamoglobin because the absorption bands of myoglobin and heamoglobin are almost identical (27, 95). Therefore, both chromophores were reported together as haemoglobin/myoglobin changes (95). The deoxygenation indices were calculated by subtracting absorbances at the wavelength that corresponds to deoxyhaemoglobin/deoxymyoglobin from those of oxyhaemoglobin/oxymyoglobin. The significant alterations of deoxygenation indices from pre-ischemic baseline value were detected in both tourniquet occlusion and induction of systemic hypoxaemia under general anesthesia condition but not unanesthetized condition (95). The

movement artifact in unanesthetized horses may mask the changes in deoxygenation indices of the muscle. There were no significant reductions of cytochrome aa3 absorbance detected in both conditions (95). The artifact induced by tourniquet application related to changes in tissue geometry may contribute to the lack of significance in reduction of cytochome aa3 (i.e the changes of tissue geometry when applying and releasing the tourniquet may affect optical pathlength). However, the results of the study suggested the potential role of noninvasive NIR spectroscopy for monitoring changes in deoxygenation of tissue (by use of deoxygenation indices) that may be useful for prevention of postanaesthetic myopathy in horses (95).

The use of NIR spectroscopy to evaluate focal and global tissue perfusion and oxygenation may be acheived by both NIR fiber optic probe and NIR camera system (94). The segmental arteriovenous occlusion and reperfusion of intestine using a pig model was utilized to test the applicability of NIR spectroscopy in detecting and assessing the tissue perfusion and oxygenation (94). Based upon Lambert-Beer law, the least squares estimation of the relative concentration of total haemoglobin was used as a measure of tissue perfusion (94). This variable could be derived from the summation of HbO_2 and Hb absorbances. The ratio of relative concentration of HbO_2 to total haemoglobin yielded a measure of tissue oxygen saturation. The estimation for both total haemoglobin and oxygen saturation (ratio) were calculated from the tissue contacted area by the use of fiber optic probe. The same method of estimation was performed for each pixel of 256 x 256 NIR spectroscopic images. Upon the segmentally arteriovenous occlusion and IR spectroscopic measurement, the affected

intestine segment demonstrated a prompt and statistically significant reduction in tissue oxygenation indicated by the reduction in oxyhaemoglobin to total haemoglobin ratio (94). The oxygenation returned to the pre-occlusion level after reperfusion (94). The NIR image system revealed similar results in response to arteriovenous occlusion and reperfusion maneuver (94). The measurement of tissue perfusion (reflected by the relative concentration of total haemoglobin) demonstrated a minimal and statistically insignificant increase over time during arteriovenous occlusion. This suggested a small residual flow which may occur due to incomplete occlusion. A statistically significant increase in total hemoglobin concentration was also observed in the early phase of reperfusion before returning to the baseline level when using NIR fiber optic probe (94). This suggested a detection of a reactive hyperemic response at the initial phase of reperfusion (94). This phenomenon was explained in the study by suggesting that the vasodilators released in response to ischemia may not be completely eliminated from the ischemic site and may still exert their effect in decreasing vascular tone (94). Once the occlusion was released, a rapid and heavy influx of blood to the site may lead to hyperemic response. The tissue perfusion could be restored to the baseline level when the normal vascular tone can be re-established (94). The changes in the intestinal tissue oxygenation and haemodynamics in response to arteriovenous occlusion and reperfusion, particularly the reactive hyperemic response assessed by NIR spectroscopy, suggested that NIR spectroscopy may provide a rapid, reliable and sensitive means to gauge the degree of

intestinal ischemia and may assist in determination of the margin of tissue for intestinal resection and anastomosis in animals (94).

Regardless of the tissue being probed, the changes in tissue perfusion and oxygenation following induction of tissue ischemia or hypoxia can be detected from spectroscopic data, revealing the status of both tissue perfusion and oxygenation (93-95). However, heavily pigmented epidermal tissue in animals, such as that found in black hoof and black hair covered areas can influence and impede the penetration of NIR radiation (96). Tissue melanin may also be a source of a strong absorber of NIR light (96). These factors have been reported as limitations of NIR haemodynamic monitoring systems in animals (96, 97). Nevertheless, these studies have suggested the potential role of non-invasive NIR monitoring system for tissue perfusion and oxygenation in veterinary surgery and anesthesiology (93-97).

1.11 Future directions

The potential role of IR spectroscopy in biomedical applications was once speculated by a renowned British physician and scientist, Thomas Henry Huxley, in 1885. In his presidential address to the Royal Society, he stated "What an enormous revolution would be made in biology, if physics or chemistry could supply the physiologist with a means of making out the molecular structure of living tissues comparable to that which the spectroscope affords to the inquirer into the nature of the heavenly bodies". Since the first discovery of IR radiation in 1800 by a distinguished astronomer, Sir William Herschel, IR spectroscopy has been

continuously developed and refined by the efforts of pioneers in this field. Nowadays, IR spectroscopy has opened up new applications and gained a lot of attention from many scientific communities including biomedical and veterinary clinical sciences. IR spectroscopy-based analyses of biological fluid, cells and tissue have been investigated with encouraging results. Several reports have demonstrated the diagnostic potential of IR spectroscopy, particularly when combined with advanced and powerful computational methods. Not only do IR spectra provide fundamental insights into pathogeneses, this revolutionizing technology holds significant promise for the development of objective and reagent-free diagnostic tests that are practical, economical and reliable. These diagnostic tests have the potential to benefit both humans and animals by offering better disease detection and monitoring methods. These in turn trigger rapid and appropriate prevention strategies and treatment regimens, thus improving the quality of life for both human and animal patients.

1.12 Objectives of the current study

The broad objective of the current research project is to develop and apply IR spectroscopy and statistical classification algorithms to the field of equine arthrology. The specific objectives of the current research project are:

1) To optimize a laboratory protocol suitable for mid-infrared (MIR) spectroscopic analysis of equine synovial fluid

2) To identify significant differences and variations due to anatomic types among joints and left and right limbs within horses on MIR spectra of equine synovial fluid

3) To determine the feasibility of using IR spectroscopy and statistical classification algorithms in differentiation of samples of clinically diseased joints from those of controls in horses with traumatic arthritis and osteochondrosis.

The studies conducted in this research project were a preliminary phase (exploratory phase) of diagnostic accuracy research in order to assess the feasibility of this new technology for the diagnosis of joint disease in horses. It is hoped that the results from this research project will support the further development of this technique in the intermediate and advanced phase of diagnostic accuracy research in the future, with the ultimate goal of developing a preclinical and economical screening test for joint disease.

References

(1) Knottnerus JA, van Weel C. General introduction: evaluation of diagnostic procedures. In: Knottnerus JA, eds. The evidence base of clinical diagnosis. London: BMJ Books, 2002:1-18.

(2) Radostits OM, Tyler JW, Mayhew IG. Making a diagnosis. In: Radostits OM, Mayhew IGJ, Houston DM, eds. Veterinary clinical examination and diagnosis. London: W.B. Saunder, 2000:11-49.

(3) Kumar V., Abbas A.K., Fausto N. Cellular Adaptations, Cell injury, and Cell death. In: Gruliow R., eds. Robbins and Cotran Pathologic basis of disease. Philadelphia: Elsevier Saunders, 2005:3-46.

(4) Bollard ME, Stanley EG, Lindon JC, Nicholson JK, Holmes E. NMR-based metabonomic approaches for evaluating physiological influences on biofluid composition. NMR Biomed 2005;18:143-162.

(5) Csako G. Present and future of rapid and/or high-throughput methods for nucleic acid testing. Clin Chim Acta 2006;363:6-31.

(6) Jackson M, Mantsch HH. Infrared Spectroscopy, Ex vivo tissue analysis by. In: Meyers R.A., eds. Encyclopedia of analytical chemistry. Chichester: John Wiley and Sons Ltd., 2000:131-156.

(7) Pearson JM, McWilliam LJ, Coyne JD, Curry A. Value of electron microscopy in diagnosis of renal disease. J Clin Pathol 1994;47:126-128.

(8) Tampoia M, Brescia V, Fontana A, Maggiolini P, Zucano A, Pansini N. Proteomic: new advances in the diagnosis of rheumatoid arthritis. Clin Chim Acta 2005; 357:219-225.

(9) Westwood ME, Kelly S, Berry E, Bamford JM, Gough MJ, Airey CM et al. Use of magnetic resonance angiography to select candidates with recently symptomatic carotid stenosis for surgery: systematic review. BMJ 2002;324:198.

(10) Gunzler H, Gremlich HU. Introduction. In: IR spectroscopy, an introduction. Weinheim: Wiley-VCH, 2002:1-7.

(11) Dubois J, Shaw RA. IR spectroscopy in clinical and diagnostic applications. Anal Chem 2004;76:361A-367A.

(12) Schultz CP. The potential role of Fourier transform infrared spectroscopy and imaging in cancer diagnosis incorporating complex mathematical methods. Technol Cancer Res Treat 2002;1:95-104.

(13) Shaw RA, Mansfield JR, Rempel SP, Low-Ying S, Kupriyanov VV, Mantsch HH. Analysis of biomedical spectra and images: from data to diagnosis. J Mol Struct (Theochem) 2000;500:129-138.

(14) Naumann D. FT-IR and FT-NIR Raman spectroscopy in biomedical research. In *proceedings*: AIP Conference 1998;430:96-109.

(15) Stuart B. Introduction. In: Infrared spectroscopy: fundamentals and applications. Chichester: John Wiley & Sons Ltd., 2004:1-13.

(16) Hsu CPS. Infrared spectroscopy. In: Settle F, eds. Handbook of instrumental techniques for analytical chemistry. New Jersey: Prentice Hall, 1997: 247-283.

(17) Gunzler H, Gremlich HU. Absorption and molecular design. In: IR spectroscopy an introduction. Weinheim: Wiley-VCH, 2002:9-36.

(18) Shaw RA, Mantsch HH. Infrared spectroscopy in clinical and diagnostic analysis. In: Meyers RA, eds. Encyclopedia of analytical chemistry. Chichester: John Wiley & Sons Ltd., 2000:83-102.

(19) Stuart BH. Infrared spectroscopy of biological Applications. In: Meyers RA, eds. Encyclopedia of analytical chemistry. Chichester: John Wiley & Sons Ltd., 2000:529-559.

(20) Stuart B. Spectral Analysis. In: Infrared spectroscopy: fundamentals and applications. Chichester: John Wiley & Sons Ltd., 2004:45-70.

(21) Eysel HH, Jackson M, Nikulin A, Somorjai RL, Thomson GTD, Mantsch HH. A novel diagnostic test for arthritis: multivariate analysis of infrared spectra of synovial fluid. Biospectroscopy 1997;3:161-167.

(22) Jackson M, Mansfield JR, Dolenko B, Somorjai RL, Mantsch HH, Watson PH. Classification of breast tumors by grade and steroid receptor status using pattern recognition analysis of infrared spectra. Cancer Detect Prev 1999;23:245-253.

(23) Liu KZ, Shaw RA, Dembinski TC, Reid GJ, Ying SL, Mantsch HH. Comparison of infrared spectroscopic and fluorescence depolarization assays for fetal lung maturity. Am J Obstet Gynecol 2000;183:181-187.

(24) Schultz CP, Liu K, Johnston JB, Mantsch HH. Study of chronic lymphocytic leukemia cells by FT-IR spectroscopy and cluster analysis. Leuk Res 1996;20:649-655.

(25) Shaw RA, Guijon FB, Paraskevas M, Ying SL, Mantsch HH. Infrared spectroscopy of exfoliated cervical cell specimens. Proceed with caution. Anal Quant Cytol Histol 1999;21:292-302.

(26) Shaw RA, Kotowich S, Leroux M, Mantsch HH. Multianalyte serum analysis using mid-infrared spectroscopy. Ann Clin Biochem 1998;35:624-632.

(27) Shaw RA, Mansfield JR, Kupriyanov VV, Mantsch HH. In vivo optical/near-infrared spectroscopy and imaging of metalloproteins. J Inorg Biochem 2000;79:285-293.

(28) Canvin JM, Bernatsky S, Hitchon CA, Jackson M, Sowa MG, Mansfield JR et al. Infrared spectroscopy: shedding light on synovitis in patients with rheumatoid arthritis. Rheumatology (Oxford) 2003;42:76-82.

(29) McIntosh LM, Jackson M, Mantsch HH, Mansfield JR, Crowson AN, Toole JWP. Near-infrared spectroscopy for dermatological applications. Vib Spectrosc 2002;28:53-58.

(30) McIntosh LM, Summers R, Jackson M, Mantsch HH, Mansfield JR, Howlett M et al. Towards non-invasive screening of skin lesions by near-infrared spectroscopy. J Invest Dermatol 2001;116:175-181.

(31) Coates J. Interpretation of infrared spectra, a practical approach. In: Meyers RA, eds. Encyclopedia of analytical chemistry. Chichester: John Wiley & Sons Ltd., 2000:10815-10837.

(32) Gunzler H, Gremlich HU. Qualitative spectral interpretation. In: IR spectroscopy, an introduction. Weinheim: Wiley-VCH, 2002:171-278.

(33) Gunzler H, Gremlich HU. Reference spectra and expert systems. In: IR spectroscopy, an introduction. Weinheim: Wiley-VCH, 2002:329-345.

(34) Jackson M, Mantsch H. Pathology by infrared and Raman spectroscopy. In: Chalmers JM, Griffiths PR, eds. Handbook of vibrational spectroscopy. Chichester: John Wiley & Sons, 2002:3227-3245.

(35) Alam MK. Noninvasive diagnoses by near-infrared spectroscopy. In: Chalmers JM, Griffiths PR, eds. Handbook of vibrational spectroscopy. Chichester: John Wiley & Sons Ltd., 2002:3266-3279.

(36) Jackson M, Sowa MG, Mantsch HH. Infrared spectroscopy: a new frontier in medicine. Biophys Chem 1997;68:109-125.

(37) Schultz CP. Role of near-infrared spectroscopy in minimally invasive medical diagnosis. In: Chalmers JM, Griffiths PR, eds. Handbook of vibrational spectroscopy. Chichester: John Wiley & sons Ltd, 2002:3246-3265.

(38) Shaw RA, Mantsch H. Vibrational spectroscopy applications in clinical chemistry. In: Chalmers JM, Griffiths PR, eds. Handbook of vibrational spectroscopy. 2002:3295-3307.

(39) Dukor R.K. Spectroscopy in the detection of cancer. In: Chalmer J.M., Griffiths P.R., eds. Handbook of vibrational spectroscopy. Chichester: John Wiley & Sons Ltd., 2002:3335-3361.

(40) Petrich W, Staib A, Otto M, Somorjai RL. Correlation between the state of health of blood donors and the corresponding mid-infrared spectra of the serum. Vib Spectrosc 2002;28:117-129.

(41) Petrich W, Dolenko B, Fruh J, Ganz M, Greger H, Jacob S et al. Disease pattern recognition in infrared spectra of human sera with diabetes mellitus as an example. Applied optics 2000;39:3372-3379.

(42) Staib A, Dolenko B, Fink DJ, Nikulin AE, Otto M, Pessin-Minsley MS et al. Disease pattern recognition testing for rheumatoid arthritis using infrared spectra of human serum. Clin Chim Acta 2001;308:79-89.

(43) Liu KZ, Shaw RA, Man A, Dembinski TC, Mantsch HH. Reagent-free, simultaneous determination of serum cholesterol in HDL and LDL by infrared spectroscopy. Clin Chem 2002;48:499-506.

(44) Low-Ying S, Shaw RA, Leroux M, Mantsch HH. Quantitation of glucose and urea in whole blood by mid-infrared spectroscopy of dry films. Vib Spectrosc 2002;28:111-116.

(45) Shaw RA, Eysel HH, Liu KZ, Mantsch HH. Infrared spectroscopic analysis of biomedical specimens using glass substrates. Anal Biochem 1998; 259:181-186.

(46) Shaw RA, Mantsch HH. Multianalyte serum assays from mid-IR spectra of dry films on glass slides. Appl Spectrosc 2000;54:885-889.

(47) Shaw RA, Low-Ying S, Leroux M, Mantsch HH. Toward reagent-free clinical analysis: Quantitation of urine urea, creatinine, and total protein from the mid-infrared spectra of dried urine films. Clin Chem 2000;46:1493-1495.

(48) Gunzler H, Gremlich HU. Quantitative spectral assertions. In: IR spectroscopy an introduction. Weinheim: Wiley-VCH, 2002:279-307.

(49) Schultz CP, Ahmed MK, Dawes C, Mantsch HH. Thiocyanate levels in human saliva: quantitation by Fourier transform infrared spectroscopy. Anal Biochem 1996;240:7-12.

(50) Stuart B. Experimental Methods. In: Infrared spectroscopy: Fundamentals and applications. Chichester: John wiley & Sons Ltd., 2004:15-44.

(51) Li G., Thomson M., Dicarlo E., Yang X., Nestor B., Bostrom M.P.G. et al. A chemometric analysis for evaluation of early-stage cartilage degradation by infrared fiber-optic probe spectroscopy. Appl Spectrosc 2006;59:1527-1533.

(52) Liu KZ, Schultz CP, Johnston JB, Lee K, Mantsch HH. Comparison of infrared spectra of CLL cells with their ex vivo sensitivity (MTT assay) to chlorambucil and cladribine. Leuk Res 1997;21:1125-1133.

(53) Boffetta P. Molecular epidemiology. J Intern Med 2000;248:447-454.

(54) Holland NT, Smith MT, Eskenazi B, Bastaki M. Biological sample collection and processing for molecular epidemiological studies. Mutat Res 2003; 543:217-234.

(55) Poole AR. Biochemical/immunochemical biomarkers of osteoarthritis: utility for prediction of incident or progressive osteoarthritis. Rheum Dis Clin North Am 2003;29:803-818.

(56) Sasse EA. Objective evaluation of data in screening for disease. Clin Chim Acta 2002;315:17-30.

(57) Adams MJ. Feature selection and extraction. In: Chemometrics in analytical spectroscopy. Cambridge: The Royal Society of Chemistry, 2004:55-95.

(58) Jackson M., Eysel HH, Shaw RA, Glen T.D., Mantsch H. Non-subjective Diagnosis of Arthritic disorders by multivaliate analysis of IR spectra of

synovial fluid. In: Merlin J.C., eds. Sixth European conference on the spectroscopy of biological molecules. Dordrecht: Kluwer Academic Publishers, 1995:499-500.

(59) Lasch P, Haensch W, Naumann D, Diem M. Imaging of colorectal adenocarcinoma using FT-IR microspectroscopy and cluster analysis. Biochim Biophys Acta 2004;1688:176-186.

(60) Liu KZ, Tsang KS, Li CK, Shaw RA, Mantsch HH. Infrared spectroscopic identification of beta-thalassemia. Clin Chem 2003;49:1125-1132.

(61) Shaw RA, Kotowich S, Eysel HH, Jackson M, Thomson GT, Mantsch HH. Arthritis diagnosis based upon the near-infrared spectrum of synovial fluid. Rheumatol Int 1995;15:159-165.

(62) Fujioka N, Morimoto Y, Arai T, Kikuchi M. Discrimination between normal and malignant human gastric tissues by Fourier transform infrared spectroscopy. Cancer Detect Prev 2004;28:32-36.

(63) Nikulin AE, Dolenko B, Bezabeh T, Somorjai RL. Near-optimal region selection for feature space reduction: novel preprocessing methods for classifying MR spectra. NMR Biomed 1998;11:209-216.

(64) Somorjai RL, Dolenko B, Nikulin A, Nickerson P, Rush D, Shaw A et al. Distinguishing normal from rejecting renal allografts: application of a three—stage classification strategy to MR and IR spectra of urine. Vib Spectrosc 2002;28:97-102.

(65) Steiner G, Shaw A, Choo-Smith LP, Abuid MH, Schackert G, Sobottka S et al. Distinguishing and grading human gliomas by IR spectroscopy. Biopolymers 2003;72:464-471.

(66) Lasch P, Schmitt J, Beekes M, Udelhoven T, Eiden M, Fabian H et al. Antemortem identification of bovine spongiform encephalopathy from serum using infrared spectroscopy. Anal Chem 2003;75:6673-6678.

(67) Martin TC, Moecks J, Belooussov A, Cawthraw S, Dolenko B, Eiden M et al. Classification of signatures of Bovine Spongiform Encephalopathy in serum using infrared spectroscopy. Analyst 2004;129:897-901.

(68) Pizzi N, Choo LP, Mansfield J, Jackson M, Halliday WC, Mantsch HH et al. Neural network classification of infrared spectra of control and Alzheimer's diseased tissue. Artif Intell Med 1995;7:67-79.

(69) Ziegler CM, Kircher P, Hassfeld S. Analysis of temporomandibular joint synovial fluid using Fourier transform/infrared spectroscopy. J Oral Maxillofac Surg 2002;60:1302-1306.

(70) Hueber DM, Franceschini MA, Ma HY, Zhang Q, Ballesteros JR, Fantini S et al. Non-invasive and quantitative near-infrared haemoglobin spectrometry in the piglet brain during hypoxic stress, using a frequency-domain multidistance instrument. Phys Med Biol 2001;46:41-62.

(71) Villringer A, Chance B. Non-invasive optical spectroscopy and imaging of human brain function. Trends Neurosci 1997;20:435-442.

(72) Nighswander-Rempel SP, Shaw RA, Mansfield JR, Hewko M, Kupriyanov VV, Mantsch HH. Regional variations in myocardial tissue oxygenation mapped by near-infrared spectroscopic imaging. J Mol Cell Cardiol 2002;34:1195-1203.

(73) Mancini DM, Bolinger L, Li H, Kendrick K, Chance B, Wilson JR. Validation of near-infrared spectroscopy in humans. J Appl Physiol 1994;77:2740-2747.

(74) Miura H, McCully K, Hong L, Nioka S, Chance B. Regional difference of muscle oxygen saturation and blood volume during exercise determined by near infrared imaging device. Jpn J Physiol 2001;51:599-606.

(75) Sowa MG, Payette JR, Mantsch HH. Near-infrared spectroscopic assessment of tissue hydration following surgery. J Surg Res 1999;86:62-69.

(76) Stranc MF, Sowa MG, Abdulrauf B, Mantsch HH. Assessment of tissue viability using near-infrared spectroscopy. Br J Plast Surg 1998;51:210-217.

(77) Boas DA, Gaudette T, Strangman G, Cheng X, Marota JJ, Mandeville JB. The accuracy of near infrared spectroscopy and imaging during focal changes in cerebral hemodynamics. Neuroimage 2001;13:76-90.

(78) Strangman G, Franceschini MA, Boas DA. Factors affecting the accuracy of near-infrared spectroscopy concentration calculations for focal changes in oxygenation parameters. Neuroimage 2003;18:865-879.

(79) Arunvipas P, VanLeeuwen JA, Dohoo IR, Keefe GP. Evaluation of the reliability and repeatability of automated milk urea nitrogen testing. Can J Vet Res 2003;67:60-63.

(80) Hansen PW. Screening of dairy cows for ketosis by use of infrared spectroscopy and multivariate calibration. J Dairy Sci 1999;82:2005-2010.

(81) Heuer C, Luinge HJ, Lutz ET, Schukken YH, van der Maas JH, Wilmink H et al. Determination of acetone in cow milk by Fourier transform infrared spectroscopy for the detection of subclinical ketosis. J Dairy Sci 2001;84:575-582.

(82) Tsenkova R, Atanassova S, Kawano S, Toyoda K. Somatic cell count determination in cow's milk by near-infrared spectroscopy: a new diagnostic tool. J Anim Sci 2001;79:2550-2557.

(83) Escolar E, Bellanato J. Analysis of feline urinary calculi and urethral plugs by infrared spectroscopy and scanning electron microscopy. Vet Rec 2003; 152:625-628.

(84) Diaz-Espineira M, Escolar E, Bellanato J, De La Fuente MA. Infrared and atomic spectrometry analysis of the mineral composition of a series of equine sabulous material samples and urinary calculi. Res Vet Sci 1997;63:93-95.

(85) Escolar E, Bellanato J. Spectroscopic and ultrastructural comparative study of cystine calculi in humans and dogs. Biospectroscopy 1999;5:237-242.

(86) Escolar E, Bellanato J, Rodriquez M. Study of cystine urinary calculi in dogs. Can J Vet Res 1991;55:67-70.

(87) Thomzig A, Spassov S, Friedrich M, Naumann D, Beekes M. Discriminating scrapie and bovine spongiform encephalopathy isolates by infrared spectroscopy of pathological prion protein. J Biol Chem 2004;279:33847-33854.

(88) Kneipp J, Lasch P, Baldauf E, Beekes M, Naumann D. Detection of pathological molecular alterations in scrapie-infected hamster brain by Fourier transform infrared (FT-IR) spectroscopy. Biochim Biophys Acta 2000;1501:189-199.

(89) Kneipp J, Beekes M, Lasch P, Naumann D. Molecular changes of preclinical scrapie can be detected by infrared spectroscopy. J Neurosci 2002; 22:2989-2997.

(90) Schmitt J, Beekes M, Brauer A, Udelhoven T, Lasch P, Naumann D. Identification of scrapie infection from blood serum by Fourier transform infrared spectroscopy. Anal Chem 2002;74:3865-3868.

(91) Muttini A, Petrizzi L, Tinti A, Bertoluzza A. Synovial fluid parameters in normal and osteochondritic hocks of horses with open physis. Boll Soc Ital Biol Sper 1994;70:337-344.

(92) Vijarnsorn M, Riley CB, Shaw RA, McIlwraith CW, Ryan DAJ, Rose P, Spangler E. Use of infrared spectroscopy for diagnosis of traumatic arthritis in the horses. Am J Vet Res 2006;67:1286-1292.

(93) Hinckley KA, Fearn S, Howard BR, Henderson IW. Near infrared spectroscopy of pedal haemodynamics and oxygenation in normal and laminitic horses. Equine Vet J 1995;27:465-470.

(94) Kohlenberg E, Payette J.R., Sowa M.G., Levasseur M.A., Riley C.B., Leonardi L. Determining intestinal viability by near infrared spectroscopy: a veterinary application. Vib Spectrosc 2005;38:223-228.

(95) Pringle J, Roberts C, Art T, Lekeux P. Assessment of muscle oxygenation in the horse by near infrared spectroscopy. Equine Vet J 2000;32:59-64.

(96) Pringle J, Roberts C, Kohl M, Lekeux P. Near infrared spectroscopy in large animals: optical pathlength and influence of hair covering and epidermal pigmentation. Vet J 1999;158:48-52.

(97) Raisis AL. Skeletal muscle blood flow in anaesthetized horses. Part I: measurement techniques. Vet Anaesth Analg 2005;32:324-330.

CHAPTER 2

DEVELOPMENT OF THE INFRARED SPECTROSCOPIC TECHNIQUES FOR THE ANALYSIS OF EQUINE SYNOVIAL FLUID

2.1 Introduction

Today's infrared (IR) spectrometers would be nearly unrecognizable to the spectroscopist of a generation ago. With the advent of the interferometer, and powerful digital data acquisition and processing (1, 2), IR spectroscopic measurements today routinely provide a wavenumber accuracy of +/- 0.01 cm^{-1}, a very high signal-to-noise ratio of 10,000:1 or better, and superb reproducibility (2). These features have paved the way to the adoption of this emerging technology in the biomedical and diagnostic arenas (1-4). The ultimate goal in the development of IR-based diagnostic methods is to provide medical practitioners with a reliable, practical, and economical diagnostic test that is suitable for routine use. The quality and reproducibility of spectroscopic data are of the utmost importance to ensuring the reliability of such tests.

The development of IR based diagnostic tests for equine joint disease rely upon both state-of-the-art IR spectroscopic hardware, and also on spectral manipulations to bring diagnostic features into prominence (5-7). Once acceptable spectra have been measured, the next step is to pre-process the digitized spectroscopic data. These manipulations are carried out prior to pattern recognition or model calibration, with the aim of optimizing the accuracy of the diagnostic or analytical test

(8-10). This chapter will focus on the optimization of laboratory technique, spectral acquisition and feature enhancement, and pre-processing procedures used in the following chapters. The effects of these preprocessing techniques on spectral classification were investigated, and are reported in this chapter. The final section of the chapter provides an overview of decision-making criteria pertaining to the preprocessing and classification of equine synovial fluid (SF) using a spectroscopic dataset from Chapter 5 as an example.

2.2 Sample preparation technique

2.2.1 Optical materials

Various materials are available as optical windows to contain samples for spectroscopic analysis. These windows must be transparent to IR radiation. The vast majority of these materials are alkali halides, including sodium chloride, potassium bromide, barium fluoride, calcium fluoride and caesium iodide (11). Since biomedical IR spectroscopy typically involves aqueous or strongly hydrated samples (biofluids and tissues), expensive water-insoluble substrates such as barium fluoride and calcium fluoride have traditionally been used as optical windows (12-17). Even though it is possible to clean and to reuse these materials, it is relatively impractical to consider reusing them when contaminated or infectious samples are involved, or when batch analyses of the samples are performed (18). Alternative optical materials that are more economical and practical may be a better solution in such cases.

The Institute of Biodiagnostics (in collaboration with Dr. Anthony Shaw), National Research Council of Canada has developed a novel sample plate made from a silicon wafer (19). The silicon is IR transparent, and is very cost effective making it a practical substitute for expensive sample substrates (18, 19). The wafer is cut to match the size of a 96-well microtiter plate. An adhesive plastic mask with 5 mm-diameter circular windows is placed on the surface of the plate to spatially define the positions of those 96 wells. The microplate is designed to use with the "High-Throughput Screening" (HTS) accessory manufactured by Bruker Optics (Billerica, Massachusetts) to interface with Bruker FT-IR spectrometers. This accessory carries out the automated, sequential acquisition of spectra from the 96 sample wells on the silicon wafer, and is therefore well-suited for batch analyses of the type used in both the development and implementation of biomedical tests (19). A prototype of this novel plate design was used for this research (Figure 2.1). One disadvantage of this sample plate is delicacy of the material. Care should be taken when working with the silicon wafer because it is very fragile under compression.

2.2.2 Mid-infrared (MIR) spectroscopy of dried films

Mid IR spectroscopic analysis of biological fluids (such as SF) is technically challenging due to the superimposition of strong water absorption bands (O-H stretching and bending vibration) upon the absorption bands of other solute species within the sample (7, 20). One technique that has come into common use to surmount this problem is to dry the sample to a film prior to the spectroscopic measurement (7, 15-17). This approach was first developed for the spectroscopic analysis of human

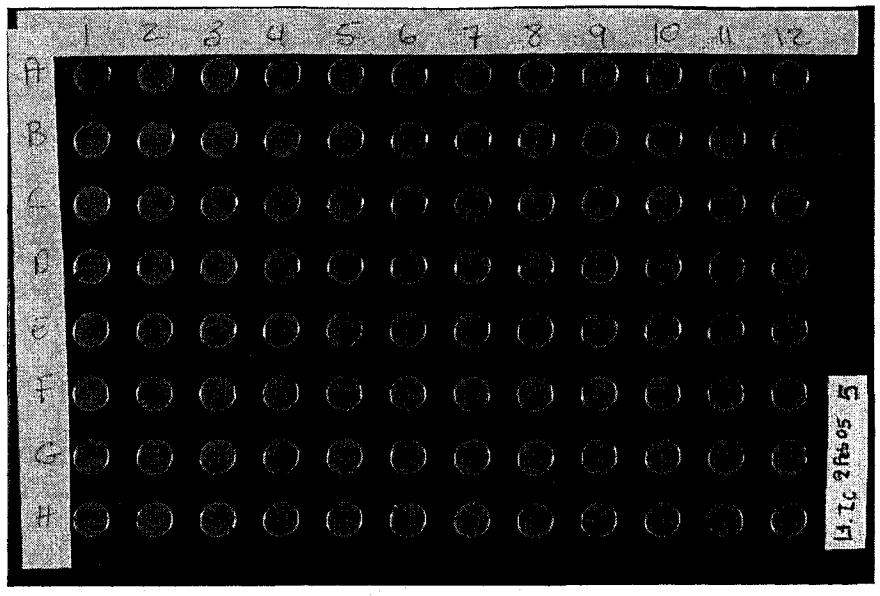

Figure 2.1. A 96-well silicon microplate with the blank position at A1 used as the background measurement.

SF samples (12, 21). The dried film technique is typically performed by spreading 5-50 μL of the biological fluid of interest onto a suitable optical substrate, and allowing it to dry completely (7). This approach not only offers a simple and convenient way to eliminate the water component of the aqueous samples, but also stabilizes the sample since degradative enzymes are likely to be inactivated (20). The method can, however, also produce artifacts associated with the spatial heterogeneity of the dried film. For example, infrared microscopic mapping of dried amniotic fluid films revealed protein deposits concentrated at the edge of the circular film (6). Some of the dried films of amniotic fluid samples have demonstrated two concentric rings, the formation of which may be associated with capillary flow during drying (6). From our experience rings are likely to occur when an air bubble is accidentally created in depositing the sample onto the plate; care should be taken to avoid the formation of these bubbles. As revealed by microscopic examination, SF desiccated films with grossly acceptable homogeneity can be obtained by either drying under mild vacuum pressure or drying at room temperature (Figure 2.2) (12, 16).

2.2.3 Dilution and deposition volume optimization

Both sample dilution and deposition volume should be optimized for the sample of interest to ensure well resolved spectra of sufficient magnitude, with minimal artifacts (6). Artifacts may be introduced into spectroscopic data, for example, by deposition of thick layer of films resulting in an overly long optical pathlength. If the pathlength is too long, the IR radiation is nearly completely

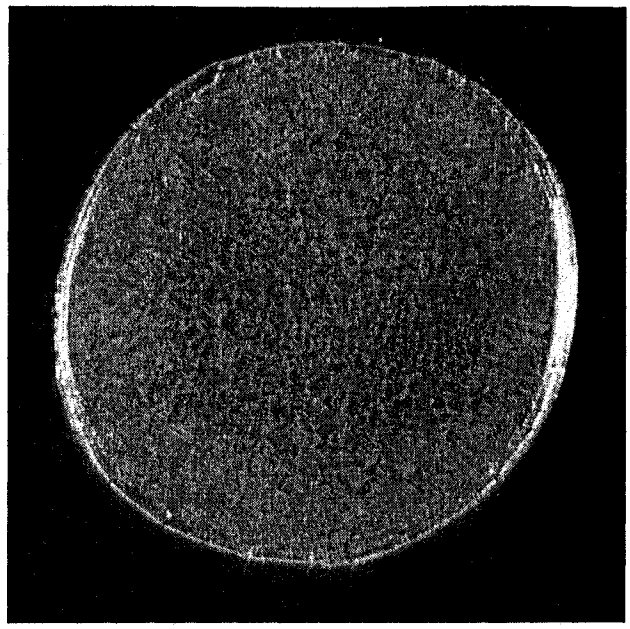

Figure 2.2. The dried film of equine synovial fluid (8 μl)

absorbed at wavenumbers corresponding to strong sample absorptions, and the spectra severely distorted as a consequence (6). To avoid such distortions, the intensity of light that transmits through the sample and reaches a detector must be within the linearity range of the detector (6). Dilution and sample deposition volume are therefore optimized to produce the spectra whose peaks remain in the linearity range of detector. One guideline that has been suggested is maintaining the maximum absorbance values within the range of 0.4 - 0.6 absorbance units (6). Once established, the optimal dilution and deposition volume should be maintained for every sample to ensure spectral reproducibility throughout the experiment.

For the current research, sample dilution and deposition volume were optimized by using 30 SF samples from 18 horses (11 females and 7 males). The samples were donated for the purpose of this study. These horses were 1-22 years old with mean age of 11.3±6.0 (mean±SD) and median age of 12 years old. Appaloosa (n=1), Quarter horse (n=3), Standardbred (n= 13) and mixed breeds (n=1) were represented. Synovial fluid samples were aspirated from joints including fetlock (n=6), antebrachiocarpal (n=5), midcarpal (n=7), stifle (n=6) and tarsocrural (n=6). The samples were centrifuged at 2700 x g for 10 minutes, and the supernatants were kept for spectroscopic measurement. An internal standard, KSCN solution (4g/L) was prepared in large volume and stored at 15 °C. This standard solution was used to dilute all samples in the current research project (16, 22, 23). The same amount of internal standard was added into each sample, in the ratio 3:1 SF-to-KSCN. Dried films of SF were made for each sample by applying 20 μL of neat SF and 3 different

deposition volumes, 15, 10 and 8 μL of the 3:1 SF-to-KSCN dilution. Triplicate films were produced for each sample using 4 different dried film preparation protocols as described. Each film was prepared by spreading the SF sample preparation evenly in a circular motion within a 5-mm circular island on the masked silicon microplate described above. For each sample, different dilutions and deposition volumes were deposited on the same well position but on different plates (a total of 4 plates were used in the optimization). The spectral acquisition was performed using a protocol described in the next section. Once the spectra of all samples were obtained, all of the replicate spectra with the same concentration and deposition volume were averaged (Figures 2.3-2.6). The 3:1 SF-to-KSCN dilution, deposited as 8 μL aliquots, was chosen as an optimal dilution and deposited volume, avoiding overly intense IR absorption by the sample. Infrared absorption bands of the average spectrum including their 95% confidence interval did not exceed the absorbance level of 0.6 (Figure 2.6) (6).

A representative spectrum of equine SF with major IR band functional molecular group assignments is illustrated in Figure 2.7. The major IR band assignment of human SF spectra reported by Jackson et al. (24) was adopted for the IR band assignment of equine SF spectra. The overall IR absorption pattern of dried film equine SF is relatively similar to the reported IR absorption pattern of human SF (24). The spectra of samples produced by the dried film technique used in the current

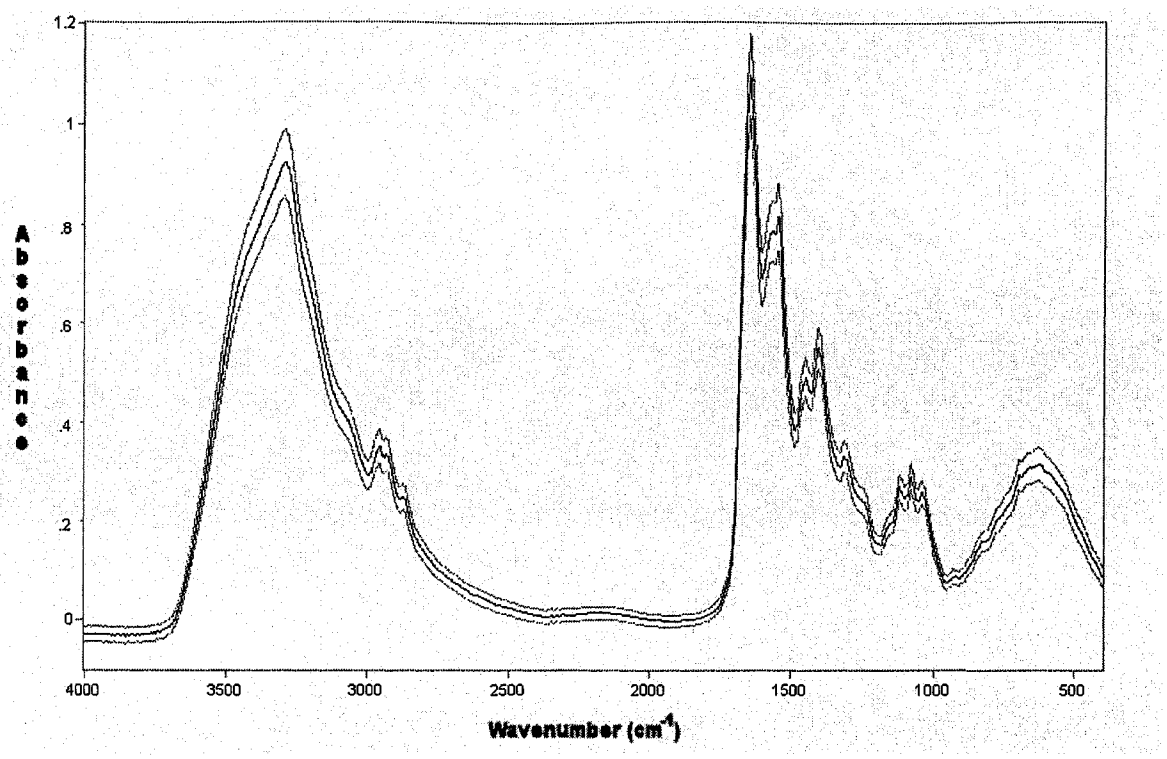

Figure 2.3. An average spectrum (black line) with 95% confidence limit (grey line) of neat synovial fluid when applying 20 μL onto silicon microplate.

Note: the magnitude of absorbencies greater than the suggested range of 0.4 – 0.6 absorbance units.

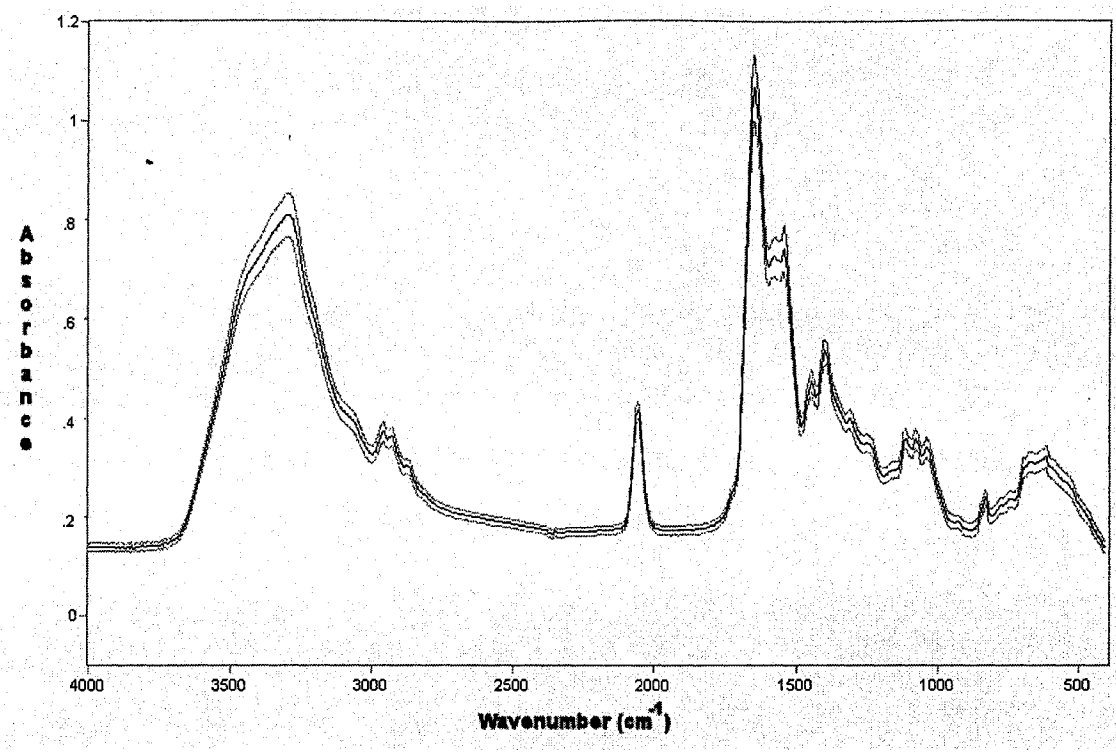

Figure 2.4. An average spectrum (black line) with 95% confidence limit (grey line) of 3:1 synovial fluid to KSCN dilution when applying 15 μL onto silicon microplate.

Note: the magnitude of absorbencies greater than the suggested range of 0.4 – 0.6 absorbance units.

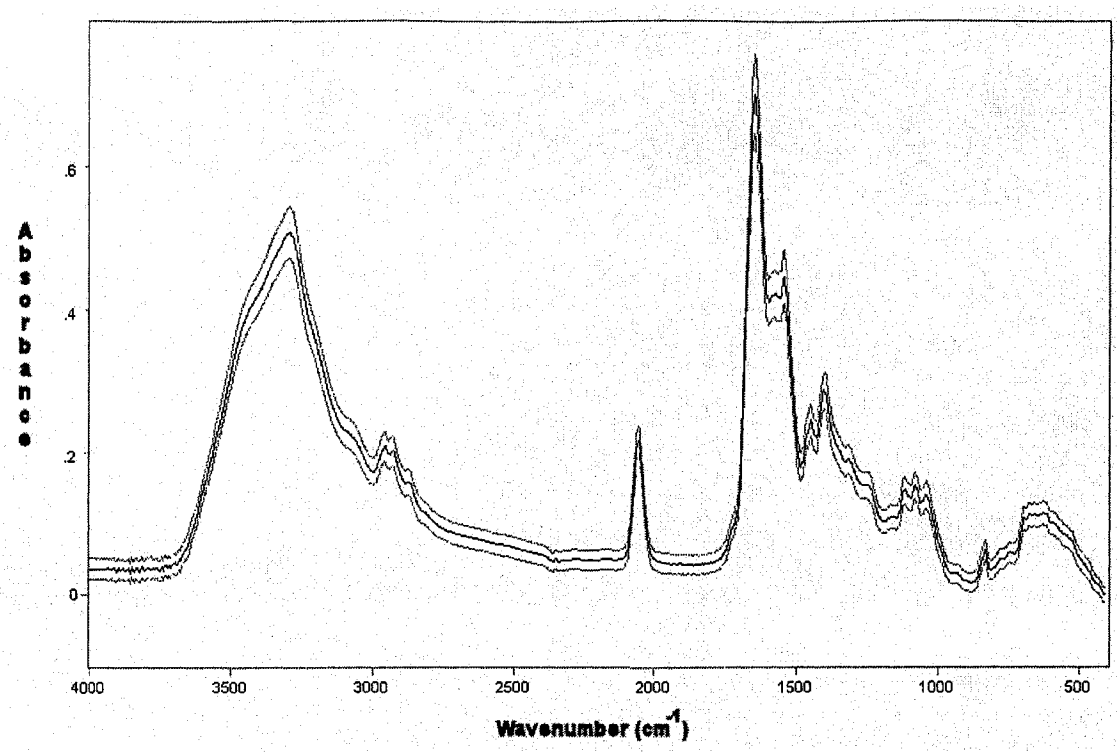

Figure 2.5. An average spectrum (black line) with 95% confidence limit (grey line) of 3:1 synovial fluid to KSCN dilution when applying 10 μL onto silicon microplate.

Note: the number of wavenumbers with a magnitude of absorbency greater than the suggested range of 0.4 – 0.6 absorbance units is markedly reduced.

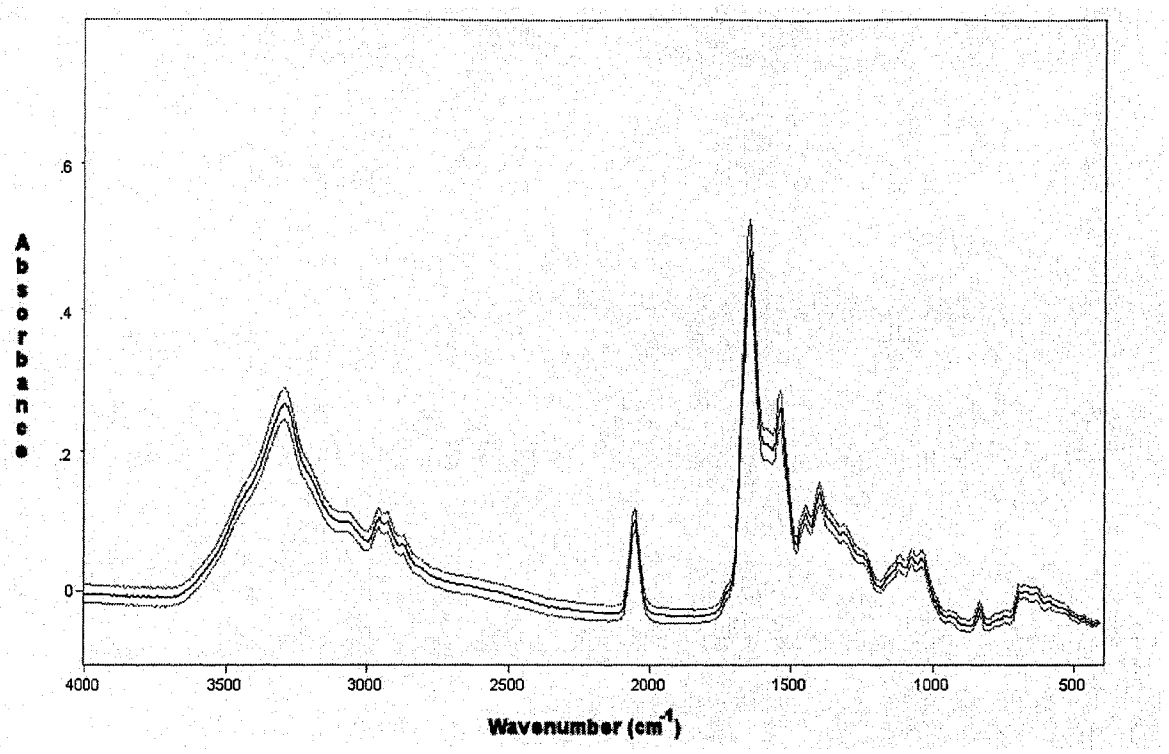

Figure 2.6. An average spectrum (black line) with 95% confidence limit (grey line) of 3:1 synovial fluid to KSCN dilution when applying 8 μL onto silicon microplate.

Note: there are no wavenumbers with a magnitude of absorbency greater that the suggested range of 0.4 – 0.6 absorbance units.

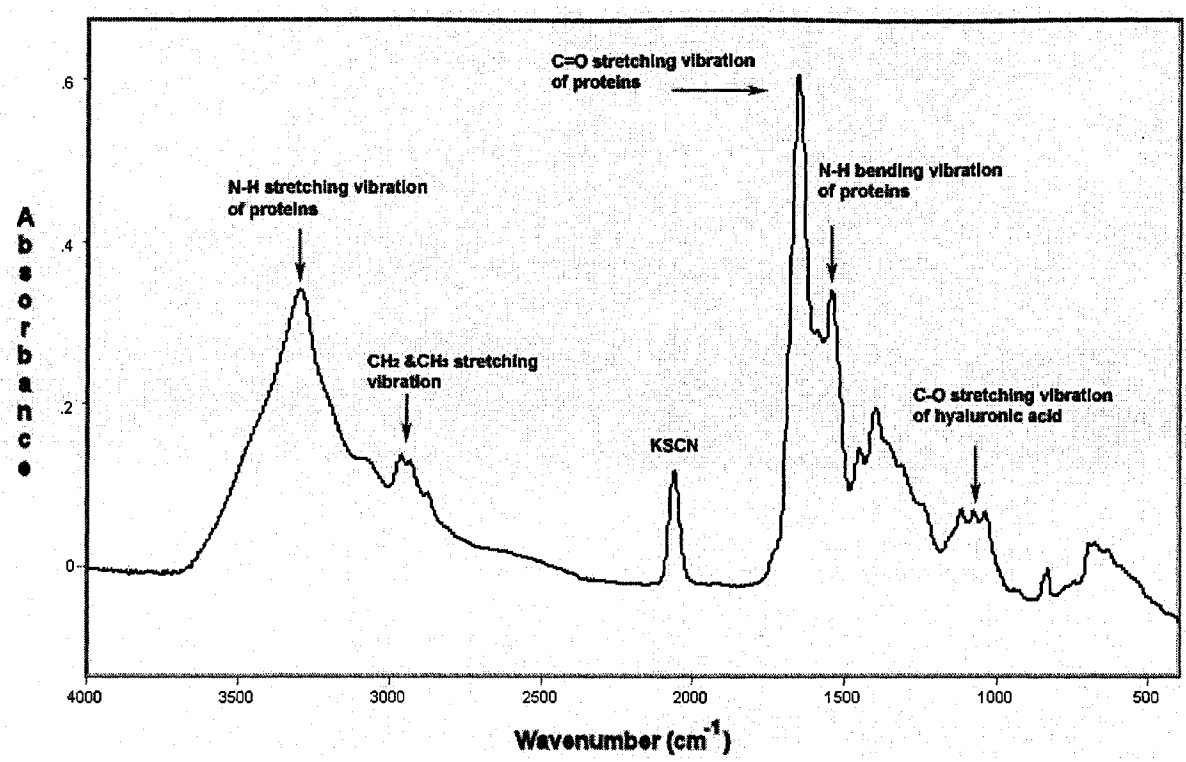

Figure 2.7. Equine synovial fluid spectrum with major IR band assignment corresponding to key molecular functional grouping indicated.

study are also dominated by the absorption bands of N-H and C=O vibrations from protein constituents, CH_2 and CH_3 stretching and bending vibrations and C-O stretching of carbohydrate (primarily hyaluronic acid) (24).

2.3 Fourier-transform infrared (FT-IR) spectral acquisition

The Fourier-transform infrared (FT-IR) spectrometer measures IR radiation transmitted through a sample of interest, but in an indirect way. Through a particular optical arrangement called an interferometer, the FT-IR spectrum is obtained by collecting signal interferograms (11, 25). The actual spectrum is derived from a co-added set of interferograms by carrying out a mathematical procedure called the Fourier Transform. This mathematical transformation converts the power density as a function of the difference in pathlength to the power density as a function of wavenumber (11, 25). The interferometer therefore lies at the heart of the FT-IR spectrometer, with the pivotal advantage of this setup being that all IR frequencies impinge on the detector simultaneously. This confers an enormous advantage in signal-to-noise for a given measurement time when compared to the traditional grating spectrometer, which transmits only a narrow band of frequencies to the detector at a time. The interferometer is an optical arrangement with three core components: a beam splitter, a stationary mirror, and a moving mirror (11, 25). Broadband (polychromatic) MIR radiation is split into two beams that interfere with each other in a constructive and destructive manner as the moving mirror is displaced (Figure 2.8). The interference results in an intensity-modulated beam exiting the

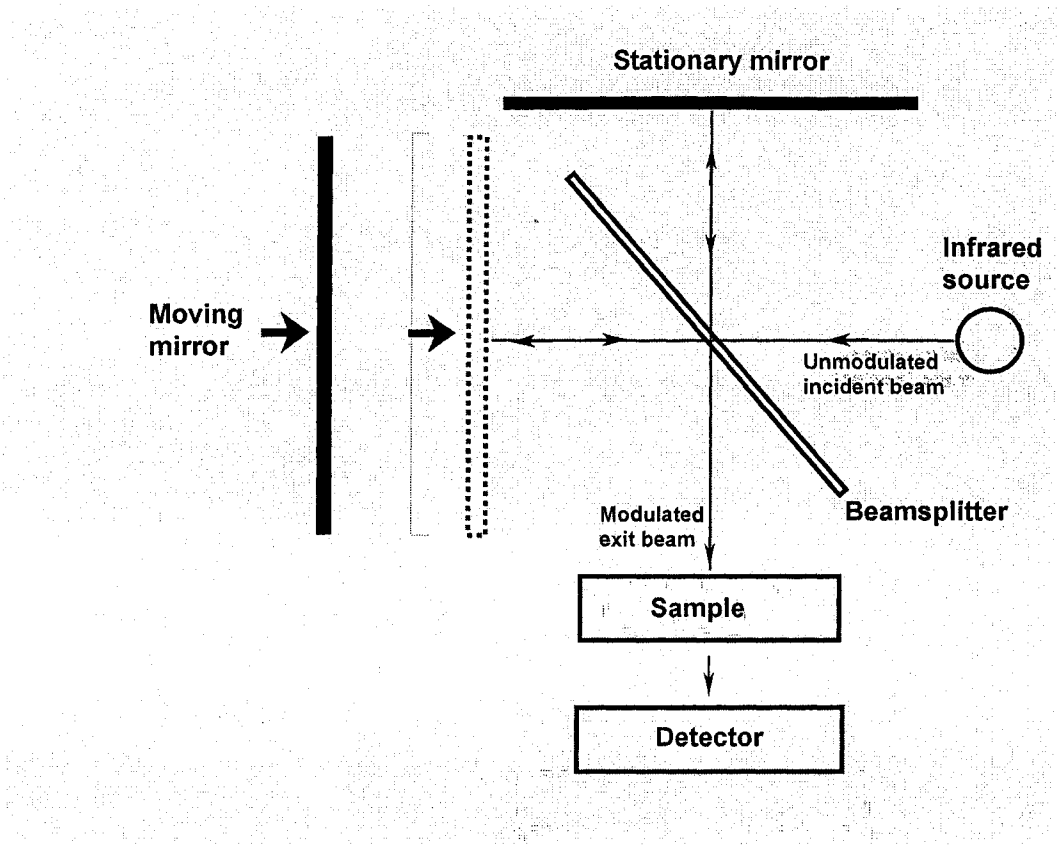

Figure 2.8. Schematic illustration of interferometer (adapted from Reference 11)

interferometer, that impinges upon the detector. The measured "interferogram" is therefore the signal intensity as a function of the pathlength difference (distance) between the two arms of the interferometer (Figure 2.8). Fourier-transformation converts the signal intensity in the distance domain (cm) dictated by the moving distance of the moving mirror into the desired signal intensity in a frequency domain (wavenumber, cm^{-1}), which is the single-beam infrared spectrum (5, 11). Since the FT-IR spectrometer analog signal from the detector is converted to digital domain for storage and Fourier transformation, the digitized signal may then be subject to mathematical manipulations as required and/or desired (5, 11, 25).

In transmission-absorbance spectroscopy, the first interferogram is obtained when the modulated exit beam reaches the detector in an absence of the sample. After Fourier transformation, a background single channel spectrum is generated (11, 25). The background spectrum is affected by instrumental and environmental factors. The overall profile reflects both the intensity of the source and the response of the detector as a function of wavenumber (frequency). Superimposed on this profile may be patterns arising through the absorption by atmospheric constituents. For example, band complexes centered approximately at 3500 cm^{-1} and 1630 cm^{-1} commonly appear and are assigned to atmospheric water vapor, while bands at approximately 2350 cm^{-1} and 667 cm^{-1} are due to carbon dioxide (11, 26, 27). To factor out both the instrumental response profile (detector response, source emission profile) and possible atmospheric absorptions, a background spectrum must be measured prior to obtaining the spectrum with the presence of sample (26, 27). Once the interferogram

of the sample is measured (identical to the background measurement, but with the sample of interest between the interferometer exit beam and the detector) and Fourier transformed, the sample spectrum is determined against the background spectrum in order to eliminate the effects from instrument and environment as much as possible (11, 25). The absorbance (**A**) is defined as the logarithm of the ratio $\mathbf{I_0/I}$ (28).

$$\mathbf{A} = \log_{10} (\mathbf{I_0/I})$$

where $\mathbf{I_0}$ and **I** are the single-beam background and sample spectra respectively. Because it is a product based upon a ratio, the absorbance unit is dimensionless. In practice, the background measurement for the projects reported in this thesis was obtained by measuring the single-beam spectrum for a particular well position (on the top left corner of the plate) with no sample in place, prior to every sample measurement. This was especially necessary for the current study, as the laboratory used for our study had limited climate control, and the humidity could vary significantly over a 24 hour period.

Since the transmittance is defined as $\mathbf{I/I_0}$, the relationship between absorbance (**A**) and transmittance (**T**) is defined by (28):

$$\mathbf{A} = - \log (\mathbf{T})$$

Using the ratio of a single-beam spectrum of the sample with its counterpart background spectrum successfully eliminates the bands attributable to atmospheric water and CO_2 only if the concentrations of these vapors remain stable when obtaining both the background and sample single-beam spectra (26, 27). However, if there is any difference in concentration of the vapors between the two measurements,

these bands appear in the resultant spectrum. To ensure that atmospheric water levels are low and stable, the sample compartment may be purged continuously with dry air (25). Any weak water absorptions that do appear in the spectrum may be minimized by using a spectral subtraction algorithm that iteratively subtracts the spectral features attributable to water vapour. Automated routines are available to minimize the intensity of residual absorptions following subtraction (27). The multisampler compartment (HTS-XT, Bruker Optics, Milton, ON) used for the present research is equipped with a desiccant cartridge without any accessible channel for purging the system. To minimize the influence of long-term drift in atmospheric water concentration, a new background measurement (predetermined at the first position of the top left corner of the silicon microplate) was performed immediately prior to each sample measurement. While this strategy minimized the influence of atmospheric factors as much as possible, a system to purge the multisampler compartment would likely be a more effective (time saving) way to eliminate atmospheric carbon dioxide vapor if installation were possible.

In the current research project, a baseline variation was observed on the IR spectra. This variation was observed in the IR spectra of empty sample wells of the silicon plates prior to the deposition of sample, and the IR spectra derived from the deposition of a sample onto the sample wells (see Appendix 1). One of the possible explanations for baseline variation (especially those observed in the spectra measured from each well of the plate prior the deposition of sample) is that it may arise from imperfect positioning of the modulated exit beam on each well position (i.e the

perimeter of the modulated beam did not fit perfectly inside the perimeter of the wells situated on the silicon plate). In such cases, the portion of the beam that falls outside the sample well cannot reach the detector. Varying negative absorbance may occur when the intensity of the single-beam background (I_0) is less than the single-beam of a particular sample well on the silicon plate (I). In the current research project, this limitation was acknowledged. Several attempts to adjust the position of the microplate on the carriage inside the multisampler compartment were made. The measurements of silicon plate without deposition of sample suggested that samples wells situated on the periphery of the plate were more likely to produce spectra with higher degree of baseline variation. Therefore, these particular wells were not used (columns 1, 11 and 12; rows A and H). The baseline variation was minimized to a level of -0.05 to 0.05 absorbance units by the adjustment of plate position and by not using the wells on the periphery as previously described. The last strategy to deal with the minimal baseline variation of the spectra is to use derivatives of the spectroscopic data. The method will be described in the following section of this chapter.

Other possible sources of measurement variation were observed in the current research. The spectra derived from the deposition of a single sample onto 3 different silicon plates demonstrated varying degree of within-plate variation and between-plate variation. These variations were observed only at some particular wavenumbers (see Appendices 2-6). The possible reasons for these phenomena are not yet fully understood. However, they appear to be related to well position on the plate. To guard

against possible sources of bias due to plate and to account for such effects, a randomized block design was used to assign samples to plate and well position prior to deposition of samples.

Acquisition parameters that must be specified in collecting FT-IR spectra include the number of scans, spectral resolution and apodization functions (4, 18, 22, 29). Where spectra of high signal-to-noise ratio are desired, signal averaging is conducted by repetitively scanning and co-adding individual interferograms (5, 11). The signal-to-noise ratio (S/N) is proportional to the square root of the number of scans, for example co-adding 512 scans is to achieve a theoretical enhancement of 22.63:1 S/N ratio (5, 11). Resolution is a measure of the instrument's ability to separate two overlapping peaks. A nominal spectral resolution of 4 cm^{-1} means that peaks whose maxima are separated by 4 wavenumbers would be resolved in the measured spectrum (25). The nominal resolution is dictated by the displacement distance of the moving mirror (11, 25). In addition to dictating the resolution, another consequence of the finite mirror travel is the presence of artificial side lobes (or pods) on the FT-IR spectra whose natural bandwidth is narrow (11). To address this concern, an "apodization function" is usually chosen to multiply an interferogram before Fourier transformation in order to minimize the artificial negative and positive side lobes of the spectral line (11). In particular, the Blackman-Harris 3-term apodization function is recommended for routine liquid and solid phase spectroscopic measurements, and has been used previously in many biomedical MIR spectroscopy studies (4, 18, 25, 29, 30).

For the current study, the MIR spectral acquisition and enhancement of spectroscopic data was carried out using the following protocol: the MIR spectra in the range of 400 - 4000 cm^{-1} were recorded using a multisampler compartment (HTS-XT, Bruker Optics, Milton, ON) interfaced with a FT-IR spectrometer (Tensor 37, Bruker Optics, Milton, ON) equipped with a deuterium tryglycine sulphate (DGTS) detector. For each spectrum, 512 interferograms were coadded at a spectral resolution of 4 cm^{-1}, and a Blackman-Harris 3-term apodization function applied to the coadded interferogram prior to Fourier transformation.

2.4 Spectral pre-processing

Spectral "pre-processing" encompasses a variety of mathematical manipulations with 3 main purposes (8):

1) to factor out irrelevant data and hence reduce the data dimensionality
2) to preserve and/or enhance meaningful diagnostic information within the spectroscopic data.
3) to transform the spectroscopic data into suitable format for further analysis (i.e. chemometric spectral classification)

Chemometric test development typically proceeds in two stages (8). In the first stage, the spectra may be subjected to differentiation and normalization (8-10), with the aim of minimizing the non-diagnostic sources of spectral variation. These include, for example, variations in spectral baseline and slope, which are remedied by second order differentiation, and variations in absolute intensity, which may be

remedied by normalization. This spectral preprocessing is then typically followed by feature extraction – a procedure that combines and transforms the spectroscopic data (as variables) into a set of new derived variables or factors to reduce the dimension of the spectroscopic data (8). Principal component analysis is one technique that is commonly used for this purpose (31, 32).

Four preprocessing techniques were frequently employed for the spectroscopic studies reported here, including spectral averaging, subtraction, normalization, and differentiation/smoothing. These techniques are reviewed below.

2.4.1 Spectral averaging

A set of spectra as defined by a user can be averaged. The idea of spectral averaging is to calculate the arithmetic mean intensity (**y**) for each data point ($\mathbf{y_i}$) of **N** input spectra (33).

$$\mathbf{y} = \sum \mathbf{y_i} / \mathbf{N}$$

The average spectrum is therefore a plot of the mean intensity of each data point versus wavenumber. The technique was exploited here most often to obtain the average of triplicate dried film spectra. The resulting representative spectrum calculated from this procedure was used for subsequent analysis.

2.4.2 Spectral subtraction

This technique is widely used in spectral analysis, and simply entails the arithmetic subtraction of the intensity for corresponding data points for pairs of spectra (28). Spectral manipulation software further allows for iterative spectral subtraction, with the subtrahend multiplied by a user-controlled continuously variable

factor. The digital subtraction technique is useful, for example, to recover solute spectroscopic information from solution spectra by subtracting the solvent spectrum from the sample spectrum (28).

Water is the main constituent in biological fluid such as SF (7, 34). For IR spectroscopic measurements in the native fluid state, the strong water absorptions overwhelm spectroscopic features of other chemical constituents (7, 34). Theoretically, digital subtraction may remove the contribution from water from the biological fluid spectrum. However the operation needs to be performed with caution. Digital subtraction of a pure water spectrum from its biological fluid counterpart by using software may induce artifacts in the resultant spectrum (20). Comparison of water absorptions in the spectrum of a biological fluid to their counterparts in the spectrum of pure water reveals subtle differences (20). One possible explanation is that the structure of water is altered by the presence of solutes, e.g. macromolecules (20). To avoid this complication, and to circumvent the practical difficulties associated with MIR spectroscopy of aqueous specimens, the dried film technique was adopted for the current project (7, 20, 34).

2.4.3 Spectral normalization

Spectral normalization is one of the most common spectral preprocessing techniques (16, 17, 23, 29, 30, 32, 34, 35, 36). The idea is to scale each spectrum in a dataset to some common constant value (36). This method is aimed to minimize variations in the overall spectral intensity, so that spectroscopic variations believed to be important for the spectral calibration or classification become more prominent

(32). There are several methods for normalization. One is to add an internal standard to all samples. For example, KSCN gives rise to a peak at approximately 2060 cm^{-1}. Normalization of the spectra to a common intensity of this KSCN peak is one common normalization method (16, 17, 23, 34). By adding the same amount of aqueous KSCN solution to each sample in a dataset, the spectra may be normalized or scaled to yield a common effective pathlength or thickness of the dried film (34).

Vector normalization is a convenient procedure for the normalization of derivative spectra in particular (29, 30, 32, 35, 36). The first step is to choose a spectral region as a basis for vector normalization, the "normalization region". Then the calculation is carried out in the following way; firstly, for each 2^{nd} derivative spectrum the sum of square absorption intensities is calculated for all data points within the normalization region. The square root of this sum is then evaluated for each spectrum, and adopted as the normalization factor for that same spectrum. When each spectrum is scaled in this way (the entire spectrum is divided by this normalization factor), the sum of square intensities within the normalization region is equal to 1. Put another way, the N-dimensional vector of spectral intensities within the normalization range has the same length (of 1) for all spectra.

The choice of normalization range is user-defined. In one study, the normalization region was chosen as the region wherein the difference between the normal and abnormal samples was believed to be most pronounced (32). In the work reported here, vector normalization was performed on the 2^{nd} derivative spectra (see

the next section), using a MATLAB script (MATLAB, MathWorks, Natick, MA, USA) developed by collaborators at the IBD, NRC, Winnipeg, MB, Canada.

2.4.4 Spectral differentiation

Spectral differentiation is commonly used to eliminate random variations in baseline offset and slope (8, 25, 28) that may otherwise obscure variations of diagnostic relevance (29, 30, 35-37) (Figure 2.9). This technique mathematically transforms an absorbance spectrum to the first, second, or higher-order derivative of that spectrum (Figure 2.9) (8, 25, 28). In addition to removing baseline and slope variations, derivation also has the benefit of narrowing the spectral band shape and hence resolving features that might otherwise be inaccessible. The spectral appearance can be altered dramatically as compared to the original absorbance spectrum. For example, peak maxima in absorption spectra correspond to the zero-crossings (y axis) in the first derivative counterparts, and are inverted to give negative peaks in second derivative spectra (8, 25, 28) (Figure 2.10).

This technique offers several advantages to the analysis of raw spectroscopic data. The effective resolution enhancement can reveal weak absorptions that might otherwise go unnoticed (8, 25, 28). However, care should be taken when applying this technique to noisy spectra - the noise component can be greatly amplified by this technique (8, 25). For this reason, spectral smoothing is almost always carried out hand-in-hand with derivation. The Savitzky-Golay algorithm is considered the most useful one for IR spectroscopic data (8, 10). This algorithm enables the differentiation

a

b

c

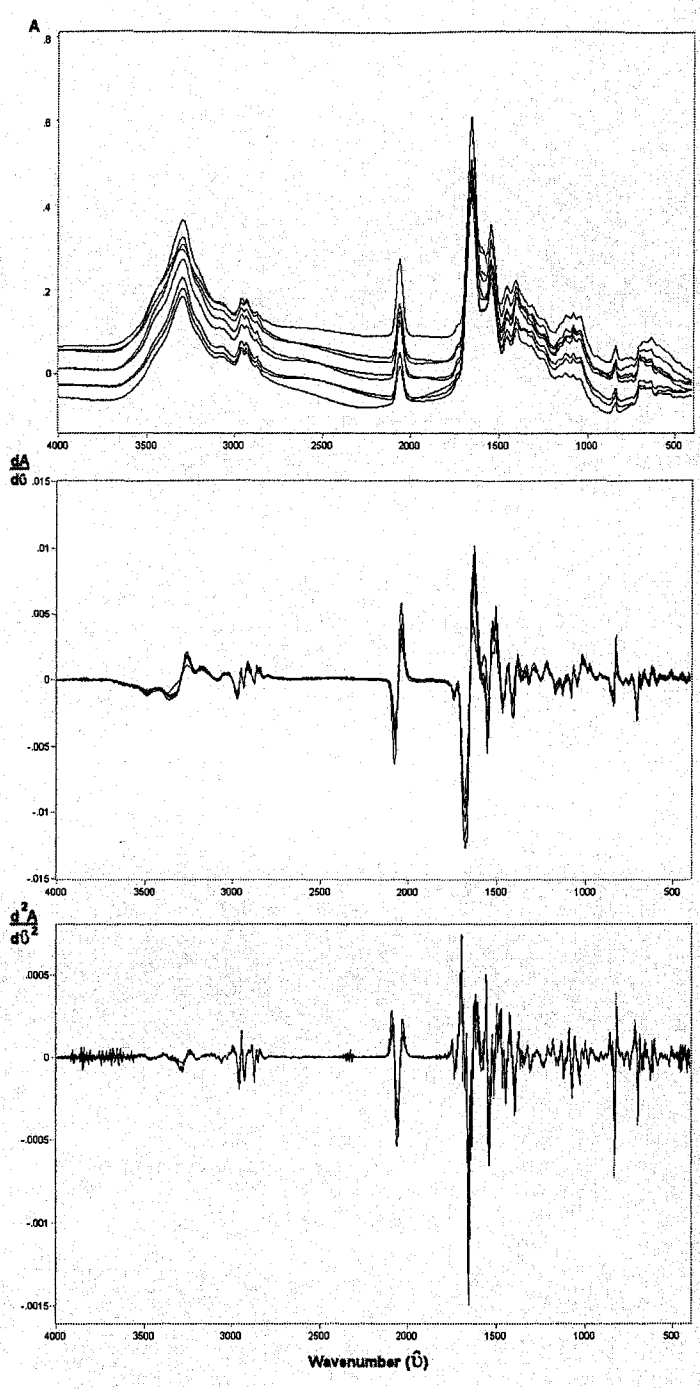

Figure 2.9. A set of 8 spectra with baseline variation shown before being subjected to spectral differentiation (a) and their corresponding first (b) and second (c) derivative spectra (A = absorbance)

a

b

c

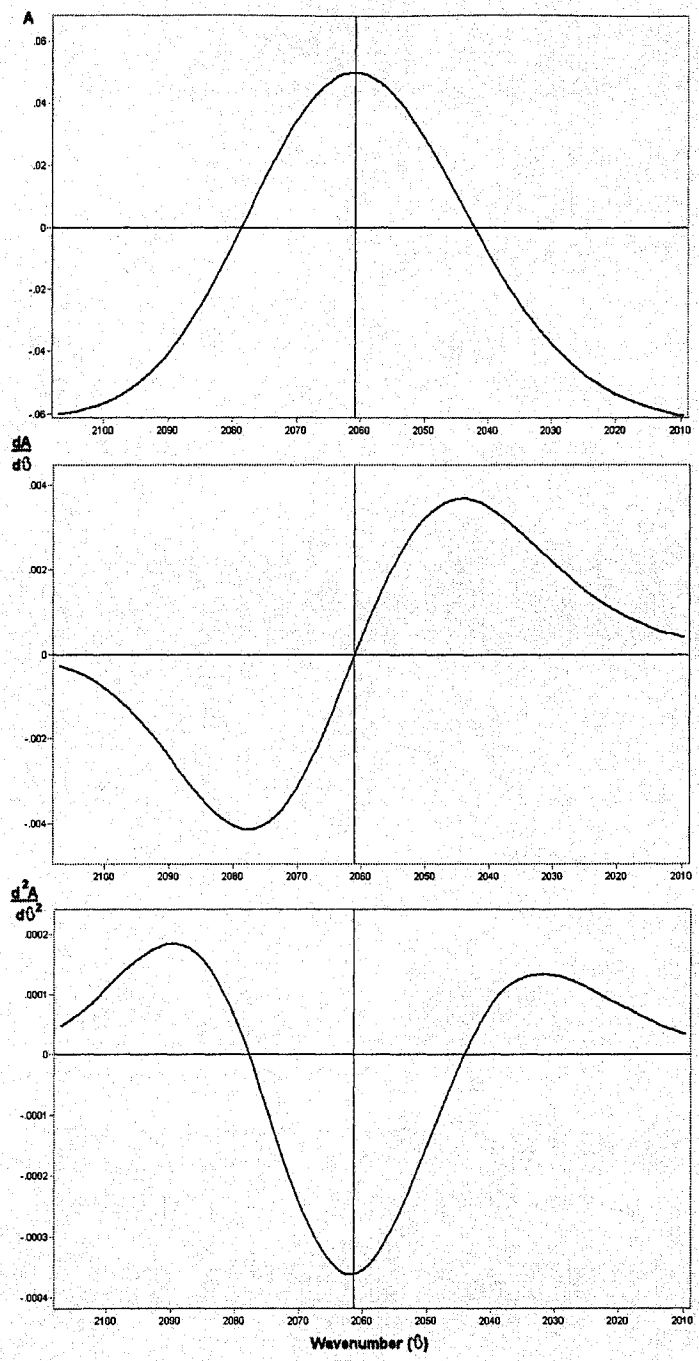

Figure 2.10. A normal spectrum (a) and its corresponding first (b), and second (c) derivative spectrum using a KSCN band as an example

of the spectra while simultaneously smoothing the data using suitable polynomial smoothing functions (a suitable array of weighting coefficients suggested by Savitzky and Golay is used as a smoothing function) (8, 10). All smoothing algorithms (including the Savitzky-Golay method) have the effect of minimizing the noise, while at the same time decreasing the effective spectral resolution (8, 10) and at the cost of spectral line distortion (8). Experience with the process teaches the practitioner the optimum trade-off between signal-to-noise and spectral resolution.

2.5 The effect of smoothing technique on spectral classification

A pilot study was conducted in the current research project in order to gain an understanding about derivation, smoothing technique and spectral classification, using MIR spectra of SF samples from joints with osteochondral fracture and those of controls. The objective of the pilot study was to investigate the effect of varying the degree of spectral smoothing on the accuracy of spectral classification by using a dataset (the traumatic arthritis dataset that was partially used in Chapter 4). The spectral differentiation and smoothing procedures (Savitzky-Golay smoothing algorithm) were simultaneously performed by the use of proprietary software (GRAMS/AI 7.02, Thermo Galactic, Salem, NH, USA).

The 2nd order differentiation was chosen for investigation in this study due to its advantages for removing baseline and slope variations, and resolving features of the overlapping bands that may be inaccessible in absorption spectra (7-8). The peak maxima in absorption spectra were inverted to give negative peaks in second

derivative spectra, therefore the positions of peak maxima are still preserved after transformation (8). Then, varying and increasing degrees of spectral smoothing were investigated. The classification of IR spectra from affected joints and those of controls was performed using a genetic algorithm for optimal region selection developed by the Institute for Biodiagnostics, National Research Council of Canada in collaboration with Dr. Anthony Shaw. Comparisons of classification results including sensitivity, specificity, and accuracy were performed among different degrees of smoothing.

The genetic algorithm used for spectral classification is programmed to seek a set of spectral subregions that can provide a basis of spectral classification, using discriminant analysis as the basis for that classification (39-40). Generally, this set of spectral regions is sought by making use of a subset of spectra, referred to as the calibration set. Once the optimal regions have been chosen, the discriminant analysis classifier is considered to be optimized. For each spectrum, the input variables for spectral classification are the set of average intensities calculated from the set of spectral subregions (an average intensity of each spectral subregion was calculated) selected by the genetic algorithm and its actual class designation (whether it is in affected or control groups) (39-40). Classification results are reported as numbers of spectra in the calibration set that are correctly classified or misclassified in each class (41-43). These numbers allow the calculations of sensitivity, specificity, and accuracy for the calibration set of spectra. The robustness and general applicability of the classification are then tested by an independent set of spectra, the so-called validation

set (40). The sensitivity, specificity, and accuracy are then calculated and compared to those from calibration set. The spectroscopic data preprocessing and classification strategy for this pilot study are schematically illustrated in Appendix 7.

A set of SF sample (n=94) from 49 horses age between 2-5 years were included in this pilot study on spectral preprocessing. The samples were collected from fetlock, antebrachiocarpal and midcarpal joints. Fifty-three samples are from joints with osteochondral fragmentation and 41 samples are from control joints. Numbers of samples according to anatomical locations of joints in affected and control groups were presented in Appendix 8. Sample preparation and spectral acquisition were as described previously (see section 2.2 and 2.3). Spectral differentiation and smoothing were applied to the set of spectra using the Savitzky-Golay algorithm (GRAMS/AI 7.02, Thermo Galactic, Salem, NH, USA). A total of 94 spectra were transformed into second derivative spectra. Three different levels of smoothing including 15 points, 25 points and 45 points were applied to the set of spectra.

In order to validate and estimate the accuracy of classification for each degree of smoothing, the random re-sampling with replacement technique was exploited to separate spectra (53 affected and 41 control spectra) into calibration and validation sets. The calibration set consisted of 35 spectra randomly selected from 53 affected spectra and 27 of those 41 control spectra (two-thirds of affected and control groups) by using computer generated random numbers (Minitab 13, Minitab Inc., College, PA, USA). The remaining spectra of those affected and control samples constituted a

validation set. Twenty iterations of re-sampling with replacement were conducted to achieve 20 sets of calibration and their corresponding validation sets. At the end of this re-sampling, there were 20 calibration sets and their corresponding validation sets for each smoothing method.

The spectroscopic data within the range of 400-1800 cm^{-1} were used in spectral analysis. In our experience, inclusion of spectroscopic information within the range of 400-1800 cm^{-1} into statistical analysis is likely to yield a better classification result than using either the entire MIR range (400-4000 cm^{-1}) or the information from 2750-4000 cm^{-1} (see Figure 2.7) in statistical analysis. In addition, restricting the IR range to 400-1800 cm^{-1} may help to reduce the high dimensionality of our data matrix, which is especially important when constrained by a limited sample size of SF samples.

Following the preprocessing and the conversion into a suitable data format (see Appendix 7), the classification of the spectra with respect to their class designation was performed using the genetic algorithm as previously described. Three optimal regions were successfully selected (see Appendices 9.1- 9.3 for optimal regions selected by genetic algorithm). Classification models based on those regions were optimized from each calibration set and tested using the spectra in the validation sets. Finally, the 95% confidence interval of the mean sensitivity, specificity and accuracy of the calibration and validation sets were calculated (see Appendices 10.1-10.3 for sensitivity, specificity, and accuracy of all calibration-validation sets). The plot of 95% confidence intervals of the mean sensitivity, specificity and accuracy of

the calibration and validation sets when subjected to 3 different levels of smoothing were placed side by side in Appendices 11.1-11.3.

There were no significant differences ($\alpha = 0.05$) among the 3 levels of smoothing based on the classification results (sensitivity, specificity and accuracy). This suggested that the smoothing procedure may not have a profound influence on classification result of this dataset. However, insignificant increases in the mean value of sensitivity, specificity and accuracy were observed in validation sets suggesting that smoothing might provide some benefits to the classification of the spectra (Appendices 11.1-11.3).

One limitation that needs to be addressed in this data analysis is the dependence of the spectra. A firm conclusion regarding to the classification results cannot be achieved because of a violation of at least one of the assumptions of independence for discriminant analysis. This multivariate statistical analysis requires an independence of the spectra being classified (i.e. each horse provides a single SF sample for spectral analysis). To meet such assumptions, a larger number of horses to provide a single sample from either affected or control joints are required. The optimal solutions for the spectral classification of this dataset were later developed and described in Chapter 4.

2.6 An overview of spectral preprocessing and classification strategy

The purpose of this section is to provide an overview and describe decision making criteria pertaining to the preprocessing techniques and classification strategy

of SF spectra of horses with osteochondrosis as an example. The optimal and final solution for spectral preprocessing and classification will be further described in Chapter 5. The process of spectral classification used in this current research began with selection of appropriate preprocessing techniques, selection of significant infrared subregions, and development and validation of a preliminary classification model based on significant subregions. These 3 key elements are crucial for the success of the classifications of equine SF spectra in this current research project (see Chapter 4 and Chapter 5). In the osteochondrosis study (see Chapter 5), the spectral classification was performed on a set of spectra consisting of 64 spectra from tarsocrural joints of 64 horses (each horse provided a single joint fluid sample). There were 33 samples from joints with osteochondrosis and 31 samples from controls. The sample preparation and spectral acquisition methods were as described previously (see section 2.2 and 2.3).

2.6.1 Selection of preprocessing technique

The spectral preprocessing and classification strategy described in this section are schematically illustrated in Appendix 12.1 and the summary of classification results is presented in Appendices 12.2 - 12.3. The spectral differentiation and smoothing procedures (Savitzky-Golay smoothing algorithm) were simultaneously performed by the use of proprietary software (GRAMS/AI 7.02, Thermo Galactic, Salem, NH, USA). Sixty-four spectra were transformed into both first and second derivative spectra. Varying degrees of spectral smoothing were applied to both first and second derivative spectra with 5, 9, 15, 19, 21, 25, 30 points. The genetic

algorithm approach was used as a method for rapid classification and optimization of differentiation and smoothing preprocessing technique for this dataset. The classification results (accuracy) of the first and second derivative with varying degree of spectral smoothing based on 6 optimal regions are graphically illustrated in Appendix 13. Six optimal regions were chosen by the genetic optimal region selection algorithm. It is recommended that the ratio of the number of spectra per class to number of optimal regions selected should be 5:1 to 10:1 (40). The 2^{nd} order derivation with 19 point smoothing was finally selected as an optimal differentiation and smoothing method based on the highest accuracy yielded.

The appropriateness of vector normalization technique (see section 2.4.3) for this dataset was also explored. For this purpose, the dataset containing 64 non-normalized 2^{nd} derivative spectra with 19 point smoothing was subjected to vector normalization. The IR regions providing the basis for normalization included 1950-2150 cm^{-1}, 1500-1700 cm^{-1}, 800-1450 cm^{-1}. These regions correspond to characteristic bands of KSCN (1950-2150 cm^{-1}), protein, lipid and carbohydrate absorptions. The region of particular interest was 800-1450 cm^{-1}. This region encompasses characteristic bands at 1000, 1035, 1115 and 1245 cm^{-1} which were reported to be associated with the presence of osteochondrosis in a previous study (44). The dataset of 64 second-derivative spectra was subjected to three different vector normalization methods as described. The non-normalized and normalized data were used in the next step.

2.6.2 Selection of significant infrared subregion

In the osteochondrosis dataset, differences of mean age in either the osteochondrosis or the control groups may introduce bias into data analysis. The horses in the osteochondrosis group were likely to be younger than the control group (see detail in Chapter 5). Analyses of covariance (ANCOVA) were employed to detect sets of wavenumbers that demonstrated a significant effect of group ($p<0.01$) after accounting for the age variable. The statistical analyses were performed on each wavenumber basis within the entire range of MIR (400-4000 cm^{-1}). Significant subregions were defined as a set of at least 4 consecutive wavenumbers that demonstrated a significant effect of group at a level of $p < 0.01$.

A significance level of $\alpha = 0.01$ was set to guard against type I error arising from multiple statistical analyses performed on entire wavenumber range of MIR spectrum. The criterion of using at least 4 consecutive wavenumbers was exclusively established in the current research based on the minimal width of the optimal range reported (1). In general, the width of the optimal region usually spans from 4 to 50 cm^{-1} and 5 to 15 optimal regions were selected to include in a classification model (1).

Before applying ANCOVA on each wavenumber, a test for parallelism was performed to ensure that the data is suitable for applying ANCOVA (45). This assumption has to be met in order to avoid misinterpretation of the results. Analysis of non-normalized data revealed an inappropriateness of applying ANCOVA with this particular dataset because substantial IR subregions failed the test for parallelism. This problem was solved with the normalization method. The dataset after

preprocessing with any of 3 normalization methods was suitable for applying ANCOVA as indicated by the test for parallelism.

There were 6, 5 and 12 significant subregions detected when data were normalized on based on wavenumber range of 1950-2150 cm^{-1}, 1500-1700 cm^{-1}, 800-1450 cm^{-1} respectively (see Appendix 12.3). The highest number of significant subregions (when using 800-1450 cm^{-1}as a basis of normalization) may reflect the ability of this particular normalization method to minimize variations in the overall spectral intensity and factor out irrelevant information, giving greater prominence to the spectroscopic variations believed to be important for successful spectral classification (32, 36). The 2^{nd} order differentiation with 19 point smoothing and vector normalization using the IR range of 800-1450 cm^{-1} as a basis of normalization were chosen as optimal methods to preprocess the spectra of SF from horses with osteochondrosis and those of controls (Chapter 5). The preprocessed spectra were used for development of classification model and model validation as the final step.

2.6.3 Classification model development and validation

Discriminant analysis is the most common supervised pattern recognition method used to classify the spectra in biomedical research (12, 14, 18, 24, 29, 31, 37, 40, 41, 43). The essence of this classification technique can be graphically illustrated by a multidimensional plot in some cases (Figure 4.3 in Chapter 4), but in other cases where there are > 3 variables an alternate representation is required (46). Each coordinate point represents each spectrum in **N** dimensional space where **N** is the number of significant regions (38, 41, 47, 48). The value on each axis corresponds to

the average intensity of each significant region. Discriminant analysis identifies the boundaries that best separate the points in multidimensional space with respect to their group membership (38, 41, 47, 48). For example, in bivariate linear discriminant analysis, these boundaries may be a straight line defined by a linear equation. The discrimination or class assignment base on discriminant analysis can be appreciated by consideration of probability and Bayes' theorem; a sample or object should be assigned to that class that having the highest conditional probability (38, 48). The class assignment based on indirect estimation of conditional probability can be achieved through calibration of discriminant function and rules (38). A comprehensive description of the principles underlying the theory of discriminant analysis is beyond the scope of this thesis, readers are referred to McLachlan (49) for details. The discriminant analysis procedures were performed in the current research project by the use of proprietary statistical software (SAS 8.02, SAS institute Inc.,Cary, USA) with the aim of deriving the preliminary classification models. The classification results can be presented in a form of a contingency table that shows the number of samples (or spectra) based on their actual class against their predicted class (8) (see table 5.2 in Chapter 5). Stepwise discriminant analysis was applied prior to calibration of classification models. This procedure is performed to select a set of subregions (from those significant subregions selected from the previous step) that most contribute to the power of discrimination (50). The significant region selection procedure based on ANCOVA and stepwise discriminant procedure are the strategies

for reducing the dimensionality of data matrix particularly when the number of variables exceeds sample size as seen in the current research project (50).

The model validation technique used in the osteochondrosis study was the leave-one-out cross-validation technique (see section 1.8.2 in Chapter 1). The classification results (sensitivity, specificity, and accuracy) of the 3 methods of normalization applied with this dataset are summarized in Appendix 12.3. The 2^{nd} order differentiation with 19 point smoothing and vector normalization by using IR range of 800-1450 cm^{-1} as a basis of normalization yielded the highest accuracy among the 3 methods. The performance of class prediction by a classification model using all 64 preprocessed spectra in the dataset was not as high as we expected (overall accuracy of 77%) when compared to the traumatic arthritis dataset for which overall accuracy of 97% was achieved from 29 spectra in the calibration set. The diagnostic features distinguishing diseased spectra from control spectra may be less prominent in the osteochondrosis dataset when compared to the traumatic arthritis dataset. The performance of the classification model may be improved and refined by inclusion of more samples in the future. However, the leave-one-out cross validation seems to be a reasonable means to estimate an overall performance of classification of osteochondrosis sample at this preliminary stage.

2.7 Conclusion

The main emphases of this chapter, practical laboratory technique, optimal spectral acquisition, effective spectral pre-processing techniques, and data

classification techniques comprise the foundation for the development of IR-based diagnosis of equine joint diseases. The optimal dilution and sample deposition volume were established as a strategy to achieve a suitable optical pathlength of SF dried films. Randomized experimental design was applied on each plate of each experiment to guard against possible bias sources due to the variability of the plate and well positions (column and row) on the prototype of silicon plate used in the study. Spectral acquisition protocol and parameters were optimized to obtain the resultant spectra with high resolution and signal-to-noise ratio. Synovial fluid spectra acquired within the optimal laboratory technique and spectral acquisition protocols are comparable to those reported in a human study (24). The same laboratory techniques and spectral acquisition protocol were maintained consistently for all studies summarized in the following chapters. The spectral pre-processing procedures as described in this chapter were utilized to enhance spectroscopic features that faithfully related to the pathological changes and to transform spectroscopic data into a form that is suitable for statistical analysis. Generally, the choice of technique was based on the nature of the spectroscopic data and the studies being undertaken, with subtle but important variations to suit each set of circumstances (8). The preprocessing techniques were carefully optimized for each data set to achieve the best possible classification result.

References

(1) Dubois J, Shaw RA. IR spectroscopy in clinical and diagnostic applications. Anal Chem 2004;76:361A-367A.

(2) Schultz CP. The potential role of Fourier transform infrared spectroscopy and imaging in cancer diagnosis incorporating complex mathematical methods. Technol Cancer Res Treat 2002;1:95-104.

(3) Diem M, Chiriboga L, Lasch P, Pacifico A. IR spectra and IR spectral maps of individual normal and cancerous cells. Biopolymers 2002;67:349-353.

(4) Naumann D. FT-IR and FT-NIR Raman spectroscopy in biomedical research. In *Proceedings*. 11th international AIP Conference 1998;430:96-109.

(5) Adams MJ. Acquisition and enhancement of data. In: Chemometrics in analytical spectroscopy. Cambridge: Royal Society of Chemistry, 2004;29-54.

(6) Jackson M., Mantsch HH. Infrared Spectroscopy, Ex vivo tissue analysis by. In: Meyers R.A., eds. Encyclopedia of analytical chemistry. Chichester: John Wiley and Sons Ltd, 2000;31-156.

(7) Shaw RA, Mantsch HH. Infrared spectroscopy in clinical and diagnostic analysis. In: Meyers RA, eds. Encyclopedia of analytical chemistry. Chichester: John Wiley & Sons Ltd, 2000;83-102.

(8) Adams MJ. Feature selection and extraction. In: Chemometrics in analytical spectroscopy. Cambridge: Royal Society of Chemistry, 2004;55-95.

(9) Fetterman MR. Fourier-transform infrared derivative spectroscopy with an improved signal-to-noise ratio. Opt Lett 2005;30:2311-2313.

(10) Savitzky A, Golay MJE. Smoothing and differentiation of data by simplified least squares procedures. Anal Chem 1964;36:1627-1639.

(11) Stuart B. Experimental Methods. In: Infrared spectroscopy: Fundamentals and applications. Chichester: John Wiley & Sons Ltd., 2004;15-44.

(12) Eysel HH, Jackson M, Nikulin A, Somorjai RL, Thomson GTD, Mantsch HH. A novel diagnostic test for arthritis: multivariate analysis of infrared spectra of synovial fluid. Biospectroscopy 1997;3:161-167.

(13) Heuer C, Luinge HJ, Lutz ET, Schukken YH, van der Maas JH, Wilmink H et al. Determination of acetone in cow milk by Fourier transform infrared spectroscopy for the detection of subclinical ketosis. J Dairy Sci 2001;84:575-582.

(14) Jackson M, Mansfield JR, Dolenko B, Somorjai RL, Mantsch HH, Watson PH. Classification of breast tumors by grade and steroid receptor status using pattern recognition analysis of infrared spectra. Cancer Detect Prev 1999;23:245-253.

(15) Liu KZ, Shaw RA, Man A, Dembinski TC, Mantsch HH. Reagent-free, simultaneous determination of serum cholesterol in HDL and LDL by infrared spectroscopy. Clin Chem 2002;48:499-506.

(16) Shaw RA, Kotowich S, Leroux M, Mantsch HH. Multianalyte serum analysis using mid-infrared spectroscopy. Ann Clin Biochem 1998;35:624-632.

(17) Shaw RA, Low-Ying S, Leroux M, Mantsch HH. Toward reagent-free clinical analysis: Quantitation of urine urea, creatinine, and total protein from the mid-infrared spectra of dried urine films. Clin Chem 2000;46:1493-1495.

(18) Martin TC, Moecks J, Belooussov A, Cawthraw S, Dolenko B, Eiden M et al. Classification of signatures of Bovine Spongiform Encephalopathy in serum using infrared spectroscopy. Analyst 2004;129:897-901.

(19) Shaw RA, Low-Ying S, Man A, Liu KZ. Reagent-free clinical analysis and diagnostics: laboratory medicine in a new light. IVD Technology 2003;9:43-49.

(20) Jackson M, Mantsch H. Pathology by infrared and Raman spectroscopy. In: Chalmers JM, Griffiths PR, eds. Handbook of vibrational spectroscopy. Chichester: John Wiley & Sons, 2002;3227-3245.

(21) Ziegler CM, Kircher P, Hassfeld S. Analysis of temporomandibular joint synovial fluid using Fourier transform/infrared spectroscopy. J Oral Maxillofac Surg 2002;60:1302-1306.

(22) Low-Ying S, Shaw RA, Leroux M, Mantsch HH. Quantitation of glucose and urea in whole blood by mid-infrared spectroscopy of dry films. Vib Spectrosc 2002;28:111-116.

(23) Shaw RA, Mantsch HH. Multianalyte serum assays from mid-IR spectra of dry films on glass slides. Appl Spectrosc 2000;54:885-889.

(24) Jackson M., Eysel HH, Shaw RA, Glen T.D., Mantsch H. Non-subjective Diagnosis of Arthritic disorders by multivaliate analysis of IR spectra of

synovial fluid. In: Merlin J.C., eds. Sixth European conference on the spectroscopy of biological molecules. Dordrecht: Kluwer Academic Publishers, 1995;499-500.

(25) Gunzler H, Gremlich HU. Spectrometers. In: IR spectroscopy an introduction. Weinheim: Wiley-VCH, 2002;37-94.

(26) Hollas JM. General features of experimental method. In: Modern spectroscopy. 2nd ed. Chichester: John Wiley & Sons, 1992;38-67.

(27) Hoult R. Atmospheric vapor compensation on the spectrum 100 FT-IR and 100N FT-NIR spectrometer. In: Technical note, infrared spectroscopy. Boston: Perkin Elmer, 2006;1-7.

(28) Stuart B. Spectral Analysis. In: Infrared spectroscopy: fundamentals and applications. Chichester: John Wiley & Sons Ltd., 2004;45-70.

(29) Lasch P, Schmitt J, Beekes M, Udelhoven T, Eiden M, Fabian H et al. Antemortem identification of bovine spongiform encephalopathy from serum using infrared spectroscopy. Anal Chem 2003;75:6673-6678.

(30) Schmitt J, Beekes M, Brauer A, Udelhoven T, Lasch P, Naumann D. Identification of scrapie infection from blood serum by Fourier transform infrared spectroscopy. Anal Chem 2002;74:3865-3868.

(31) Canvin JM, Bernatsky S, Hitchon CA, Jackson M, Sowa MG, Mansfield JR et al. Infrared spectroscopy: shedding light on synovitis in patients with rheumatoid arthritis. Rheumatology (Oxford) 2003;42:76-82.

(32) Cohenford MA, Godwin TA, Cahn F, Bhandare P, Caputo TA, Rigas B. Infrared spectroscopy of normal and abnormal cervical smears: evaluation by principal component analysis. Gynecol Oncol 1997;66:59-65.

(33) OPUS Reference manual version 4.2. Ettlingen: Bruker Optik GmbH, 2003:95-160.

(34) Shaw RA, Mantsch H. Vibrational spectroscopy applications in clinical chemistry. In: Chalmers JM, Griffiths PR, eds. Handbook of vibrational spectroscopy. 2002;3295-3307.

(35) Liu KZ, Shaw RA, Dembinski TC, Reid GJ, Ying SL, Mantsch HH. Comparison of infrared spectroscopic and fluorescence depolarization assays for fetal lung maturity. Am J Obstet Gynecol 2000;183:181-187.

(36) Lasch P, Haensch W, Naumann D, Diem M. Imaging of colorectal adenocarcinoma using FT-IR microspectroscopy and cluster analysis. Biochim Biophys Acta 2004;1688:176-186.

(37) McCrae KC, Mantsch HH, Thliveris JA, Scott JE, Shaw RA. Analysis of neoplastic changes in mouse lung using Fourier-transform infrared microspectroscopy. Vib Spectrosc 2002;28:189-197.

(38) Adams MJ. Pattern recognition II: Supervised Learning. In: Chemometrics in analytical spectroscopy. Cambridge: Royal Society of Chemistry, 2004;129-160.

(39) Nikulin AE, Bolenko B, Bezabeh T, Somorjai, RL. Near-optimal region selection for feature space reduction: novel preprocessing methods for classifying MR spectra. NMR Biomed 1998;11:209-216.

(40) Somorjai RL, Dolenko B, Nikulin A, Nickerson P, Rush D, Shaw A, et al. Distinguishing normal from rejection renal allografts: application of a three-stage classification strategy to MR and IR spectra of urine. Vib Spectros 2002;28:97-102.

(41) Shaw RA, Guijon FB, Paraskevas M, Low-Ying S, Mantsch, HH. Infrared spectroscopy of exfoliates cervical cell specimens, proceed with caution. Anal Quant Cytol Histol 1999;21:292-302.

(42) Steiner G, Shaw A, Choo-Smith L, Abuid MH, Schackert G, Sobottaka S, et al. Distinguishing and grading human gliomas by IR spectroscopy. Biopolymers 2003;72:464-471

(43) McIntosh LM, Summers R, Jackson M, Mantsch HH, Mansfield JR, Howlett M, et al. Toward non-invasive screening of skin lesions by near-infrared spectroscopy. J Invest Dermatol 2001;116:175-181.

(44) Muttini A, Petrizzi L, Tinti A, Bertoluzza A. Synovial fluid parameters in normal and osteochondritic hocks of horses with open physis. Boll Soc Ital Biol Sper 1994;70:337-344.

(45) Rutherford A. Assumptions underlying ANOVA, traditional ANCOVA, and GLMS. In: Introducing ANOVA and ANCOVA: a GLM approach. London: SAGE, 2001;105-121

(46) Somorjai RL, Dolenko B, Demko A, Mandelzweig M, Nikulin AE, Baumgartner R, Pizzi NJ. Mapping high-dimensional data onto a relative distance

plane-an exact method for visualizing and characterizing high-dimensional patterns. J Biomed Inform. 2004;37:366-79.

(47) Shaw RA, Mansfield JR, Rempel SP, Low-Ying S, Kupriyanov VV, Mantsch HH. Analysis of biomedical spectra and image: from data to diagnostic. J Mol Struct (Theochem) 2000;500:129-138.

(48) Naes T, Isaksson T, Fearn T, Davies T. Qualitative analysis/classification. In: A user-friendly guide to multivariate calibration and classification. Chichester: NIR publications, 2002;221-259

(49) McLachlan GF. General introduction. In: Discriminant analysis and statistical pattern recognition. Indianapolis: John Wiley & Sons Inc, 1992;1-26

(50) Khattree R, Naik DN. Discriminant analysis. In: Multivariate data reduction and discrimination with SAS software. Cary: SAS Institute Inc, 2000;211-345.

CHAPTER 3

AN ANALYSIS OF INTRA-HORSE BIOCHEMICAL VARIATIONS BETWEEN HIGH MOTION JOINTS BASED ON THE INFRARED SPECTRAL CHARACTERISTICS OF SYNOVIAL FLUID

3.1 Abstract

Infrared spectroscopy relies upon the absorption characteristics of chemical bonds of infrared active molecules when exposed to IR light. The absorption pattern is very specific to the molecular species within the samples. The infrared spectrum of a sample is often referred to as a molecular fingerprint that reflects the structure of chemical constituents with the intensity of absorptions being directly related to their concentrations. In the development of IR-based analysis of synovial fluid (SF) for diagnosis and assessment of joint diseases in horses, the proper selection of normal control joints and an appropriate method of comparison are crucial factors in study design and data analysis. Intrinsic sources of variation, other than those due to disease, may cause differences in composition of SF samples. These inturn, may lead to differences in IR absorption patterns. The objective of this study is to identify significant differences due to natural variation among different anatomic types of joints and left versus right limbs that may affect the pattern of mid-infrared (MIR) spectra derived from SF of clinically normal joints. Synovial fluid samples were collected from joints with no abnormalities detected in radiographic examination and/or necropsy. The left versus right comparison was conducted by use of 78

bilateral SF samples from antebrachiocarpal (AC), midcarpal (MC), and tarsocrural (TC) joints obtained from 13 horses. The between-joint comparisons were conducted by use of 66 ipsilateral SF samples from AC, MC, and TC joints of 22 horses. Mid-infrared spectra were acquired and mathematically manipulated. Analyses of variance for a complete block design using horse as a blocking factor were performed on each wavenumber. The wavenumbers that demonstrated significant effect ($p<0.01$) of side (left versus right) and significant differences ($p<0.01$) among joints were the primary outcomes of interest. Significant differences among AC, MC, and TC joints in SF composition were identified in MIR spectra. The MIR absorption patterns of SF samples derived from pairs of contralateral joints were similar supporting their use as within subject control in appropriately designed studies. The finding of a broad range of biomolecular differences among these joints indicates that interarticular variation within the horse needs to be considered in prospective study design, as well as studies of naturally occurring joint disease. Further normal samples should be evaluated to better characterize the range and significance of MIR spectral changes detected.

3.2 Introduction

The synovial fluid (SF) from normal joints is a unique dialysate of plasma with the addition of hyaluronate and other molecules secreted by synoviocytes (1-3). This specialized fluid plays important roles in articular cartilage nourishment, joint lubrication and disease (3). Analyses of SF using conventional and novel molecular (biomarker) approaches have been used to assist the clinical diagnosis of arthritic

conditions in veterinary and human medicine (4-8). Conventional SF analysis consists of evaluations of color, viscosity, volume, clot formation, total protein and cytologic examination (6, 8). Although useful in cases of septic arthritis, these parameters provide limited information about the degree of synovitis, and are of little value in identifying articular cartilage or subchondral bone damage in the osteoarthritic joint (9). In recent years the focus of osteoarthritis (OA) research has shifted from microscopic changes in cell number and total protein parameters, to the search for biomarkers (direct or indirect molecular indicators of abnormal skeletal turnover) for joint disease in humans and horses (4-8, 10, 11). Various biomarker assays have been developed to identify qualitative and quantitative changes in intra-articular catabolism and anabolism using biochemical analysis, radioimmunoassay or ELISA (4-8, 10, 11). Early results are promising but complex multiple assays may be required to characterize cases of joint disease, and further study is required to determine their usefulness for routine osteoarthritis assessment (11). Other tools including genetic array analysis are under development, but as yet are either too expensive for routine screening, or have limited availability (12).

Infrared (IR) spectroscopy is revolutionizing the assessment of biological molecules and the biochemical response to disease (13-18). This technology relies upon the absorption characteristics of biomolecules when exposed to IR light (14, 16, 17). The absorption pattern is very specific to the nature and distribution of molecular species within a sample, with the intensity of absorptions being directly related to both the concentration and composition of the various constituents (14, 16, 17).

Within an animal species and for a particular disease, the IR spectra of a biological sample may be referred to as a "molecular fingerprint" that is correlated to the presence or absence of that disease (14, 16, 17). The feasibility and usefulness of IR-based analyses of various types of biological fluids have been investigated in previous studies (13, 15, 16, 18). The advantages of this approach are that no specific reagents are required because all IR active species within the samples give rise to IR absorption bands without a need for chemical or immunological modification. Automated repetitive analyses can be performed with low cost (16). It is a potentially powerful technique because an enormous amount of biochemical information (qualitative and quantitative) is extracted from the sample constituents, with features contained within the IR spectrum characterizing the sum of all IR active components in a sample (14, 16).

Recently the application of IR spectroscopy to evaluate human arthritis has been pioneered resulting in a novel diagnostic methodology (13, 15). However there are no published studies comparing the IR profiles among normal joints, or identifying the effect of anatomic location on spectral variables used to characterize joint disease. In order to advance this technique of SF analysis, an understanding of the IR spectroscopic information gathered from 'normal' horse or joint populations is as important as that derived from diseased horses. It is clear from other published reports that significant mechanical and biochemical differences occur among different joints within the same organism (5, 6, 19-23). These intrinsic differences among joints may result in an altered response to disease among joints, even though the

inciting cause is similar (20). The proper selection of normal controls and appropriate methods of comparison are crucial in study design, data analysis, and the application of IR spectroscopy in the disease diagnosis and assessment of joints. Intrinsic sources of variance, other than those due to disease, may cause differences in composition of SF attributable to biological rather than pathological reasons (1-3).

The authors hypothesized that the anatomic location from which SF is sampled may affect the pattern of mid-infrared spectra derived from SF of clinically normal antebrachiocarpal (AC), midcarpal (MC) and tarsocrural (TC) joints. The objective of this study is to identify significant differences in the IR absorption spectra attributable to the natural biochemical variation among these three high motion joints.

3.3 Materials and methods

This study was approved by the Animal Care Committee in accordance with the University of Prince Edward Island policy and the principles outlined in the *Guide to the Care and Use of Experimental Animals* prepared by the Canadian Council on Animal Care.

3.3.1 Study design and sample population

The effect of anatomical location of 3 high motion joints (AC, MC, and TC) and side (left versus right) on mid-infrared (MIR) absorbance spectra of SF (wavenumber range 400-4000 cm^{-1}) was investigated. Synovial fluid samples were collected from multiple joints in each horse. Inclusion criteria for joint selection were

radiographically normal AC, MC and TC and/or AC, MC and TC with no gross pathological lesions of synovium and articular cartilage detected by necropsy. Samples of SF were collected from 22 horses (105 joints) that met the criteria for inclusion (a pool of ~ 30 horses was examined; exclusions were mostly due to abnormal radiographic findings despite a normal clinical appearance). Breeds represented included Standardbred (n=18), Quarter horse (n=1), and mixed breeds (n=3). There were 10 females and 12 males. Mean age for all study horses was 4.3±2.3 (mean±SD) years. Of these 22 horses, 13 provided bilateral and 9 provided unilateral ipsilateral SF samples from AC, MC, and TC joints. All SF samples collected were stored at -80 °C in plain cryovials for later IR spectroscopic batch analysis.

3.3.2 Fourier transform infrared (FT-IR) spectroscopy

Synovial fluid samples were thawed at 22 °C, centrifuged at 2700 g for 10 minutes, and the supernatants were used for IR spectroscopic analysis. Sample preparation was a modification of a previously described technique (24, 25). Briefly, for each sample, an aliquot was drawn and diluted in aqueous 4 g/L potassium thiocyanate (KSCN, Sigma-Aldrich Inc., St.Louis, MO) solution in the ratio 3 parts SF: 1 part KSCN solution. The KSCN absorption band at approximately 2060 cm^{-1} served as one basis for spectral normalization (24, 25).

Triplicate dry films were made for each sample by depositing 8 μL aliquots of the diluted SF, spread evenly in circular motion onto 5 mm diameter circular islands within a custom made, adhesive masked, 96 well-silicon microplate (18). The

adhesive mask attached on the surface of the microplate served to spatially define and systematically separate the 5 mm islands on the microplate so as to correctly align samples with the IR radiation beam and detector. Samples from each horse were randomly assigned to well positions on the microplate. The SF films were left to dry at room temperature for 12 h. Once thoroughly dried, the microplate was mounted within the multisampler (HTS-XT, Bruker optics, Milton, ON) interfaced with the Fourier transform infrared (FT-IR; Tensor 37, Bruker optics, Milton, ON) spectrometer to allow for the acquisition of IR spectra.

Infrared absorbance spectra in the MIR region of 400-4000 cm^{-1} were recorded using the FT-IR spectrometer equipped with a deuterium tryglycine sulphate detector. For each acquisition, 512 interferograms were signal averaged and Fourier transformed to generate a spectrum with a nominal resolution of 4 cm^{-1} (18, 24, 25).

3.3.3 Data preprocessing

Triplicate spectra of each sample were averaged. Preprocessing included differentiation and smoothing procedures (Savisky-Golay 2nd order derivatives using a 2nd degree polynomial function, with 7 point smoothing) which were performed on all spectra to resolve and enhance weak spectral features, and remove the variation in baselines, using spectral calibration software (GRAM/AI 7.02 Thermo Galactic, Salem, NH) (26).

The preprocessed spectra were then normalized by using a wavenumber range of 800-1450 cm^{-1} as a basis of vector normalization using scripts written in MATLAB (MATLAB 6.5, The Math Works Inc., Natick, MA). Vector normalization was

carried out for each 2nd derivative spectrum by first summing the squares of absorption intensities for all data points (1 data point corresponded to ~1 wavenumber) within the spectral basis range of 800-1450 cm^{-1} (27). The square root of this sum of squares calculated from each spectrum was used as the normalization factor for that same spectrum; the intensities of the entire range within each spectrum were divided by this vector normalization factor prior to statistical analysis.

3.3.4 Statistical analysis

Two statistical comparisons were performed in order to study the effect of anatomical location of 3 high motion joints (AC, MC, and TC) and side (left versus right).

3.3.4.1 Comparison of left and right MIR spectra

Seventy-eight preprocessed spectra of bilateral SF samples from AC, MC, and TC joints were used for this part of the analysis. The relative intensity at each wavenumber in the spectrum was the dependent variable. Analyses of variance for a randomized block model using horse as a blocking factor were performed (PROC MIXED, SAS 8.02, SAS institute Inc., Cary, NC) on each intensity-wavenumber basis for the entire MIR regions. The effect of side (left versus right side) was considered significant for any wavenumber within MIR region if the p value < 0.01.

3.3.4.2 Inter-joint comparison of the MIR spectra

Following comparisons of left and right joints within horse, preprocessed spectra from the remaining 9 horses (unilateral samples) and a randomly selected spectrum (left or right) from each of the 13 bilaterally sampled horses were compared

under the assumption of no significant differences between contralateral joints. These constituted a second set of 66 spectra from ipsilateral AC, MC, and TC joints. Analyses of variance were performed (PROC MIXED, SAS 8.02, SAS institute Inc.,Cary, NC) as described above to detect the significant effect of joint ($p < 0.01$). Pairwise comparisons were performed among the 3 joints of interest (e.g. AC-MC, AC-TC, MC-TC). The differences between joints for any wavenumber within MIR region were considered significant if the p value < 0.01.

3.4 Results

Analyses of variance were performed on 3731 wavenumbers on the set of preprocessed spectra ranging from wavenumbers 402.15 to 3999.28 cm^{-1}. The only significant effects of side (left versus right) that were demonstrated occurred at wavenumbers 2568.14 cm^{-1} ($p = 0.0079$) and 2699.29 cm^{-1} ($p = 0.0052$).

Significant differences (193 wavenumbers) based on pairwise comparisons of AC and MC IR spectra were observed, and were most concentrated in the 1000-1100 cm^{-1}, 1550-1600 cm^{-1}, and 3500-3650 cm^{-1} regions; differences within the 2000-2500 cm^{-1} region were few. For AC-TC comparisons, significant differences (364 wavenumbers) were most concentrated in the 560-650 cm^{-1}, 790-840 cm^{-1}, 890-900 cm^{-1}, 940-1240 cm^{-1}, 1400-1440 cm^{-1}, 1650-1700 cm^{-1}, 2260-2270 cm^{-1}, 3000-3020 cm^{-1}, and 3620-3830 cm^{-1} regions. The significant IC-TC differences were more broad ranging (995 wavenumbers), and were concentrated in the 600-740 cm^{-1}, 810-900 cm^{-1}, 950-1050 cm^{-1}, 1070-1090 cm^{-1}, 1120-1140 cm^{-1}, 1160-1800 cm^{-1}, 2030-

2200 cm^{-1}, and 2830-3400 cm^{-1} bands. The AC and MC joints shared in common 158 significant wavenumber differences with the TC joint. The difference spectra and wavenumbers demonstrating the significant differences ($p < 0.01$) between pairwise spectra (AC compared to MC joints and AC compared to TC joints) are illustrated in Figures 3.1 - 3.8. These illustrations show group frequencies in the fingerprint (600-1500 cm^{-1}), double-bond (1500-2000 cm^{-1}), triple-bond (2000-2500 cm^{-1}) and X-H stretching regions (2500-4000 cm^{-1}, X = oxygen, carbon, or nitrogen atoms) (27, 28).

3.5 Discussion

Comparisons of IR absorption patterns of SF of different high motion joints of the horse demonstrated significant spectral differences among the joints of interest. Given the scarcity of significant IR spectral differences with the MIR bandwidth detected between left and right clinically normal AC, MC and TC joints, the biomolecular composition of the SF as characterized by the IR spectroscopy may be considered to be equivalent in non-diseased joints. A previous study found good agreement in oncotic pressure between contralateral joints, suggesting similar concentrations of molecular solutes (29). Contralateral joints have been widely used as controls in a variety of joint related studies, and these results support this approach in studies where effects are localized to the joint of interest (30, 31). However some

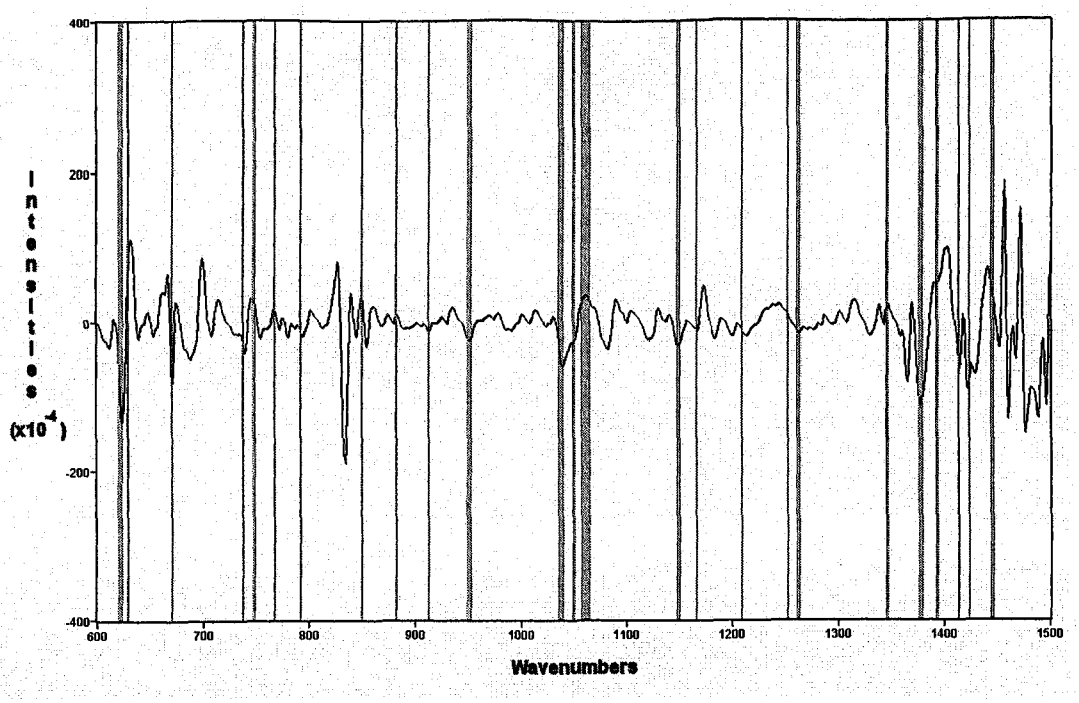

Figure 3.1 Difference spectrum (2nd derivative) of antebrachiocarpal-midcapal spectra in the fingerprint region. The shaded areas represent the series of wavenumbers that demonstrate significant differences between the antebrachiocarpal and midcarpal joints ($p<0.01$).

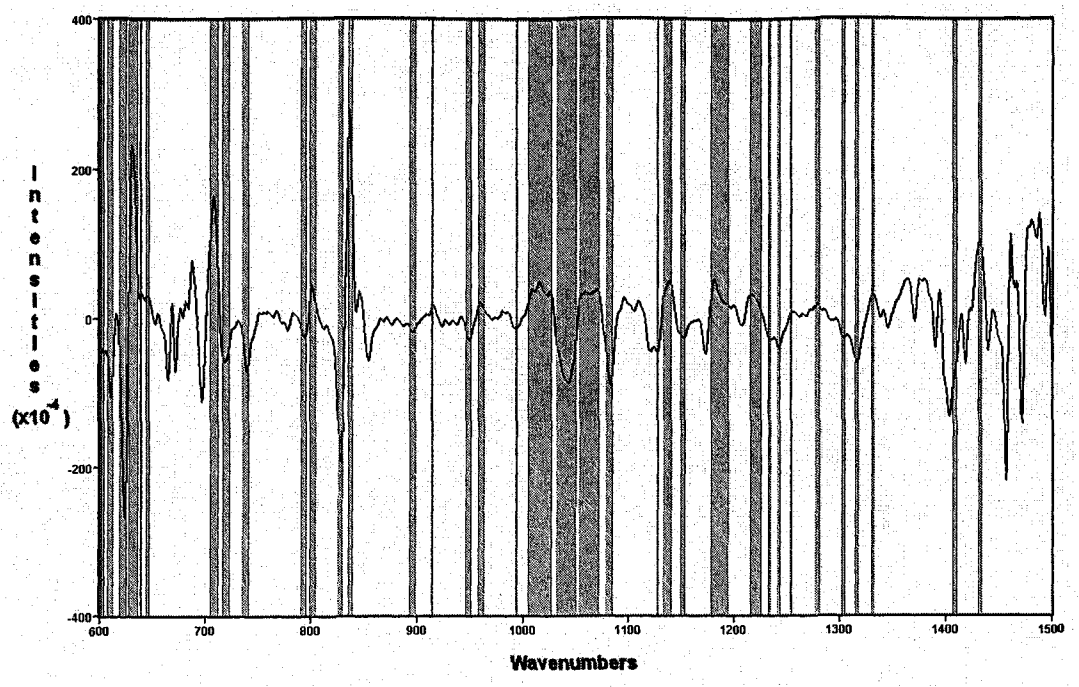

Figure 3.2 Difference spectrum (2nd derivative) of antebrachiocarpal-tarsocrural spectra in the fingerprint region. The shaded areas represent the series of wavenumbers that demonstrate significant differences between the antebrachiocarpal and tarsocrural joints ($p<0.01$).

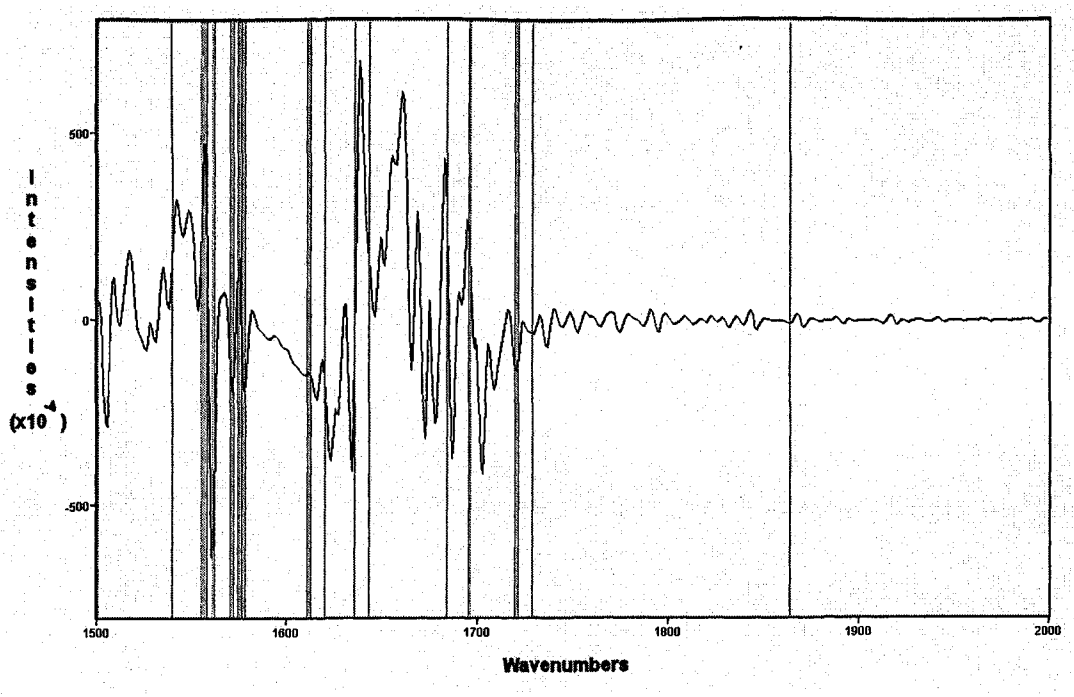

Figure 3.3 Difference spectrum (2nd derivative) of antebrachiocarpal-midcarpal spectra in the double bond region. The shaded areas represent the series of wavenumbers that demonstrate significant differences between the antebrachiocarpal and midcarpal joints ($p<0.01$).

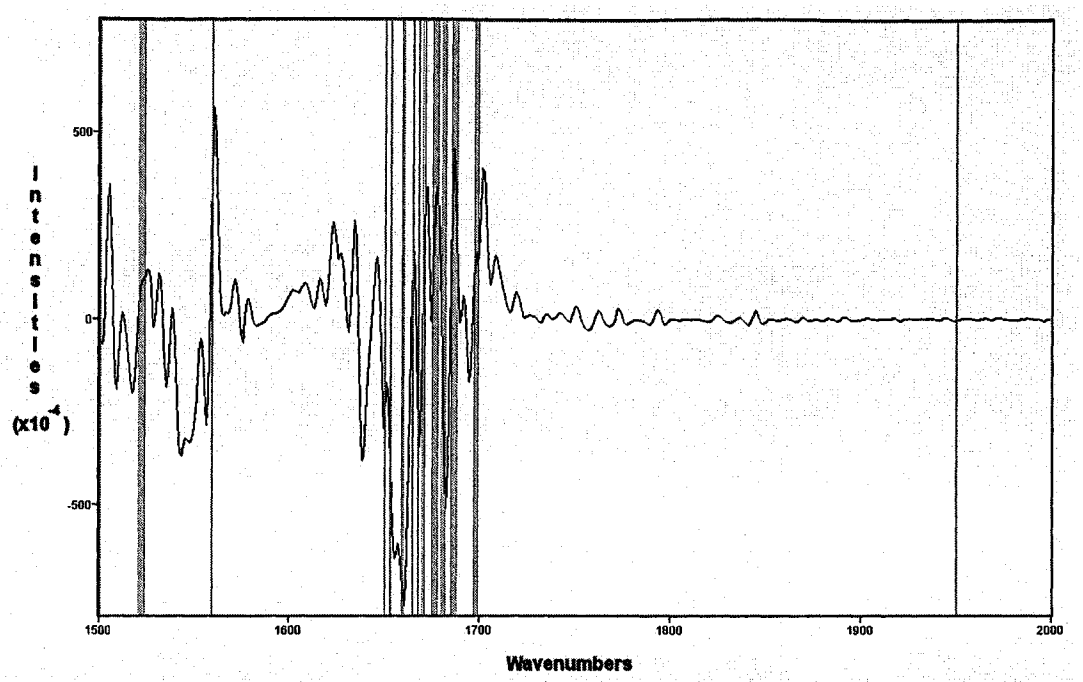

Figure 3.4 Difference spectrum (2nd derivative) of antebrachiocarpal-tarsocrural spectra in the double bond region. The shaded areas represent the series of wavenumbers that demonstrate significant differences between the antebrachiocarpal and tarsocrural joints ($p<0.01$).

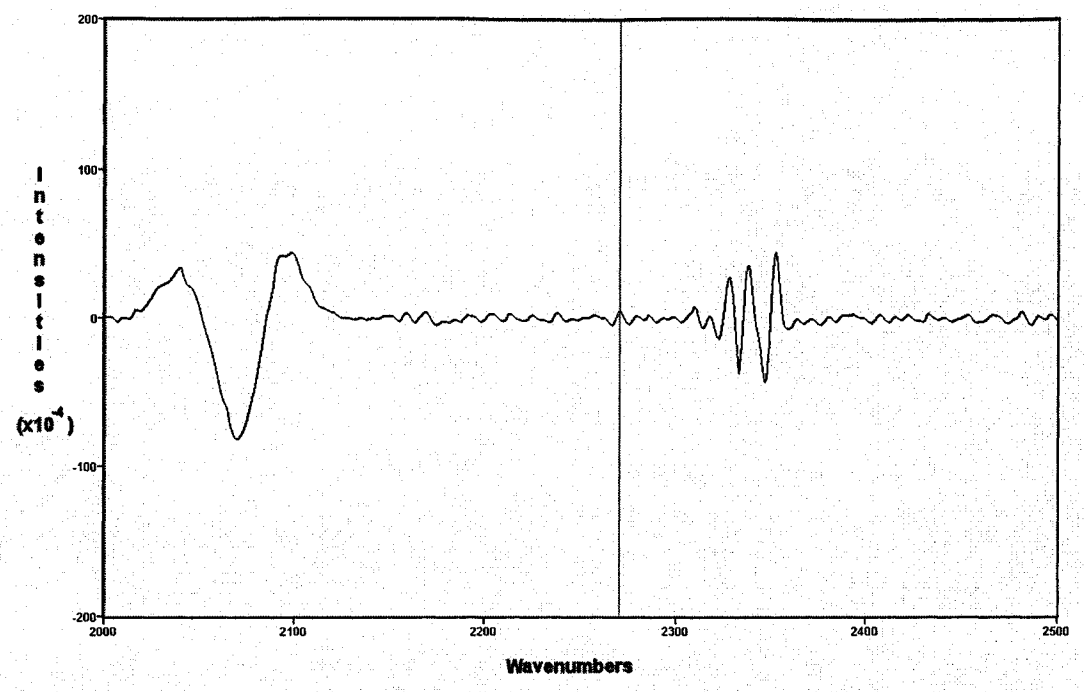

Figure 3.5 Difference spectrum (2nd derivative) of antebrachiocarpal-midcapal spectra in the triple bond region. The shaded areas represent the series of wavenumbers that demonstrate significant differences between the antebrachiocarpal and midcarpal joints ($p<0.01$).

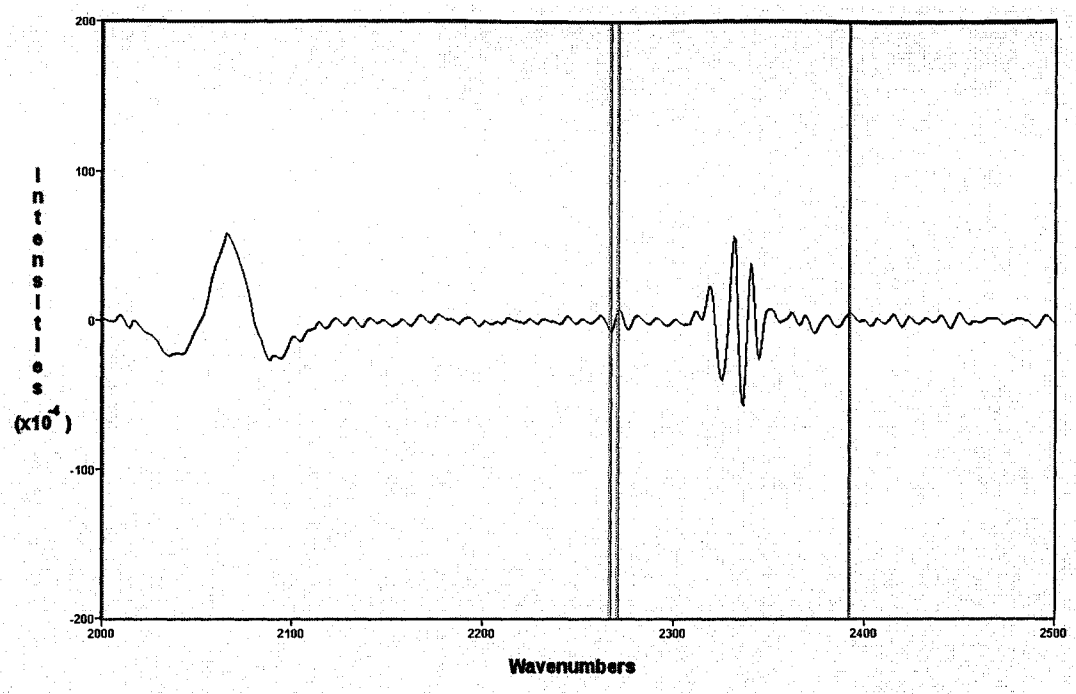

Figure 3.6 Difference spectrum (2nd derivative) of antebrachiocarpal-tarsocrural spectra in the triple bond region. The shaded areas represent the series of wavenumbers that demonstrate significant differences between the antebrachiocarpal and tarsocrural joints ($p<0.01$).

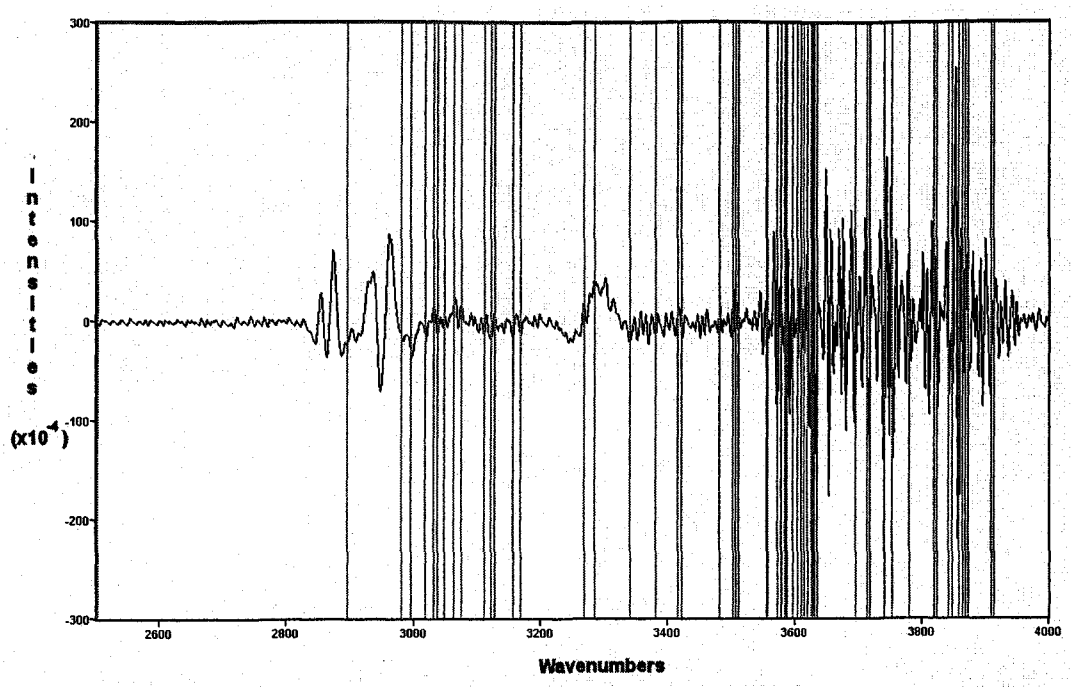

Figure 3.7 Difference spectrum (2nd derivative) of antebrachiocarpal-midcapal spectra in the X-H stretching region (X = O,C or N). The shaded areas represent the series of wavenumbers that demonstrate significant differences between the antebrachiocarpal and midcarpal joints ($p<0.01$).

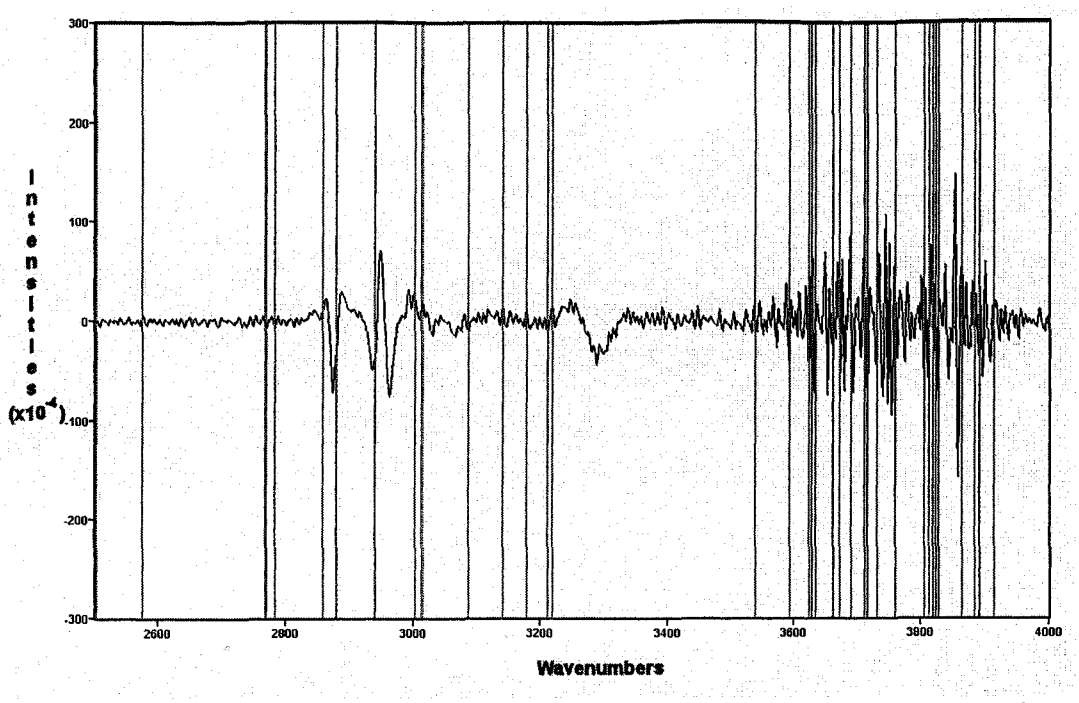

Figure 3.8 Difference spectrum (2nd derivative) of antebrachiocarpal-tarsocrural spectra in the X-H stretching region (X = O,C or N). The shaded areas represent the series of wavenumbers that demonstrate significant differences between the antebrachiocarpal and tarsocrural joints ($p<0.01$).

pharmacologic and mechanical studies have documented that changes may occur in contralateral control joints (32, 33). The biochemical changes occurring within the contralateral control joints may be objectively assessed by IR spectroscopy of SF in a future study to confirm the validity of the use of contralateral joint as a normal control.

In contrast, the dissimilarities in IR absorption patterns observed among ipsilateral joints of different anatomical locations were marked, even when the joints were immediately adjacent. However, the IR absorption patterns of SF samples from adjacent joints (AC and MC) showed fewer differences than comparisons between more anatomically distant joints (TC). Given the biomechanical and functional differences between the carpal and tarsal regions, it is reasonable to expect that biochemical differences as determined by IR analysis of SF, reflecting the full range of molecules present, would be more marked than those occurring between functionally similar joints (19, 21, 22, 29, 34). Despite biomechanical differences, earlier workers have found no quantitative differences in total protein content (TP) between hocks and carpi (the precise joints sampled were not described), but TP was lower in the fetlock (35). Differences in the concentration of total glycosaminoglycans, keratan sulfate and cartilage oligomeric matrix protein between the interphalangeal and metacarpophalangeal joints have been reported in normal horses (23). Different values for total glycosaminoglycans and keratan sulphate concentrations in SF were also reported between AC and TC joints, but data were insufficient for statistical conclusions to be drawn (19). In the current study the range

of biochemical differences among the joints was more clearly demonstrated because unlike specifically targeted assays, investigation by IR spectroscopy of SF reflects both quantitative and qualitative molecular differences of known and unknown biomolecules (14, 16).

The interpretation and correlation of the features of the MIR spectra to specific molecules is possible when examining a pure solute or a solution of a few distinct molecules (14, 36). For more complex biological mixtures such as the SF examined in the current study, the absorption bands are no longer simple and well-resolved – the absorption profile reflects the superposition of literally thousands of individual absorptions spread across the MIR region (14). In the case of SF, the major molecular contributions to the mixture are water, albumin, α-, β- and γ-globulins, transferrin, glucose, urea, hyaluronate and proteoglycans (5, 6, 8, 35). It is the pattern of overlapping absorptions rather than individual molecular moieties that provide a biochemical signature, referred to as a molecular fingerprint, reflecting the complexity and relative abundance of the chemical constituents.

Hyaluronate has been supported as a marker for osteoarthritis, as have total glycosaminoglycans and keratan sulfate (4, 6, 19, 23, 31). Cartilage extracted preparations of proteoglycans (containing chondroitin sulfate and keratan sulfate) have a wide absorption band (1550-1640 cm^{-1}) with a maximum at ~1635 cm^{-1} due to the overlapping of the combined absorption of carbonyl groups of acetamide residues (amide I), the antisymmetrical stretching of carboxylate groups of hexuronic acid (COO^-), and other contributions (37-39). Absorption at 1550 cm^{-1} is associated with

the amide II band, and 1413 cm^{-1} with the symmetrical COO^- vibration (37-39). In the current study significant differences with joint type were detected in areas corresponding to these peaks. Unless the SF samples are fractionated, and molecules separated prior to IR spectroscopy, the specific origins of the differences are not readily interpreted (14, 39). The current study also identified significant spectral differences among the AC, IC, and TC joints spread across several spectral regions. These included subregions that would include, for example, absorption bands associated with proteoglycan sulfate groups, and hyaluronante primary and secondary alcohol hydroxyl groups (37-39). While further fractionation and analysis is clearly necessary to confirm the actual origin of these spectroscopic changes, these observations are consistent with the work of others suggesting differences among joints in concentrations of proteoglycans and glucosaminoglycans (19).

Caution should be exercised in interpreting the significance of absorptions in the X-H stretching region. While the broad 3000-3600 cm^{-1} profile encompasses the O-H stretching bands of water and polysaccharides (37, 39), both hyaluronate (HA) and chondroitin sulfate (CS) have a high capacity for water binding, resulting in a significant contribution to the MIR spectra that varies with atmospheric humidity even though the samples were dried prior to spectral acquisition (39). The apparatus used in the study does not permit control of humidity within the sample chamber. The authors suggest that future IR spectroscopy studies control relative humidity in order to prevent dilution of the IR signal attributable to HA and CS, and to minimize the small spectral shift that occurs with varying OH bandwidth (39). The authors of the

current study suggest the fingerprint region of the spectra may be more suitable for comparing joints in cases where controlling humidity is difficult, as this region is less affected (39).

The sample size used in the current study is comparable to that used in similar reports examining synovial constituents (23, 30, 31). However the large number of variables examined increases the rate of type I error, limiting the utility of the data in the current study for linear discriminant analysis to model the significant spectral differences which best characterize each joint. Data reduction strategies were employed and a high significance level set (15, 18). Despite these steps a large number of differences among joints were found. As a result the study was limited to pairwise comparisons of MIR spectra of different joints. Recruitment of further samples from normal joints is necessary to facilitate more advanced modeling of the differences between normal joints.

In conclusion, significant differences among AC, MC, and TC joints in SF composition were confirmed as characterized by IR spectroscopy. The MIR absorption patterns of SF samples derived from pairs of contralateral joints were comparable supporting their use as within subject control in appropriately designed studies. The finding of a broad range biomolecular differences among these joints indicates that interarticular variation within the horse needs to be considered in prospective study design, and well as studies of joint disease (19, 23, 31). Further normal samples should be evaluated to better characterize the range and significance of MIR spectral changes detected.

References

(1) Coleman PJ, Scott D, Ray J, Mason RM, Levick JR. Hyaluronan secretion into the synovial cavity of rabbit knees and comparison with albumin turnover. J Physiol 1997;503:645-656.

(2) Iwanaga T, Shikichi M, Kitamura H, Yanase H, Nozawa-Inoue K. Morphology and functional roles of synoviocytes in the joint. Arch Histol Cytol 2000;63:17-31.

(3) Levick JR. Microvascular architecture and exchange in synovial joints. Microcirculation 1995;2:217-233.

(4) McIlwraith CW. Use of synovial fluid and serum biomarkers in equine bone and joint disease: a review. Equine Vet J 2005;37:473-482.

(5) Pascual E, Jovani V. Synovial fluid analysis. Best Pract Res Clin Rheumatol 2005;19:371-386.

(6) Punzi L, Oliviero F, Plebani M. New biochemical insights into the pathogenesis of osteoarthrits and the role of laboratory investigations in clinical assessment. Crit Rev Clin Lab Sci 2005;42:279-309.

(7) Swan A, Amer H, Dieppe P. The value of synovial fluid assays in the diagnosis of joint disease: a literature survey. Ann Rheum Dis 2002;61:493-498.

(8) Van Pelt RW. Interpretation of synovial fluid findings in the horse. J Am Vet Med Assoc 1974;16:91-95.

(9) McIlwraith CW, Billinghurst RC, Frisbie DD. Current and future diagnostic means to better characterize osteoarthritis in the horse- routine synovial fluid analysis and synovial fluid and serum markers. In *Proceedings.* 47th AAEP annual convention 2001;47:171-179.

(10) Bertone AL, Palmer JL, Jones J. Synovial fluid cytokines and eicosanoids as markers of joint disease in horse. Vet Surg 2001;30:528-538.

(11) Poole AR. Biochemical/immunochemical biomarkers of osteoarthritis: utility for prediction of incident or progressive osteoarthritis. Rheum Dis Clin North Am 2003;29:803-818.

(12) Gu W, Bertone AL. Generation and performance of an equine-specific large-scale gene expression microarray. Am J Vet Res 2004;65:1664-1673.

(13) Canvin JM, Bernatsky S, Hitchon CA, Jackson M, Sowa MG, Mansfield JR et al. Infrared spectroscopy: shedding light on synovitis in patients with rheumatoid arthritis. Rheumatology (Oxford) 2003;42:76-82.

(14) Dubois J, Shaw RA. IR spectroscopy in clinical and diagnostic applications. Anal Chem 2004;76:361A-367A.

(15) Eysel HH, Jackson M, Nikulin A, Somorjai RL, Thomson GTD, Mantsch HH. A novel diagnostic test for arthritis: multivariate analysis of infrared spectra of synovial fluid. Biospectroscopy 1997;3:161-167.

(16) Shaw RA, Mantsch HH. Infrared spectroscopy in clinical and diagnostic analysis. In: Meyers RA, eds. Encyclopedia of analytical chemistry: applications theory and instrumentation. Chichester: John Wiley & Sons Ltd, 2000: 83-102.

(17) Shaw RA, Mantsch HH. Vibrational biospectroscopy: from plants to animals to humans. A historical perspective. Journal of Molecular Structure 1999; 481:1-13.

(18) Vijarnsorn M, Riley CB, Shaw RA, McIlwraith CW, Ryan DA, Rose PL et al. Use of infrared spectroscopy for diagnosis of traumatic arthritis in horses. Am J Vet Res 2006;67:1286-1292.

(19) Fuller CJ, Barr AR, Dieppe PA, Sharif M. Variation of an epitope of keratan sulphate and total glycosaminoglycans in normal equine joints. Equine Vet J 1996;28:490-493.

(20) Fuller CJ, Barr AR, Dieppe PA. Variations in cartilage catabolism in different equine joints in response to interleukin-1 in vitro. Vet Rec 2001;148:204-206.

(21) Hodson E, Clayton HM, Lanovaz JL. The forelimb in walking horses: 1. Kinematics and ground reaction forces. Equine Vet J 2000;32:287-294.

(22) Hodson E, Clayton HM, Lanovaz JL. The hindlimb in walking horses: 1. Kinematics and ground reaction forces. Equine Vet J 2001;33:38-43.

(23) Viitanen M, Bird J, Maisi P, Smith R, Tulamo RM, May S. Differences in the concentration of various synovial fluid constituents between the distal interphalangeal joint, the metacarpophalangeal joint and the navicular bursa in normal horses. Res Vet Sci 2000;69:63-67.

(24) Low-Ying S, Shaw RA, Leroux M, Mantsch HH. Quantitation of glucose and urea in whole blood by mid-infrared spectroscopy of dry films. Vib Spectrosc 2002;28:111-116.

(25) Shaw RA, Mantsch HH. Multianalyte serum assays from mid-infrared spectra of dry films on glass slides. Appl spectrosc 2000;54:885-889.

(26) Adams MJ. Feature selection and extraction. In: Barnett NW, eds. Chemometrics in analytical spectroscopy. Cambridge: Royal Society of Chemistry, 2004:55-95.

(27) Gunzler H, Gremlich HU. Qualitative spectral interpretation. In: IR spectroscopy, an introduction. Weinheim: Wiley-VCH, 2002:171-278.

(28) Stuart B. Spectral Analysis. In: Infrared spectroscopy: fundamentals and applications. Chichester: John Wiley & Sons Ltd, 2004:45-70.

(29) Simkin PA, Pickerell CC. Interarticular differences in oncotic pressure of canine synovial fluid. J Rheumatol 1984;11:14-16.

(30) Celeste C, Ionescu M, Robin PA, Laverty S. Repeated intraarticular injections of triamcinolone acetonide alter cartilage matrix metabolism measured by biomarkers in synovial fluid. J Orthop Res 2005;23:602-610.

(31) Fuller CJ, Barr AR, Sharif M, Dieppe PA. Cross-sectional comparison of synovial fluid biochemical markers in equine osteoarthritis and the correlation of these markers with articular cartilage damage. Osteoarthritis Cartilage 2001;9:49-55.

(32) Richardson DW, Clark CC. Effects of short-term cast immobilization on equine articular cartilage. Am J Vet Res 1993;54:449-453.

(33) Todhunter RJ, Altman NS, Kallfelz FA, Nersesian P, Lust G. Use of scintimetry to assess effects of exercise and polysulfated glycosaminoglycan on equine carpal joints with osteochondral defects. Am J Vet Res 1993;54:997-1006.

(34) Simkin PA, Benedict RS. Hydrostatic and oncotic determinants of microvascular fluid balance in normal canine joints. Arthritis Rheum 1990;33:80-86.

(35) Liberg P, Magnusson LE, Schougaard H. Studies on the synovia in healthy horses with particular reference to the protein composition. Equine Vet J 1977;9:87-91.

(36) Coates J. Interpretation of infrared spectra, a practical approach. In: Meyers RA, eds. Encyclopedia of analytical chemistry. Chichester: John Wiley & Sons Ltd, 2000:10815-10837.

(37) Alkrad JA, Mrestani Y, Stroehl D, Wartewig S, Neubert R. Characterization of enzymatically digested hyaluronic acid using NMR, Raman, IR, and UV-Vis spectroscopies. J Pharm Biomed Anal 2003;31:545-550.

(38) Haxaire K, Marechal Y, Milas M, Rinaudo M. Hydration of polysaccharide hyaluronan observed by IR spectrometry. I. Preliminary experiments and band assignments. Biopolymers 2003;72:10-20.

(39) Servaty R, Schiller J, Binder H, Arnold K. Hydration of polymeric components of cartilage--an infrared spectroscopic study on hyaluronic acid and chondroitin sulfate. Int J Biol Macromol 2001;28:121-127.

CHAPTER 4

USE OF INFRARED SPECTROSCOPY FOR DIAGNOSIS OF TRAUMATIC ARTHRITIS IN HORSES

4.1 Abstract

Infrared spectroscopy measures infrared absorption patterns of molecules in a sample when exposed to infrared radiation. The Infrared absorption pattern or spectrum reflects the chemical structure of all infrared-active components in the sample and their relative abundance. The spectrum of biological fluid is often referred to as a biochemical fingerprint that may correlate with the presence or absence of diseases. The objective of the study is to determine the feasibility of using infrared spectroscopy to differentiate synovial fluid samples from equine joints with traumatic arthritis from those of controls. Synovial fluid samples were collected from 77 joints in 48 horses with traumatic arthritis. Of these 29 horses provided paired samples (affected and control) used for model calibration. The remaining 19 horses provided independent samples from a diseased (n=12) or a control (n=7) joint used for model validation. A second validation set of normal SF samples (n=20) was collected from 5 clinically and radiographically normal horses. Fourier transform infrared spectra of SF were acquired, manipulated, and data from diseased joints were compared to controls to identify statistically significant ($p<0.01$) spectroscopic features that differentiated between the groups. A classification model using linear discriminant analysis was developed. Performance of the model was determined using the two validation datasets. A classification model based upon 3 infrared regions classified

spectra from the calibration dataset with overall accuracy of 97 % (sensitivity 93%; specificity 100%). The same model with cost-adjusted prior probabilities of 0.60:0.40 produced an overall accuracy of 89% (sensitivity 83%; specificity 100%) for the first validation sample dataset, and 100% correct classification of the second set of independent normal control joints. The IR spectroscopic patterns of SF from joints with traumatic arthritis differ significantly from the corresponding patterns for controls. These alterations in IR absorption patterns may be exploited via an appropriate classification algorithm to differentiate the spectra of diseased joints from those of controls.

4.2 Introduction

Osteoarthritis (OA) is a commonly encountered cause of lameness in performance horses, and has been implicated as a cause of lameness in 54% of horses (1). Lameness problems have been estimated to result in 68% of days lost in training among racehorses (2). Timely diagnosis and aggressive treatment of traumatically induced OA are important to alleviate the effects of inflammation, including pain and reduced function, and are essential to prevent or minimize the development of OA (3).

Evaluation of joint disease in a horse is facilitated by clinical examination to detect signs of pain and gross anatomical or functional change, evaluate the horse's gait, and localize the problem by use of diagnostic analgesia (3). Other diagnostic aids include radiography, ultrasonography, computed tomography (CT), magnetic

resonance imaging (MRI), nuclear medical imaging, arthroscopy, and routine synovial fluid analysis (3-5). Although radiography is presently the most practical imaging technique used to aid diagnosis, pathologic changes in articular cartilage cannot be readily assessed, and a lack of sensitivity in the detection of subchondral fragmentation has been reported (6). Nuclear scintigraphy is an advanced diagnostic tool for musculoskeletal disease with high sensitivity but low specificity (7). Factors such as age, breed, and occupation of horses can affect the radiopharmaceutical uptake and image interpretation (7). Magnetic resonance imaging generates excellent anatomic and pathoanatomic information on articular structures but the high cost of acquiring and maintaining equipment, the limited availability for use in horses, and the need for general anesthesia for high resolution images have prevented its widespread use (8). None of these tools yield useful biochemical information.

Conventional synovial fluid analyses are not widely used for evaluation of non-infectious joint disease because they rarely provide clinicians with a specific diagnosis (5-9). Recently, ELISA and radioimmunoassay-based evaluations of biomarkers within SF have been described (9-11). Complex multiple assays are required (9-12). Individual testing by use of these techniques is expensive (12). The relationships of the concentrations of the biomarkers to age, breed, sex and circadian rhythms are poorly understood (12). Early results are promising, but further study is required to determine the clinical usefulness of biomarkers for classifying OA (9-12). Presently the means to objectively identify the level of pathologic progression in most cases of traumatic and other forms of OA are not available primarily because no

generally accepted objective standards exist (6-9). There is a real need for a rapid, economical, practical, and reliable diagnostic test for objective evaluation of joint disease, as well as the unbiased monitoring of responses to treatment.

Infrared (IR) spectroscopy is rapidly emerging as a powerful diagnostic probe for biological molecules in humans and other animals (13, 14). Infrared spectroscopy measures IR absorption patterns of molecules when exposed to IR light (14). An IR spectrum is obtained when IR radiation is transmitted through a sample in a Fourier transform IR spectrometer (FT-IR). The fraction of the incident radiation absorbed at a particular wavenumber (cm^{-1}) is determined and displayed as absorption bands on the spectrum (15). These absorption bands correspond to carbon skeletal and functional group vibrations (16). Simple molecules yield simple spectra with well-resolved absorption bands that reflect both structure and concentration (13, 17). In a complex sample, compared with a simple sample, the number of chemical functional groups increases, causing the number of absorption bands and the extent of band overlap to increase (17). The IR spectrum of a biological sample becomes more complex, but the fundamental rule still applies. The IR spectrum of body fluids or tissues reflects both the structure of the individual IR active constituents and their relative abundance (14, 17). The absorption patterns in the IR spectra of biological samples may be viewed as biochemical fingerprints that correlate directly with the presence or absence of diseases (14, 18). For example, IR spectroscopy has been used in diagnosis of human diseases such as diabetes mellitus (19), Alzheimer's disease (20), breast tumors (21) and arthritic disorders (22-25). The advantages of an IR

spectroscopic approach in clinical diagnosis are that no reagents are required, and automated repetitive analyses can be carried out at very low cost (14). In addition, because the IR spectrum of biological samples such as synovial fluid reflects the sum of all IR-active components (26), the infrared spectra of such samples may carry infrared signatures of known and unknown biomarkers rather than relying upon a few novel disease markers.

We hypothesized that traumatic arthritis in horses leads to changes in equine synovial fluid composition, altering the IR absorption pattern of synovial fluid samples, and that these spectroscopic changes can be detected and used to differentiate the synovial fluid spectra of joints with traumatic arthritis from the spectra of control samples. The objective of the present study was to determine the feasibility and to evaluate the accuracy of IR spectroscopy for diagnosis of traumatic arthritis in horses.

4.3 Materials and methods

This study was approved by the Animal Care Committee in accordance with the University of Prince Edward Island policy and the principles outlined in the *Guide to the Care and Use of Experimental Animals* prepared by the Canadian Council on Animal Care.

4.3.1 Horses and samples

Synovial fluid samples (n=77) were collected from 48 horses evaluated for arthroscopic removal of osteochondral fragments or intra-articular fracture repair

after clinical and radiographic assessments. Samples for model development (calibration) and initial model validation were from Californian racing Thoroughbred (n=25) and Quarter horses (n=23). These horses were 2 to 5 years old with a mean age of 3.2 ± 1.1 years (mean ± SD). There were 37 males and 11 females. All horses had clinical evidence of osteochondral fracture of the antebrachiocarpal, midcarpal or metacarpophalangeal joints. Synovial samples were collected aseptically prior to arthroscopic surgery, and samples from contralateral joints with no evidence of articular fragmentation were also collected as controls. In bilaterally osteochondral fragmentation cases, samples from ipsilateral antebrachiocarpal or midcarpal joint with no evidence of articular fragmentation were used as control samples.

Of the 48 horses, paired samples were collected from 29 (one each from affected and control joints); these were used for calibration of the model. From the remaining 19 horses with traumatic arthritis, independent samples from either an affected (n=12) or a control (n=7) joint only; were used for initial model validation. A second set of control synovial fluid samples (n=20) was collected for further independent validation. These samples were from the (left and right) antebrachiocarpal and midcarpal joints of 5 horses. The mean age of the horses was 4.2 ± 1.5 (mean ± SD) years. Two were Trakehner crosses, 3 were Standardbreds, 4 were females, and 1 was male. On the basis of history and result of clinical evaluations, these 5 horses had no evidence of joint disease. A general physical examination and lameness examination were performed by two evaluators. Bilateral radiographs of carpal, metacarpophalangeal, stifle, and tarsal joints were evaluated by

a radiologist. Conventional synovial fluid analysis was also performed. All evaluators were unaware of clinical status of the horses. The anatomic locations from which all the synovial samples were recovered are described in Table 4.1, and their random assignment into calibration or validation datasets (see below) described. All synovial fluid samples collected for the study were stored at -80 °C in plain cryovials for later batch IR spectroscopic analysis.

4.3.2 Fourier transform (FT-IR) infrared spectroscopy

Synovial fluid samples were thawed at room temperature (approximately 22 °C) and centrifuged at 2700 x g for 10 minutes; the supernatants were kept for analyses. Synovial fluid samples were prepared as described previously with the following modification (27). Briefly, for each sample, an aliquot was drawn and diluted in aqueous 4 g/L potassium thiocynate (KSCN, SigmaUltra, Sigma-Aldrich Inc.,St.Louis, USA) solution in the ratio 3 parts synovial fluid: 1 part KSCN solution. The isolated KSCN absorption peak at approximately 2060 cm^{-1} served as a reference band for normalization of the spectral intensities (27, 28).

Triplicate dried films were made for each sample by applying 8 μL of the diluted synovial fluid preparation evenly in a circular motion onto 5-mm-diameter circular islands on a custom-made, adhesive-masked, silicon microplate; the adhesive mask serves to spatially define and systematically separate the 5 mm islands on the microplate so that sample islands are correctly aligned with the FT-IR detector). The synovial films were left to dry at room temperature for 12 hours. After the films were thoroughly dried, the microplate was mounted in a multisampler interfaced to the

Table 4.1 Description of the anatomical locations and diagnoses of the study joints

Joint	Diagnosis	Number of synovial fluid samples within each category		
		Step 1A&1B	Step 2	Step 3
Antebrachiocarpal	Osteochondral fracture	8 (2)	1	0
	Ipsilateral/contralateral control	8 (6)	1	10
Midcarpal	Osteochondral fracture	19 (11)	1	0
	Ipsilateral/contralateral control	19 (8)	5	10
Metacarpophalangeal	Osteochondral fracture	2 (1)	4	0
	Condylar fracture of the third metacarpus	0 (0)	3	0
	Proximal sessamoid fracture	0 (0)	3	0
	Contralateral control	2 (1)	1	0

Number in parenthesis indicates the number of joints randomly selected from step1A and used in step 1B.

Step 1A = Infrared (IR) region selection, Step 1B = Calibration for classification model,

Step 2 = Validation of model using independent within-population samples,

Step 3 = Validation of model using independent normal control samples

FTIR spectrometer (Tensor 37, Bruker optics, Milton, Canada) to enable acquisition of IR spectra. Infrared spectroscopic analyses of all samples were performed during the same period of time.

Infrared absorbance spectra in the range of 400-4000 cm^{-1} were recorded using a FT-IR spectrometer (HTS-XT, Bruker optics, Milton, Canada) equipped with a deuterium tryglycine sulfate detector. For each acquisition, 512 interferograms were signal averaged and Fourier transformed (Opus 4.2, Bruker Optik GmbH, Ettlingen, Germany) to generate a spectrum with a nominal resolution of 4 cm^{-1} (27).

4.3.3 Data preprocessing

Triplicate spectra of each sample yielded mean values. By use of spectral manipulation software (GRAMS/AI 7.02, Thermo Galactic, Salem, USA), differentiation and smoothing procedures (Savitsky Golay 2^{nd}-order derivative with 2^{nd}-degree polynomial function and 15-point smoothing) were performed on all spectra to resolve and enhance weak spectral features and to remove variation in baselines (29). The approach to the spectral classification is outlined schematically in Figure 4.1.

4.3.4 Statistical Analysis

4.3.4.1 Infrared region selection

The strategy employed to find significant ($p<0.01$) differences between affected and control joints was to examine the spectroscopic differences for horses that provided paired samples, one for an affected joint and the other for a contralateral or ipsilateral control. Twenty-nine horses yielded such paired synovial fluid samples

Figure 4.1 Infrared spectral classification and model development strategy

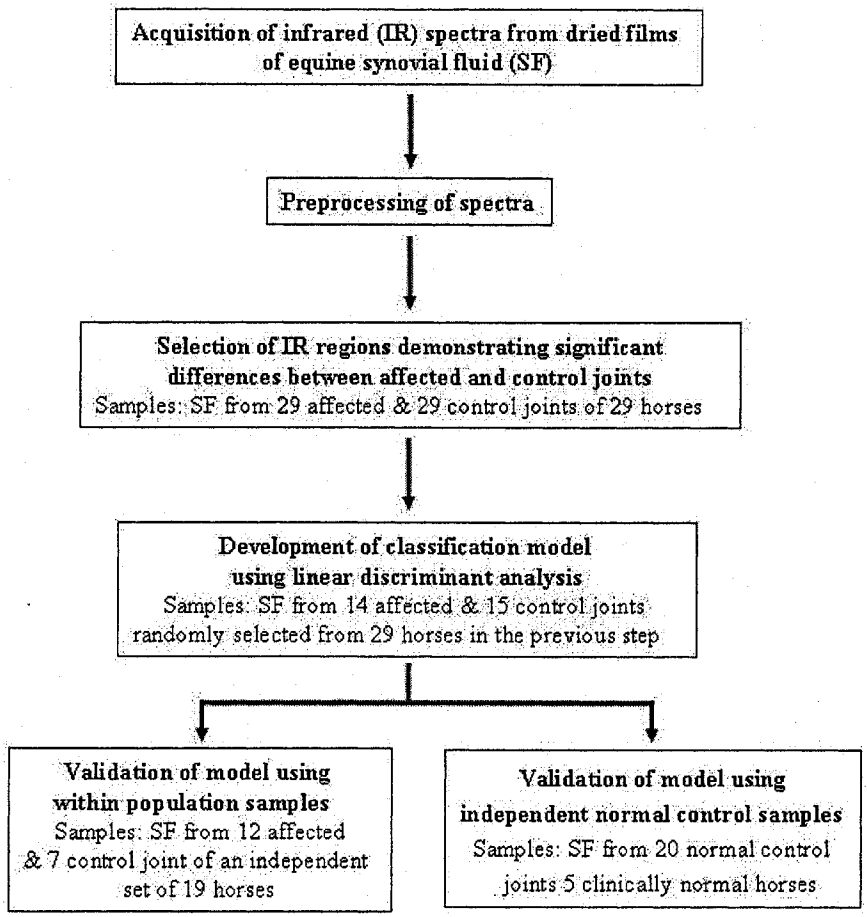

resulting in 58 averaged spectra. The pairwise spectroscopic differences in the corresponding spectra (control minus diseased) were evaluated within the IR range 400-1800 cm^{-1} (molecular fingerprint region) (15). The next step was to seek those subregions where the difference (control minus affected) was significant ($p<0.01$). These subregions were identified by use of paired t-tests performed with statistical software (SAS 8.02, SAS institute Inc.,Cary, USA). The regions which had significant differences between affected and control samples were identified, and the spectral intensities in each region were then averaged. The average value of each of the selected regions was then considered as a variable for inclusion in a classification model (30).

4.3.4.2 Development and calibration of the classification model

In order to avoid violation of assumptions of independence necessary for discriminant analysis, the 29 horses described previously were randomly assigned into group 1 (n=15) and group 2 (n=14). For group 1 (control group), only the spectra from the control joints (n=15) were used. For group 2 (affected group), only the spectra from the joints with osteochondral fracture (n=14) were used. This set of 29 spectra provided the basis to calibrate the classification model. By use of the set of averaged regional intensities as input variables for each case, stepwise discriminant analysis was then performed by use of proprietary statistical software (SAS 8.02, SAS institute Inc.,Cary, USA) to select the subset of variables that most contributed to the power of the discriminatory function (31). That subset of variables was then subjected to linear discriminant analysis (LDA) to find the discriminatory function and rule that

best separated the two groups (affected versus control), by use of statistical software (SAS 8.02, SAS institute Inc.,Cary, USA). Two sets of cost-adjusted prior probabilities of group membership (31), 0.60:0.40 or 0.50:0.50 (affected to control ratio), were selected for this preliminary classification. The posterior probabilities of group membership were calculated for each spectrum. The membership of the spectrum was thus predicted, and the spectrum assigned to the affected or control group on the basis of its posterior probability. A classification table then revealed the correct classifications for the 29 randomly selected spectra composing the calibration sample set (14, 18, 32).

4.3.4.3 Validation of the model by use of within-population samples

The remaining 19 of 48 horses that were not used to calibrate the model yielded 19 spectra (7 control and 12 affected spectra) for use as a validation dataset, to test the predictive accuracy of the classification model. The classification success rate for this set of spectra was determined and compared with the results for the calibration set (14, 18, 32).

4.3.4.4 Validation of the model by use of independent normal control samples

The second independent set of samples from 5 normal control horses that yielded 20 averaged spectra from bilateral antebrachiocarpal and midcarpal joints was used to further characterize the predictive accuracy of the classification model. The classification success rate for this set of spectra was determined and compared with the results for the calibration set.

4.4 Results

Paired t-tests revealed 24 spectral regions in the 400-1800 cm^{-1} wavenumber range that had significant differences ($p<0.01$) between the affected and control synovial fluid spectra. From this set of regions, stepwise discriminant procedures resulted in the final selection of 3 regions that most contributed to the discriminatory power of the classification algorithm. These encompassed the wavenumber ranges 1245 to 1257 cm^{-1}, 1681 to 1684 cm^{-1}, and 1691 to 1694 cm^{-1} (Figure 4.2).

The classification model developed by use of LDA, with these 3 regional intensities as input for each of the 29 calibration samples, correctly classified 28 of the 29 calibration spectra (Table 4.2), yielding an overall accuracy of 97%, specificity of 100%, and sensitivity of 93%. Both sets of cost-adjusted prior probabilities give the same classification result.

When the classification algorithm was applied to the within-population validation set (n=19), the LDA classifier with cost-adjusted prior probabilities of 0.60:0.40 (affected to control) achieved an overall accuracy of 89%, with 100% specificity and 83% sensitivity (Table 4.3). With equal prior probabilities of group membership (0.50:0.50), the overall accuracy decreased to 79% (specificity, 100%; sensitivity, 67%). All of the normal control samples that composed the second validation set were classified correctly by use of both sets of cost-adjusted prior probabilities.

The basis for these classifications was depicted in Figure 4.3. With each measured spectrum represented by the triplet of averaged intensities in the 3

Figure 4.2 The average spectrum (2^{nd} derivative) of the control group and the corresponding average difference spectrum (control minus diseased spectra). The shaded areas represent the IR regions optimal for diagnostic classification of the spectra.

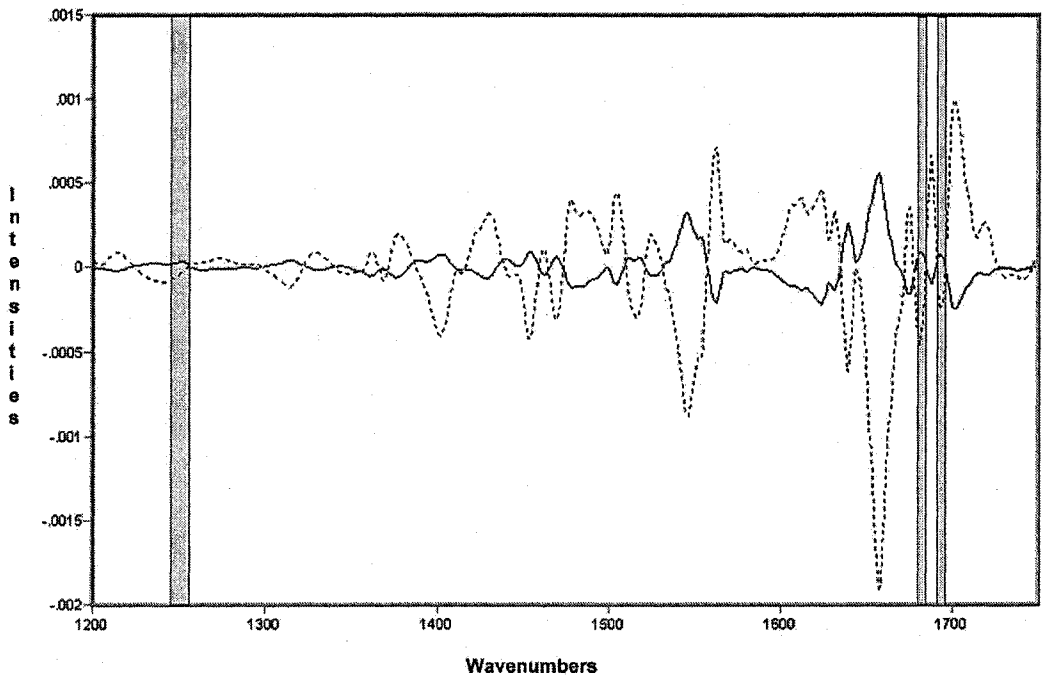

..... Average spectrum of the control group, _____ Average difference spectrum

Note: Negative features in the 2^{nd} derivative spectrum of the control group correspond to positive features (absorptions) in the original spectrum. The highlighted regions are 1245-1257 cm^{-1}, 1681-1684 cm^{-1}, and 1691-1694 cm^{-1}.

Table 4.2 Classification table for the calibration dataset

	Infrared-based diagnosis		
	Control	Osteochondral fracture	Total
Clinical diagnosis			
Control	**15**	0	15
Osteochondral fracture	1	**13**	14
Total	16	13	**29**

Number of spectra classified into control and osteochondral fracture categories for both sets of cost-adjusted prior probabilities

Sensitivity = 93%, Specificity = 100%, Accuracy = 97%

Table 4.3 Classification table for the validation dataset

	Infrared-based diagnosis		
	Control	Osteochondral fracture	Total
Clinical diagnosis			
Control	**7 (7)**	0 (0)	7 (7)
Osteochondral fracture	2 (4)	**10 (8)**	12 (12)
Total	9 (11)	10 (8)	**19 (19)**

Number of spectra classified into control and osteochondral fracture categories when setting cost-adjusted prior (diseased:control) = 0.60:0.40 (sensitivity = 83%, specificity = 100%, accuracy = 89%)

Numbers in parenthesis indicates results when setting equal cost-adjusted prior (sensitivity = 67%, specificity = 100%, accuracy = 79%)

Figure 4.3 Three-dimensional representation of the spectral datasets preprocessed for classification, and their division into the calibration and validation sets

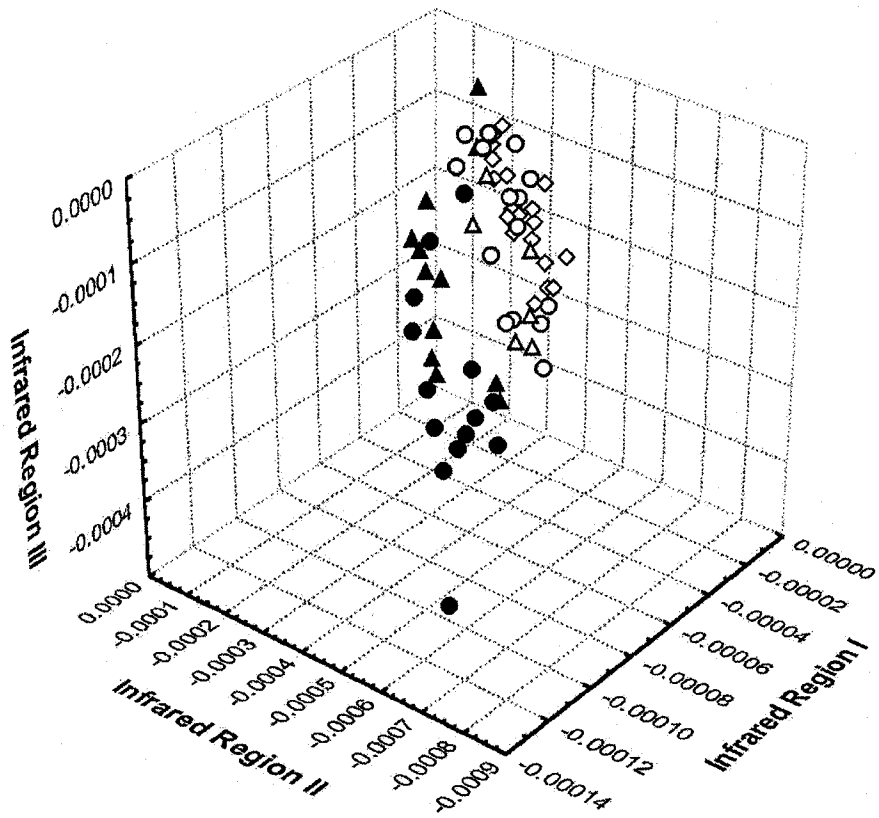

○ Control spectra in calibration set

● Osteochodral fracture spectra in calibration set

△ Control spectra in validation set I (within-population samples)

▲ Osteochondral fracture spectra in validation set I (within-population samples)

◇ Normal control spectra in validation set II (independent normal control samples)

Note: Each observation is represented by the triplet of intensities within the regions 1245-1257 cm^{-1} (IR region I), 1681-1684 cm^{-1} (IR region II) and 1691-1694 cm^{-1} (IR region III) for the 2nd derivative spectrum

subregions that provided optimal classification accuracy, the scatter plot graphically illustrates the separation of affected from control (clustering) spectra for the calibration and both validation datasets.

4.5 Discussion

In this study, significant differences in the IR absorption pattern of synovial fluid samples were demonstrated for comparison of samples from joints with traumatic arthritis to control samples. The IR spectra successfully served as biochemical fingerprints to permit diagnosis of traumatic arthritis by means of LDA classification of the processed data. These results support our hypothesis that characteristic IR absorption patterns may be detected and used to differentiate the synovial fluid spectra of the joints with traumatic arthritis from spectra for control samples.

The ultimate goal of this type of research is to develop a novel test that aids clinical and perhaps preclinical diagnosis of joint disease in horses. In agreement with published recommendations for the development of a new diagnostic test, an exploratory phase was conducted in a limited number of subjects to determine its feasibility and accuracy as a first step (33). Naturally occurring traumatic arthritis was chosen as a model to determine the feasibility and accuracy of the IR spectroscopic technique. It was thought that if this methodology was determined to be incapable of detecting more severe forms of equine joint disease, then its future use to develop a test for subclinical or mild joint disease would be limited. Intra-articular fracture, one

of the subtypes of traumatic arthritis entities in horses, is often preceded by subchondral bone changes, and may lead to osteoarthritis if diagnosis and treatment are not prescribed in a timely and appropriate fashion (3, 34).

Although the features distinguishing the IR spectra of synovial fluid samples of affected from control joints are not readily interpreted, IR spectra of biological specimens reflect chemical composition and conformation, as well as possible intermolecular interactions (14, 16, 35). Articular cartilage damage associated with articular fracture or other types of joint injury induces biochemical changes in the affected joints (3, 10). The release of wear-and-tear particles as well as articular cartilage-breakdown products activates synovial resident cells and chondrocytes to increase the productions of cytokines, metalloproteinase enzymes and inflammatory mediators or other biomarkers that can lead to further damage of the cartilage and joint inflammation (3, 10, 36-40). It is possible that the IR changes detected correlated to one or all of these molecules. However, because of the complex mixture of organic molecules in synovial fluid, the specific origins of the features that underpinned the successful classifications have not been readily identified. Further study is required to establish the precise linkages between IR spectra and biomarkers of OA, if any.

One other veterinary study (41) used a limited IR spectroscopic technique for the evaluation of synovial fluid in 14 clinically normal horses and 2 horses with osteochondrosis. Gross visually apparent differences between spectra of normal and osteochondritic joints were reported, but a multivariate classification algorithm was

not developed. In particular, differences in the relative intensity of the IR absorption bands at 1000, 1035, 1115 and 1245 cm^{-1} were recovered and suggested to be useful in differentiation between normal and osteochondritic joints. However, both the laboratory technique and the etiology of disease differ from the present study, and it is now well established that a larger number of samples must be examined in each class to derive diagnostic tests applicable to a larger population. Infrared spectroscopy of dried SF films has also been used in the diagnosis of human arthritis, with LDA classifications based upon an optimally selected set of 15 IR regions between 2800 and 3050 cm^{-1}(23). The fact that different spectral regions are required for the present study may be attributable to the differences both in species and the nature of the arthritic conditions examined.

The cost-adjusted prior probabilities represent the group-prior probability that a spectrum belongs to one of the two study groups adjusted for the cost of misclassification (31). Henceforth this will be referred to as the cost-adjusted prior. Because there is no evidence suggesting true prevalence of traumatic arthritis in the study population nor guidelines suggesting the exact cost of misclassification, in the present study, the cost-adjusted priors of affected horses compared with control horses were explored based on two sets of values, 0.50:0.50 (equal) and 0.60:0.40. If the cost-adjusted prior is set to be equal, the cost of misclassification and the group-prior probability are assumed to be equal. Ability of the test to detect traumatic arthritis cases (test sensitivity) was lower in the validation compared with calibration sets when cost-adjusted prior was set to equal. This weakness may be improved by

choosing an appropriate cost-adjusted prior. In screening for equine traumatic arthritis in horses, the aim is to identify as many affected horses as possible. The misclassification cost for failure of the clinician to identify affected horses would be delayed treatment, prolonged recovery period, or an unfavorable treatment outcome because of delayed diagnosis. If an intra-articular fracture is not diagnosed early enough, or treatment is not started early enough, it may lead to OA. The implications of false positives are clinically less serious because follow up diagnostic methods (eg. radiography, arthroscopy) will subsequently triage out the false positive cases. In the present study, the authors suggest setting cost-adjusted priors in favor of disease diagnosis because of the unequal cost of misclassification as described above. At this preliminary stage, the authors presently favor setting the cost-adjusted priors of affected to control ratio at 0.60 to 0.40, which implies the cost that is 1.5 times as great for classifying a horse with traumatic arthritis as normal relative to classifying a normal as having traumatic arthritis.

For the earlier diagnostic study of human arthritis using IR spectroscopy of SF, the spectral classification method was developed by combining an optimal region selection algorithm with LDA classification (23). The differentiation of IR spectra of joint fluid from 12 nonarthritic and 74 arthritic patients was achieved, and subsequently, the sub-classification of 3 categories of human conditions (rheumatoid arthritis, osteoarthritis and spondyloarthropathy) was detected with overall specificity and sensitivity of 100% and 96.5%, respectively. The classification success rates were therefore comparable to those achieved for the present study, despite the differences

in species and disease etiology, suggesting that IR spectroscopy may be generally useful to accurately diagnose a variety of joint diseases in a broad spectrum of species.

The classification accuracy for the within-population validation set of spectra was marginally lower than that for the calibration set when a 60:40 cost-adjusted prior was used. However, the accuracy and sensitivity of the algorithm for the validation set (79% and 67% respectively) are considerably reduced when setting a 50:50 cost adjusted prior. Although the specificity remains at 100% for either ratio of priors and in all 3 data sets, the sensitivity appeared to vary according to cost adjusted prior values in this preliminary study. The authors of the present study found that cost adjusted prior values were helpful tools in optimizing the classification of spectra from populations of limited sample size. An objective estimation of cost-adjusted priors may not be feasible for the equine population at large. The authors suggest that spectral and prevalence data from a larger sample size may be more useful for the future development and optimization of the specificity and sensitivity of this test for clinical use (31, 33). This would better enable the scope of spectral variation in the affected population at large to be encompassed, and reduce the reliance of the test on estimating cost adjusted prior values, possibly increasing the number of discriminatory variables for inclusion in the final classification model, and thus increasing sensitivity and accuracy.

The spectroscopic data from the 3 significant spectral regions found in our proof-of-concept study yielded robust results in classifying control spectra but is less

accurate in classifying affected spectra. This was not unexpected given the number of samples available for this study, which allowed for inclusion of only 3 of the 24 significant variables in the classification model (on the basis of IR region and stepwise selection procedure). These 3 variables were selected statistically and were the important variables that most contributed to the power of discrimination (31). The discriminatory function and rule based on these selective variables were considered sufficient for accurate classification between groups in the calibration set but clearly did not encompass all possible variations of the diseased population. This is indicated by the lower sensitivity (67-83%) of the validation set when classifying affected spectra on the basis of 3 significant variables. It is expected that the differences in performance between the calibration and the validation sets will be reduced as more samples become available for analysis. With a larger number of samples in the calibration set, the varying degree of articular cartilage changes and other changes associated with the traumatic injuries in the population of affected horses will be better represented. Similarly, the larger the number of samples in the validation set, the more confidence we can have in the ability of the discriminatory algorithm to discriminate spectra correctly (32). These preliminary results do address our initial objective, and favor the further development of this method of joint disease diagnosis in horses.

In the present study, the misclassification of certain affected spectra as controls may have been attributable to variation of the degree and duration of inflammation among traumatic joints. Possibly, a sample from a joint with mild

arthritis was difficult to differentiate from the controls because of the limited number of spectral regions in the present classification model. Such variation in the degree of severity is inevitable when studying joint disease in a naturally occurring setting, and may contribute substantially to the variability of synovial fluid variables of affected horses, has been reported in arthritis biomarker studies in horses (38). Other OA induced models such as osteochondral fragment and forced exercise models may provide more control for the degree of inflammation in the affected group (42). Nonetheless, the ability of the approach in this report to correctly identify control or normal joints (test specificity) in both validation sets clearly revealed the diagnostic potential for this classification algorithm in the normal equine population.

The current results demonstrate the feasibility of a novel IR-based approach for the diagnosis of equine traumatic arthritis. Further recruitment of cases and normal control horses is anticipated to develop and expand the scope of applications, and is necessary to validate the clinical value and accuracy of the method for screening and diagnosing patients with joint disease in the larger equine population.

References

(1) Kidd JA, Fuller C, Barr ARS. Osteoarthritis in the horse. Equine Vet Educ 2001;13:160-168.

(2) Rossdale PD, Hopes R, Wingfield Digby NJ, et al. Epidemiological study of wastage among racehorses 1982 and 1983. Vet Rec 1985;116:66-69.

(3) McIlwraith CW. Diseases of joints, tendons, ligaments, and related structures. In: Stashak TS, eds. Adams' lameness in horses. 5th ed. Philadelphia: Lippincott Williams & Wilkins, 2002;459-644.

(4) Park RD, Wrigley RH, Steyn PF. Equine diagnostic imaging. In: Stashak TS, eds. Adams' lameness in horses. 5th ed. Philadelphia: Lippincott Williams & Wilkins, 2002;185-375.

(5) Van Pelt RW. Interpretation of synovial fluid findings in the horse. J Am Vet Med Assoc 1974;16:91-95.

(6) Kawcak CE, McIlwraith CW, Norrdin RW, et al. Clinical effects of exercise on subchondral bone of carpal and metacarpophalangeal joints in horses. Am J Vet Res 2000;61:1252-1258.

(7) Twardock AR. Equine bone scintigraphic uptake patterns related to age, breed, and occupation. Vet Clin North Am Equine Pract 2001;17:75-94.

(8) Kraft SL, Gavin P. Physical principle and technical considerations for equine computed tomography and magnetic resonance imaging. Vet Clin North Am Equine Pract 2001;17:115-130.

(9) McIlwraith CW, Billinghurst RC, Frisbie DD. Current and future diagnostic means to better characterize osteoarthritis in the horse- routine synovial fluid analysis and synovial fluid and serum marker. In *Proceedings.* 47th AAEP annual convention 2001;47:171-179.

(10) Bertone AL, Palmer JL, Jones J. Synovial fluid cytokines and eicosanoids as markers of joint disease in horse. Vet Surg 2001;30:528-538.

(11) Trumble TN, Trotter GW, Oxford JR, et al. Synovial fluid gelatinase concentrations and matrix metalloproteinase and cytokine expression in naturally occurring joint disease in horses. Am J Vet Res 2001;62:1467-1477.

(12) Poole AR. Biochemical/immunochemical biomarkers of osteoarthritis: utility for prediction of incident or progressive osteoarthritis. Rheum Dis Clin N Am 2003;29:803-818.

(13) Shaw RA, Mantsch HH. Vibrational biospectroscopy: from plants to animals to humans. A historical perspective. J Mol Structure 1999;480-481:1-13.

(14) Shaw RA, Mantsch HH. Infrared spectroscopy in clinical and diagnostic analysis. In: Meyers RA, eds. Encyclopedia of analytical chemistry: applications theory and instrumentation. Chichester: John Wiley & Sons Ltd, 2000;83-102.

(15) Stuart B. Introduction. In: Infrared spectroscopy: fundamentals and applications. Chichester: John Wiley & Sons Ltd, 2004;1-13.

(16) Coates J. Interpretation of infrared spectra, a practical approach. In: Meyers RA, eds. Encyclopedia of analytical chemistry. Chichester: John Wiley & Sons Ltd, 2000;10815-10837.

(17) Dubois J, Shaw RA. IR spectroscopy in clinical and diagnostic applications. Anal Chem 2004;76:361A-367A.

(18) Jackson M, Mantsch HH. Infrared spectroscopy, ex vivo tissue analysis by. In: Meyers RA, eds. Encyclopedia of analytical chemistry. Chichester: John Wiley & Sons Ltd, 2000;131-156.

(19) Petrich W, Staib A, Otto M, et al. Correlation between the state of health of blood donors and the corresponding mid-infrared spectra of the serum. Vib Spectrosc 2002;28:117-129.

(20) Pizzi N, Choo LP, Mansfield J, et al. Neural network classification of infrared spectra of control and Alzheimer's diseased tissue. Artif Intell Med 1995;7:67-79.

(21) Jackson M, Mansfield JR, Dolenko B, et al. Classification of breast tumors by grade and steroid receptor status using pattern recognition analysis of infrared spectra. Cancer Detect Prev 1999;23:245-253.

(22) Canvin JM, Bernatsky S, Hitchon CA, et al. Infrared spectroscopy: shedding light on synovitis in patients with rheumatoid arthritis. Rheumatology (Oxford) 2003;42:76-82.

(23) Eysel HH, Jackson M, Nikulin A,et al. A novel diagnostic test for arthritis: multivariate analysis of infrared spectra of synovial fluid. Biospectroscopy 1997;3:161-167.

(24) Shaw RA, Kotowich S, Eysel HH, et al. Arthritis diagnosis based upon the near-infrared spectrum of synovial fluid. Rheumatol Int 1995;15:159-165.

(25) Staib A, Dolenko B, Fink DJ, et al. Disease pattern recognition testing for rheumatoid arthritis using infrared spectra of human serum. Clin Chim Acta 2001;308:79-89.

(26) Jackson M, Sowa MG, Mantsch HH. Infrared spectroscopy: a new frontier in medicine. Biophys Chem 1997;68:109-125.

(27) Shaw RA, Mantsch HH. Multianalyte serum assays from mid-IR spectra of dry films on glass slides. Appl Spectrosc 2000;54:885-889.

(28) Low-Ying S, Shaw RA, Leroux M, et al. Quantitation of glucose and urea in whole blood by mid-infrared spectroscopy of dry films. Vib Spectrosc 2002;28:111-116.

(29) Adams MJ. Feature selection and extraction. In: Chemometrics in analytical spectroscopy. Cambridge: The Royal Society of Chemistry, 2004;55-95.

(30) Nikulin AE, Dolenko B, Bezabeh T, et al. Near-optimal region selection for feature space reduction: novel preprocessing methods for classifying MR spectra. NMR Biomed 1998;11:209-216.

(31) Khattree R, Naik DN. Discriminant analysis. In: Multivariate data reduction and discrimination with SAS software. Cary: SAS Institute Inc, 2000;211-345.

(32) Adams MJ. Pattern Recognition II: supervised learning. In: Chemometrics in analytical spectroscopy. Cambridge: The Royal Society of Chemistry, 2004;129-160.

(33) Zhou XH, Obuchowski NA, McClish DK. The design of diagnostic accuracy studies. In: Statistical methods in diagnostic medicine. New York: John Wiley & Sons, Inc, 2002;57-99.

(34) Kawcak CE, McIlwraith CW, Norrdin RW, et al. The role of subchondral bone in joint disease: a review. Equine Vet J 2001;33:120-126.

(35) Stuart B. Spectral analysis. In: Infrared spectroscopy: fundamentals and applications. Chichester: John Wiley & Sons Ltd, 2004:45-70.

(36) Clegg PD, Carter SD. Matrix metalloproteinase-2 and -9 are activated in joint diseases. Equine Vet J 1999;31:324-330.

(37) Dimock AN, Siciliano PD, McIlwraith CW. Evidence supporting an increased presence of reactive oxygen species in the diseased equine joint. Equine Vet J 2000;32:439-443.

(38) Frisbie DD, Ray CS, Ionescu M, et al. Measurement of synovial fluid and serum concentrations of the 846 epitope of chondroitin sulfate and of carboxy propeptides of type II procollagen for diagnosis of osteochondral fragmentation in horses. Am J Vet Res 1999;60:306-309.

(39) Fuller CJ, Barr AR, Sharif M, et al. Cross-sectional comparison of synovial fluid biochemical markers in equine osteoarthritis and the correlation of these markers with articular cartilage damage. Osteoarthritis Cartilage 2001;9:49-55.

(40) Misumi K, Vilim V, Clegg PD, et al. Measurement of cartilage oligomeric matrix protein (COMP) in normal and diseased equine synovial fluids. Osteoarthritis Cartilage 2001;9:119-127.

(41) Muttini A, Petrezzi L, Tinti A, et al. Synovial fluid parameters in normal and osteochondritic hocks of horses with open physis. Boll Soc Ital Biol Sper 1994;70:337-344.

(42) Kawcak CE. Models of equine joint disease. In: Ross MW, Dyson SJ, eds. Diagnosis and management of lameness in the horse. St.Louis: Saunders, 2003;594-598.

CHAPTER 5

IDENTIFICATION OF INFRARED ABSORPTION SPECTRAL CHARACTERISTICS OF SYNOVIAL FLUID OF HORSES WITH TARSOCRURAL OSTEOCHONDROSIS

5.1 Abstract

Fourier-transform infrared (FT-IR) spectroscopy is a measurement of infrared (IR) absorption pattern (IR spectrum) of a sample when exposed to IR light. A biological fluid sample such as synovial fluid (SF) gives rise to a unique IR spectrum, which reflects the chemical constituents within it. Mid-infrared spectroscopic analysis of SF was employed in this study. Sixty-four SF samples of the tarsocrural joints from 64 horses were collected (one sample for each horse). Of these horses, 33 samples are from joints with radiographic evidence of osteochondrosis (OC) and the remaining 31 samples are from joints with no clinical or radiographic evidence of OC. Disease-associated characteristics within MIR spectra of SF have been studied and statistically selected for further spectral classification purposes. These disease-associated features were used as variables in a classification model. By use of linear discriminant analysis and leave-one-out cross validation, SF spectra derived from samples of joints with OC can be differentiated from the control samples with accuracy of 77% (81% specificity and 73% sensitivity). The misclassification rate within the OC group aged less than 2 years was lower than the misclassification rate for horses aged greater than 2 years of age (overall misclassification rate is 23%). The disease-associated characteristics in MIR spectra of SF from joints with OC may be

exploited via appropriate feature selection and classification algorithms to differentiate the spectra of SF from joint with OC from those of controls. Further study with larger sample size including varying degree of OC and age-, breed-, and gender-matched controls would further validate the clinical value of IR spectroscopy in diagnosis of equine OC.

5.2 Introduction

Disturbances occurring in the development of articular or periarticular structures may prevent horses from reaching their full athletic potential, particularly if diagnosis and treatment are not provided in a timely manner. Of these disorders, osteochondrosis (OC; dyschondroplasia) has been documented to have significant impact on equine performance, industry economics and welfare (1-4). The disease is characterized by a failure of endochondral ossification occurring at the physes and the articular-epiphyseal cartilage complex during the growing phase of the bones (3). Commonly found in many equine breeds, the reported incidence ranges from 10-31.5% depending upon the study design and subpopulation examined (5-8). Lesions have been reported in most equine joints, but the tarsocrural joint is the most commonly affected site (9).

The routine diagnosis of OC is based upon orthopaedic examination and radiography (10). In clinical cases, orthopedic examination is usually prompted by signs of effusion or lameness. The severity of lameness may vary from none to marked and the response to intra-articular anesthesia varies among horses (10).

However in many cases of OC in young horses, a radiographic diagnosis of subclinical or "occult" disease is made during routine pre-purchase or pre-insurance screening (10). Radiographic evaluation is the most common approach to diagnosis, but the cost and time required for evaluating large numbers of horses to identify subclinical OC remains an obstacle for early intervention (6, 8). Such an assessment of young horses is not always diagnostic. Radiographic screening has previously been shown to be of benefit for preclinical diagnosis and the initiation of management changes which may impede the progression of OC (11). Although this modality is generally useful, cases of OC have been diagnosed by arthroscopy which were neither clinically nor radiographically apparent (12). Scintigraphy and ultrasonography have also been useful in selected cases of OC, but all of these image modalities provide only gross pathoanatomic information (10, 13). None of these tools yields information about biochemical changes in response to pathological processes occurring in OC affected joints.

Recently there has been a move to the identification of serum and synovial fluid biomarkers of joint disease (14-18). With the exceptions of sepsis or severe acute traumatic arthritis, conventional synovial fluid analysis has had limited value for the diagnosis and staging of OC or osteoarthritis (16). Anabolic and catabolic markers for equine OC have been isolated and quantified from both synovial fluid and serum. Keratan sulphate (KS) epitope concentration in synovial fluid from OC affected joints was found to be significantly lower compared to controls (15). The insignificant elevation of plasma KS concentration was also detected in OC affected

horses (18). Significant changes in concentrations of chondroitin sulfate epitope 846 (CS-846), and carboxy propeptide of type II procollagen (CPII) in synovial fluid have also been associated with OC lesions in young horses (15). Age has been identified as a significant factor in the expression of these markers (15). Other serum biomarkers for OC investigated include CS-846, CPII, collagenase-generated neoepitope of type-II collagen fragments (234 CEQ), collagenase-generated neoepitope of type-I and type-II collagen fragments ($COL2\text{-}3/4C_{short}$) and cross-linked telopeptide degradation fragment of type-I collagen (CTx1) (14). The latter have been correlated with lesion severity (14). Early results of these ELISA and radioimmunoassay based evaluations have provided insights into the pathogenesis of OC and may assist clinical evaluation and screening for OC in future. However, complex multiple assays may be required to characterize cases of OC, and individual testing using these techniques is expensive (14, 15, 17).

Fourier transform infrared (FT-IR) spectroscopy remains one of the most important tools in analytical chemistry (19). Recently its application has been extended to solving clinical diagnostic problems in human and veterinary medicine (20-27). Based on the measurement of infrared (IR) absorption patterns of biological specimens, this technique is rapidly emerging as a powerful diagnostic tool for probing biological molecules in humans and animals (26, 28). Within this field of study, applications using IR absorption spectroscopy are showing promise in the development of biomedical tests (20-28). Measurement simply entails transmitting IR radiation through the sample of interest (eg. synovial fluid) and measuring the

absorbance as a function of wavelength or wavenumber (the reciprocal of the wavelength) (28). Each molecular species gives rise to a unique spectrum of absorptions, each component of which corresponds to a unique intramolecular vibration of the carbon skeleton and the functional groups attached to it (29).

In biomedical FT-IR spectroscopy, the IR spectrum of each body fluid or tissue reflects both the structure of the individual IR active constituents and their relative abundance (28, 30). Unlike a simple molecular spectrum, the IR spectrum of a biological sample is more complex because the number of chemical functional groups is increased, causing the number of absorption bands and the extent of band overlap to increase (30). The absorption patterns within the IR spectra of biological samples may be viewed as biochemical "fingerprints" that correlate directly with the presence or absence of diseases (28, 31). Recent proof-of-principle studies have demonstrated the potential of IR analyses of serum and synovial fluid as a new diagnostic tool for human arthritis (20, 21, 25, 27). One decisive advantage of an IR spectroscopic approach to clinical diagnosis is that no reagents are required. The IR spectrum can be derived directly from IR-active constituents within a sample without a need of chemical modification or the aid of comparative substances (28, 29). Therefore automated repetitive analyses can be carried out at very low cost. Moreover, since the IR spectrum of biological samples reflects the sum of all IR active components, the IR spectra of such samples may carry signatures of both known and unknown biomarkers rather than relying upon a few novel disease markers.

We hypothesized that OC leads to changes in equine synovial fluid composition, altering the IR absorption pattern of synovial fluid samples. The objective of this study is to determine the feasibility of using mid-infrared FT-IR spectroscopy to differentiate between synovial fluid samples of joints with OC from those of control samples.

5.3 Materials and methods

This study was approved by the Animal Care Committee in accordance with the University of Prince Edward Island policy and the *Guide to the Care and Use of Experimental Animals* prepared by the Canadian Council on Animal Care.

5.3.1 Horses and samples

A synovial fluid sample (n=64) was collected from a tarsocrural joint of each of 64 equine patients presented to the Veterinary Teaching Hospital, Atlantic Veterinary College for clinical and radiographic assessment of the hocks. The age of study horses ranged from 8 months to 7 years old (mean ± SD; 2.6 ± 1.3 years). There were 32 females and 32 males consisting of Appaloosa (n = 1), Belgian (n = 1), Percheron (n = 1), Thoroughbred (n = 1), Shire (n = 1), Trakehner cross (n = 2), Warmblood (n = 5), Quarter horse (n = 5), and Standardbred (n = 47) breeds. Thirty-three samples were from horses with radiographic evidence of OC affecting the intermediate ridge of the distal aspect of the tibia, lateral trochlear ridge of the talus, or medial maleolus of the tibia. The samples were collected aseptically after radiographic examination or prior to arthroscopic removal of the OC fragment. The

remaining 31 control samples were collected from joints with no clinical evidence of OC based upon radiographic examination and/or necropsy findings. All synovial fluid samples collected for the study were stored at -80 °C in plain cryovials for later batch FT-IR spectroscopic analysis.

5.3.2 Fourier transform (FT-IR) infrared spectroscopy

Synovial fluid samples were thawed at room temperature, centrifuged at 2700 x g for 10 minutes, and the supernatants used for analyses. The samples were prepared as described previously with the following modification (32). Briefly, for each sample, an aliquot was drawn and diluted in aqueous 4 g/L potassium thiocyanate (KSCN, SigmaUltra, Sigma-Aldrich Inc., St.Louis, MO, USA) solution in the ratio 3 parts synovial fluid: 1 part KSCN solution. Triplicate dry films were made for each sample by applying 8 μL of the diluted synovial fluid, spread evenly in circular motion onto 5 mm diameter circular islands within a custom made, adhesive masked, 96-well, silicon microplate (the adhesive mask serves to spatially define and systematically separate the 5 mm islands on the microplate so that sample islands are correctly aligned with the FT-IR radiation source and detector). Synovial fluid samples from all study horses were randomly assigned to well positions on the microplate. The synovial films were left to dry at room temperature for 12 h. Once the films were thoroughly dried, the microplate was mounted within a multisampler (HTS-XT autosampler, Bruker Optics, Milton, ON, Canada) interfaced with a FT-IR spectrometer equipped with a deuterium tryglycine sulfate detector (Tensor 37, Bruker Optics, Milton, ON, Canada) to allow for the acquisition of MIR spectra.

Infrared spectroscopic measurements of all samples were performed during the same period of time. Absorbance spectra in the range of 400-4000 cm^{-1} were recorded. For each acquisition, 512 interferograms were signal averaged and Fourier transformed to generate a spectrum with a nominal resolution of 4 cm^{-1} (32).

5.3.3 Data preprocessing

A data processing strategy was used to extract and to enhance relevant features within MIR spectra that contributed to the success of classification. Triplicate spectra of each sample were first averaged, and then differentiation and smoothing procedures (Savitsky Golay 2^{nd} order derivatives using 2^{nd} degree polynomial functions, with 19 point smoothing) were performed on all spectra to resolve and enhance weak spectral features and to remove variation in baselines (33), using spectral manipulation software (GRAMS/AI 7.02, Thermo Galactic, Salem, NH, USA).

The spectra were then normalized by using a wavenumber range of 800-1450 cm^{-1} as a basis of vector normalization, using scripts written in MatLab (MATLAB 6.5, The Math Works Inc., Natick, MA, USA). The script was developed by the Institute of Biodiagnostics (in collaboration with Dr. R. Anthony Shaw, Institute of Biodiagnostics, National Research Council of Canada). Vector normalization employed scaling the 2^{nd} derivative spectra in the dataset, by defining the sum of square intensities over the wavenumber range of 800-1450 cm^{-1} as equal to unity (23). Vector normalization was carried out for each 2^{nd} derivative spectrum by first summing the squares of absorption intensities for all data points (1 data point

corresponded to approximately 1 wavenumber) within the spectral basis range of 800-1450 cm^{-1}. The square root of this sum of squares calculated from each spectrum was used as the normalization factor for that same spectrum. The intensities of the entire range within each spectrum were divided by this normalization factor based on the square root of the sum of square intensities within the wavenumber range of 800-1450 cm^{-1} being assigned a value equal to 1.

5.3.4 Statistical analysis

5.3.4.1 Selection of significant subregions

The following strategy was employed to identify spectral subregions wherein the significant effect of group (OC versus control) was demonstrated in the normalized 2nd derivative of the MIR spectra. The relative intensity of normalized spectra at each wavenumber was used as a dependent variable. Statistical analysis was performed on each wavenumber basis for the entire mid-IR range of 400-4000 cm^{-1} (SAS 8.02, SAS institute Inc.,Cary, NC, USA). The set of independent variables included group (fixed effect), age (covariate), microplate (random effect), within microplate row (random effect), and within microplate column (random effect). Analyses of covariance were employed to detect the sets of wavenumbers that demonstrated the significant effect of group ($p<0.01$), accounting for the age variable. Significant subregions were defined as a set of at least 4 consecutive wavenumbers which demonstrated a significant effect of group at a level of $p < 0.01$. The spectral intensities within each region were then averaged. The average value of each of the

selected regions was then considered as a variable for inclusion within a classification model (34).

5.3.4.2 Classification model development and validation

Using the set of averaged regional intensities as input variables for each case, stepwise discriminant analysis was performed using proprietary statistical software (SAS 8.02, SAS institute Inc., Cary, NC, USA) to select the subset of variables that most contributed to the power of the discriminatory function (35). These subsets of variables (optimal regions) were then subjected to linear discriminant analysis (LDA) to find the discriminatory function and rule that best separated the two groups (OC versus control), using statistical software (SAS 8.02, SAS institute Inc., Cary, NC, USA). An equal prior probability was set. The performance of classification models indicated by accuracy, specificity and sensitivity were estimated based on the cross-validation (leave-one-out) method (21).

5.4 Results

Analysis of covariance revealed 12 significant subregions that met the selection criteria (Table 5.1; Figure 5.1). From this set of significant subregions, the stepwise discriminant procedure resulted in the final selection of 6 optimal regions that most contributed to the discriminatory power of the classification algorithm (Table 5.1). Linear discriminant analysis resulted in classification results of 77% overall accuracy, 81% specificity and 73% sensitivity estimated by the cross-validation method (Table 5.2). Age, accounted for in the final model, was found to

Table 5.1 Significant infrared absorption spectrum subregions found to discriminate between osteochondrosis and control groups

Infrared regions (wavenumber)	P value
[a]536 – 542 cm^{-1}	0.0024 – 0.0066
762 – 766 cm^{-1}	0.0029 – 0.0065
[a]851 – 855 cm^{-1}	0.0046 – 0.0084
[a]866 – 872 cm^{-1}	0.0006 – 0.0073
[a]923 – 927 cm^{-1}	0.0053 – 0.0091
958 – 968 cm^{-1}	0.0006 – 0.0099
985 – 991 cm^{-1}	0.0008 – 0.0027
[a]996 – 1019 cm^{-1}	0.0002 – 0.0069
1027 – 1036 cm^{-1}	0.0005 – 0.0074
1073 – 1083 cm^{-1}	0.0015 – 0.0073
1093 – 1100 cm^{-1}	0.0014 – 0.0083
[a]1763 – 1772 cm^{-1}	0.0001 – 0.0064

[a] Indicates the regions selected by the stepwise discriminant procedure for inclusion in the final classification model.

Figure 5.1 Graphic representation of normalized 2nd derivative spectra (2nd order derivative intensity value). The shade areas represent the significant wavenumber regions identified by analyses of covariance.

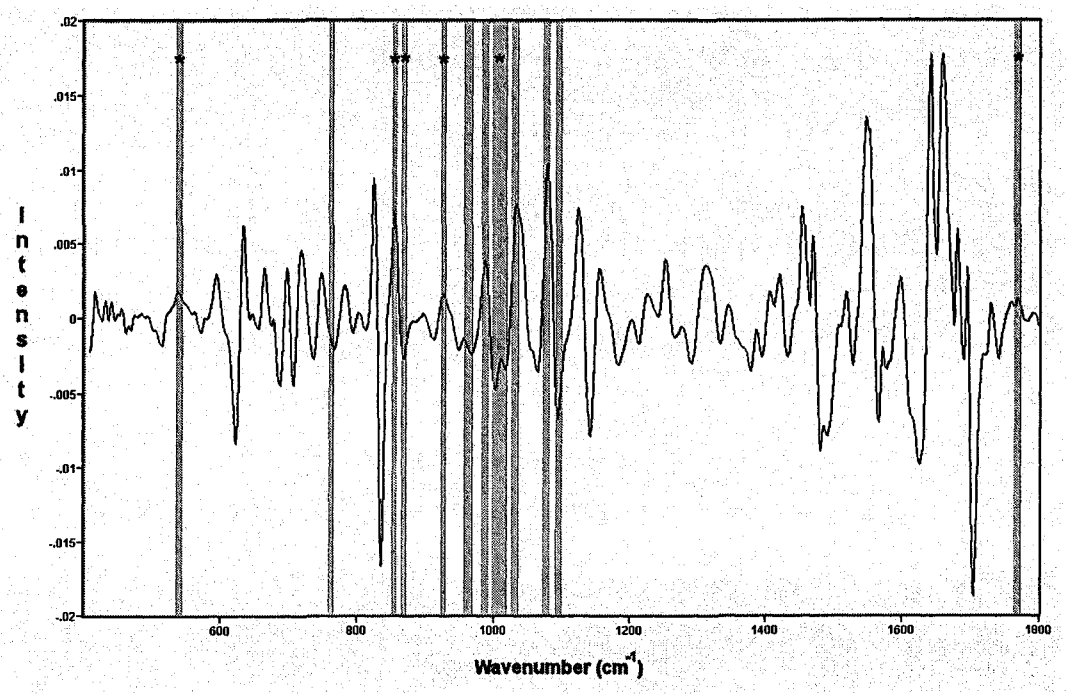

*Regions selected by the stepwise discriminant procedure for inclusion in the final classification model

Table 5.2 Classification table comparing clinical diagnosis to infrared-based diagnosis by use of LDA leave-one-out cross validation.

	Infrared-based diagnosis		
	Control	Osteochondrosis	Total
Clinical diagnosis			
Control	**25**	6	31
Osteochondrosis	9	**24**	33
Total	34	30	**64**

Numbers in bold indicate number of samples that were correctly classified

significantly influence the analysis. Based upon the identification of age as a significant determinant of outcome, the distributions of horses correctly classified and misclassified in each of 3 age categories are demonstrated in Table 5.3.

5.5 Discussion

Infrared spectroscopy in combination with feature extraction and selection methods may be successfully used to differentiate samples of OC affected horses from those of controls with an overall accuracy of 77%. Specifically, the alterations in features within 6 significant subregions may be associated with the presence or absence of disease, forming the basis for a classification algorithm. The information may be useful in designing studies for further infrared spectral classification in larger sample populations.

An alteration in the MIR spectra of synovial fluid from 2 horses with tarsocrural OC compared to control joints was first observed in horses less than 12 months old using reflectance spectroscopy (36). A visual comparison of the MIR spectra obtained from 8 control samples and 4 samples from OC affected joints revealed spectroscopic differences at 1000, 1035, 1115 and 1245 cm^{-1} (36). Statistical significance was not determined, and a multivariate classification algorithm was not developed. Despite the differences in the type of FT-IR spectroscopy employed (transmission versus reflectance) and sample preparation techniques between the studies, the wavenumbers of 1000 and 1035 cm^{-1} reported previously (36) were captured in 2 significant subregions (996 - 1019 cm^{-1} and 1027 - 1036 cm^{-1}) also

Table 5.3 Distribution of horses correctly classified and misclassified in each of 3 age categories

Group	Subgroup	Age category (years)			
		age < 2	2 ≤ age < 5	5 ≤ age < 7	Total
Control	Correct classification	0	21	4	25
	Misclassification	0	5	1	6
	Total	0	26	5	31
Osteochondrosis	Correct classification	14	10	0	24
	Misclassification	3	6	0	9
	Total	17	16	0	33

identified in this study. However, only one of these spectral features (1000 cm^{-1}) was captured with the spectral ranges contributing (996 - 1019 cm^{-1}) to the current final classification algorithm. The reason for this difference is unknown, but sample size and population differences between the 2 studies, particularly in age distribution of cases and controls, may be a contributing factor. For the current study, the inclusion of a larger number of samples within each disease class may be crucial for optimizing the extraction of the disease-relevant information from MIR spectra, thus permitting the meaningful detection of a greater number of statistically significant discriminatory MIR regions. The present classification success rate, although encouraging at 77%, may improve further in future FT-IR based studies of equine OC by using a still larger sample size. Such a large scale study would not only to improve the accuracy of this diagnostic test but also the range of applicability to a larger and more diverse diseased (clinical and subclinical) population.

The central concept underpinning the current study is that characteristic alterations in molecular synovial fluid constituents associated with joint disease lead to characteristic changes in IR absorption patterns (20, 21, 25, 27). While the specific molecular changes and species contributing to the features distinguishing the MIR spectra of OC from control joints have not been identified to date, it has been well established that IR spectra of biological samples reflect both the structure of the individual IR active constituents (including known and unknown biomarkers) and their relative abundance (28, 30). Alterations in known biomarker concentrations in synovial fluid have been reported in studies of equine OC using other methods. The

authors of these studies have proposed that alterations in biomarker concentrations are associated with either growth or pathogenesis of equine joint disease (15, 18, 37). The differences attributable to disease and age in the current IR study support this contention. To the authors' knowledge, none of the assays for known markers has been developed for routine diagnostic screening of horses for OC, and significant intra and inter assay variation may limit their accuracy in this role (14). The results of radiographic screening have also been shown to vary depending upon the age of the horse when examined and the joint affected, but may fail to diagnose cases with non-radiographic signs (6, 12). Similarly, the variation in correct classification rates in different age groups in the current study using FT-IR spectroscopy will need to be addressed before the test may be applied to screening of the general equine population for tarsocrural OC.

Alterations in CS-846 epitope and CPII associated with OC have been observed in young horses during musculoskeletal development, but not in mature horses (15). The presence of proteoglycan components in synovial fluid and serum may reflect both physiologic and pathologic cartilage extracellular matrix turnover (14, 16, 18, 38). In OC free equine joints, the highest concentration of glycosaminoglycans was detected in neonates (38). This parameter decreased with increasing age, with the effect of aging disappearing at 4 years (38). In the current feasibility study, the IR-based approach identified several spectral subregions within which the absorptions of proteoglycans would be expected to contribute prominently,

in particular the 996-1019 cm^{-1} region that lies within the range characteristic of carbohydrate C-O stretching vibrations (31, 39).

In agreement with the findings of previous studies investigating synovial fluid markers of OC, the search for the optimal IR signature of OC within the spectra may have to consider the dynamic nature of the disease process and to take into account physiological factors such as age, breed, and gender that may influence the pattern of MIR spectra (15, 17, 18, 37, 38, 40). In the current study, the wide age range of horses was controlled for in the statistical analysis to minimize bias. However it was clear from the rates of misclassification in the different age groups (Table 5.3) that this variable remains a possible confounder. Age has been shown to influence the expression of known biomarkers for OC (18, 37). Taking the age factor into account and quantifying group effects when adjusted for age are logical next steps toward the refinement and implementation of this diagnostic test. While the present samples were collected from clinical cases presented for evaluation, future studies designed to develop the IR-based test for application to the equine population at large should consider age, gender, and perhaps breed matched control selection (18, 37).

The conditions of prior probability may be adjusted based upon criteria such as the cost of misclassification and the proportion of sample size (35). Adjustment of this ratio may influence the sensitivity and specificity estimation. For this preliminary study, an equal prior probability was set assuming no prior knowledge on how the spectra should be classified or no preference for any group (35). The leave-one-out cross validation is a model validation method requires that each discriminatory

function is constructed by taking one spectrum out of the dataset (31). That spectrum is then used to validate the discriminatory model. This process is repeated for all spectra in the dataset until every single spectrum takes its turn to validate the model (31). This method was employed to enhance robustness of LDA classifier and has been proposed to be useful in classification of human arthritic disorders (21). With a limited numbers of horses, the total error rate of the dataset based on the cross validation method was 23%. A more accurate rate of classification of OC and control spectra may be achieved through the larger numbers of classification attributes (or spectral subregions) derived from larger sample size.

The misclassification rate within the OC group aged < 2 years was lower (18%) than the misclassification rate for horses > 2 years of age (37%) (Table 5.3). As alluded to above, it is possible that the significant features associated with OC in MIR spectra may be less prominent in older horses (38). In future studies it may also be possible to identify different age-dependent spectral features that allow the development of classifiers for OC that encompass variations attributable to growth as well as pathologic progression. Combination of theses attributes may probe a "real signature" within MIR spectra that is highly specific to the presence or absence of OC for all ages.

In conclusion, the current study demonstrated significant features in the FT-IR absorption pattern that were associated with OC. The differentiation of MIR spectra obtained from OC and control synovial fluid samples is feasible. The ultimate goal of this type of research is to develop novel tests that aid clinical and preclinical

diagnosis of joint disease in horses. Further study with a larger sample size including occult cases, and using matched controls, would further validate the clinical value of IR-based diagnosis of equine OC, and complete the transition to clinical utility.

References

(1) Beard WL, Bramlage LR, Schneider RK, Embertson RM. Postoperative racing performance in standardbreds and thoroughbreds with osteochondrosis of the tarsocrural joint: 109 cases (1984-1990). J Am Vet Med Assoc 1994;204:1655-1659.

(2) Grondahl AM, Engeland A. Influence of radiographically detectable orthopedic changes on racing performance in standardbred trotters. J Am Vet Med Assoc 1995;206:1013-1017.

(3) Jeffcott LB, Henson FM. Studies on growth cartilage in the horse and their application to aetiopathogenesis of dyschondroplasia (osteochondrosis). Vet J 1998;156:177-192.

(4) van Weeren PR, Barneveld A. Study design to evaluate the influence of exercise on the development of the musculoskeletal system of foals up to age 11 months. Equine Vet J 1999; Suppl 31:4-8.

(5) Alverado AF, Marcoux M, Breton L. The incidence of osteochondrosis in a Standardbred breeding farm in Quebec. 35th Am Assoc Equine Pract Proc, 1989:293-307.

(6) Carlsten J, Sandgren B, Dalin G. Development of osteochondrosis in the tarsocrural joint and osteochondral fragments in the fetlock joints of Standardbred trotters. I.a radiological survey. Equine Vet J Suppl 1993;16:42-47.

(7) Hoppe F, Philipsson J. A genetic study of osteochondrosis dissecans in Swedish horses. Equine Pract 1985;7:7-15.

(8) Sandgren B, Dalin G, Carlsten J. Osteochondrosis in the tarsocrural joint and osteochondral fragments in the fetlock joints in Standardbred trotters. I.Epidemiology. Equine Vet J 1993; Suppl 16:31-37.

(9) Harrison LJ, Edwards GB. Radiographic investigation of osteochondrosis. Eqiune Vet Educ 1996;8:172-176.

(10) Richardson DW. Diagnosis and management of osteochondrosis and osseous cyst-like lesions. In: Ross MW, Dyson SJ, eds. Diagnosis and management of lameness in the horse. Missouri: Saunders, 2003:549-556.

(11) McIntosh SC, McIlwraith CW. Natural history of femoropatellar osteochondrosis in three crops of Thoroughbreds. Equine Vet J 1993;Suppl 16:54-61.

(12) McIlwraith CW, Foerner JJ, Davis DM. Osteochondritis dissecans of the tarsocrural joint: results of treatment with arthroscopic surgery. Equine Vet J 1991;23:155-162.

(13) Tomlinson JE, Redding WR, Sage A. Ultrasonographic evaluation of tarsocrural joint cartilage in normal adult horses. Vet Radiol Ultrasound 2000;41:457-460.

(14) Billinghurst RC, Brama PA, van Weeren PR, Knowlton MS, McIlwraith CW. Evaluation of serum concentrations of biomarkers of skeletal metabolism and results of radiography as indicators of severity of osteochondrosis in foals. Am J Vet Res 2004;65:143-150.

(15) Laverty S, Ionescu M, Marcoux M, Boure L, Doize B, Poole AR. Alterations in cartilage type-II procollagen and aggrecan contents in synovial fluid in equine osteochondrosis. J Orthop Res 2000;18:399-405.

(16) McIlwraith CW, Billinghurst RC, Frisbie DD. Current and future diagnostic means to better characterize osteoarthritis in the horse- routine synovial fluid analysis and synovial fluid and serum markers. In *Proceedings.* 47th AAEP annual convention 2001;47:171-179.

(17) Poole AR. Biochemical/immunochemical biomarkers of osteoarthritis: utility for prediction of incident or progressive osteoarthritis. Rheum Dis Clin North Am 2003;29:803-818.

(18) Todhunter RJ, Fubini SL, Freeman KP, Lust G. Concentrations of keratan sulfate in plasma and synovial fluid from clinically normal horses and horses with joint disease. J Am Vet Med Assoc 1997;210:369-374.

(19) Gunzler H, Gremlich HU. Introduction. In: IR spectroscopy, an introduction. Weinheim: Wiley-VCH, 2006:1-7.

(20) Canvin JM, Bernatsky S, Hitchon CA, Jackson M, Sowa MG, Mansfield JR et al. Infrared spectroscopy: shedding light on synovitis in patients with rheumatoid arthritis. Rheumatology (Oxford) 2003;42:76-82.

(21) Eysel HH, Jackson M, Nikulin A, Somorjai RL, Thomson GTD, Mantsch HH. A novel diagnostic test for arthritis: multivariate analysis of infrared spectra of synovial fluid. Biospectroscopy 1997;3:161-167.

(22) Lasch P, Schmitt J, Beekes M, Udelhoven T, Eiden M, Fabian H et al. Antemortem identification of bovine spongiform encephalopathy from serum using infrared spectroscopy. Anal Chem 2003;75:6673-6678.

(23) Lasch P, Haensch W, Naumann D, Diem M. Imaging of colorectal adenocarcinoma using FT-IR microspectroscopy and cluster analysis. Biochim Biophys Acta 2004;1688:176-186.

(24) Schmitt J, Beekes M, Brauer A, Udelhoven T, Lasch P, Naumann D. Identification of scrapie infection from blood serum by Fourier transform infrared spectroscopy. Anal Chem 2002;74:3865-3868.

(25) Shaw RA, Kotowich S, Eysel HH, Jackson M, Thomson GT, Mantsch HH. Arthritis diagnosis based upon the near-infrared spectrum of synovial fluid. Rheumatol Int 1995;15:159-165.

(26) Shaw RA, Mantsch HH. Vibrational biospectroscopy: from plants to animals to humans. A historical perspective. J Mol Struct 1999;480-481:1-13.

(27) Staib A, Dolenko B, Fink DJ, Nikulin AE, Otto M, Pessin-Minsley MS et al. Disease pattern recognition testing for rheumatoid arthritis using infrared spectra of human serum. Clin Chim Acta 2001;308:79-89.

(28) Shaw RA, Mantsch HH. Infrared spectroscopy in clinical and diagnostic analysis. In: Meyers RA, ed. Encyclopedia of analytical chemistry. Chichester: John Wiley & Sons Ltd, 2000:83-102.

(29) Stuart BH. Infrared spectroscopy of biological Applications. In: Meyers RA, ed. Encyclopedia of analytical chemistry. Chichester: John Wiley & Sons Ltd., 2000:529-559.

(30) Dubois J, Shaw RA. IR spectroscopy in clinical and diagnostic applications. Anal Chem 2004;76:361A-367A.

(31) Jackson M, Mantsch HH. Infrared spectroscopy, ex vivo tissue analysis by. In: Meyers RA, ed. Encyclopedia of analytical chemistry. Chichester: John Wiley & Sons Ltd., 2000:131-156.

(32) Shaw RA, Mantsch HH. Multianalyte serum assays from mid-infrared spectra of dry films on glass slides. Appl Spectrosc 2000;54:885-889.

(33) Adams MJ. Feature selection and extraction. In: Barnett NW, ed. Chemometrics in analytical spectroscopy. Cambridge: Royal Society of Chemistry, 2004:55-95.

(34) Nikulin AE, Dolenko B, Bezabeh T, Somorjai RL. Near-optimal region selection for feature space reduction: novel preprocessing methods for classifying MR spectra. NMR Biomed 1998;11:209-216.

(35) Khattree R, Naik DN. Discriminant analysis. In: Multivariate data reduction and discrimination with SAS software. Cary: SAS Institute Inc, 2000:211-345.

(36) Muttini A, Petrizzi L, Tinti A, Bertoluzza A. Synovial fluid parameters in normal and osteochondritic hocks of horses with open physis. Boll Soc Ital Biol Sper 1994;70:337-344.

(37) Brama PAJ, TeKoppele JM, Beekman B, van Weeren PR, Barneveld A. Matrix metalloproteinase activity in equine synovial fluid: influence of age, osteoarthritis, and osteochondrosis. Ann Rheum Dis 1998;57:697-699.

(38) van den Boom R, Brama PA, Kiers GH, de Groot J, van Weeren PR. Assessment of the effects of age and joint disease on hydroxyproline and glycosaminoglycan concentrations in synovial fluid from the metacarpophalangeal joint of horses. Am J Vet Res 2004;65:296-302.

(39) Jackson M., Eysel HH, Shaw RA, Glen T.D., Mantsch H. Non-subjective Diagnosis of Arthritic disorders by multivaliate analysis of IR spectra of synovial fluid. In: Merlin J.C., ed. Sixth European conference on the spectroscopy of biological molecules. Dordrecht: Kluwer Academic Publishers, 1995:499-500.

(40) Brama PA, van den BR, DeGroott J, Kiers GH, van Weeren PR. Collagenase-1 (MMP-1) activity in equine synovial fluid: influence of age, joint pathology, exercise and repeated arthrocentesis. Equine Vet J 2004;36:34-40.

CHAPTER 6

CONCLUDING REMARKS

This dissertation focuses on 4 main topics; the technical development of methods for infrared spectroscopy-based analysis of synovial fluid (SF) in horses, the natural variation in mid-infrared (MIR) absorption patterns of SF attributable to the differences in anatomical location of the joints, the characteristic features of MIR absorption patterns that differentiate the SF samples of diseased joints from controls, and the feasibility assessment of using MIR spectroscopy for diagnosis of joint diseases in horses. The ultimate goal of the current research was to develop MIR spectroscopic techniques for the diagnosis and characterization of equine joint diseases.

The research project met the criteria for an exploratory (early) phase project with regards to a guideline for the design of diagnostic accuracy studies (1), to determine the feasibility of MIR spectroscopy and classification algorithms in the diagnosis of equine joint diseases. The essence of the current research project will be encapsulated in this chapter within the three following sections: summary of the main findings, significance and implications of the results, and recommendations and suggestions for the direction of future research.

6.1 Summary of the main findings

In Chapter 2, the techniques required for MIR spectroscopy of dried films were optimized for SF collected from the joints of horses. The sample preparation,

the MIR spectral acquisition, and the procedures to enhance spectroscopic data were optimized to yield the following protocol, which was followed for all spectroscopic measurements conducted during the current research project. Sample preparations of 3:1 SF to aqueous potassium thiocyanate solution were deposited as 8 μL aliquots onto the custom-made silicon plate (2). A randomized block design was applied to randomly assign samples to the plate and the well position prior to deposition of samples. It was felt that this experimental design helps guard against possible sources of bias involving the instruments and measurement techniques in the early phase of the development of a new diagnostic test. The MIR spectra were recorded using a Fourier transform infrared (FT-IR) spectrometer. For each spectrum, 512 interferograms were coadded at a spectral resolution of 4 cm^{-1}, and a Blackman-Harris 3-term apodization function applied to the coadded interferogram prior to Fourier transformation. The overall MIR absorption pattern of equine SF derived from our laboratory protocol is similar to the MIR absorption pattern of human SF reported in the literature (3). Four main preprocessing techniques were employed for the spectroscopic studies in this dissertation including spectral averaging, subtraction, normalization, and differentiation/smoothing. We found the spectral preprocessing techniques useful for the enhancement of spectroscopic features and transformation of spectroscopic data into a form that was suitable for statistical analysis. The preprocessing techniques were carefully optimized for each data set to achieve the best possible classification results.

In Chapter 3, inter-articular variability was studied with the objective of identifying significant differences due to natural variations among anatomical types of high motion joints (antebrachiocarpal (AC), midcarpal (MC) and tarsocrural (TC)), and left versus right limbs in the same horses. Inter-articular variability may affect the pattern of MIR spectra derived from SF of clinically normal joints. In this study, we found that the pattern of MIR spectra of SF samples from the same type of joint is likely to be similar when the left and right side were compared within a horse. Differences in spectral features between ipsililateral AC and MC spectra within the same horse were significant, but comparisons between the spectra of carpal and TC joints revealed many more discriminatory absorption bands. Although there were sufficient data to demonstrate these differences, the sample size was not sufficient to characterize the typical IR signature for each of the joint types, or to develop a classification strategy that might identify which of the many significant features identified contributed most to discriminating among these joints. The results from the current study were sufficient to suggest that the inter-articular variation within the same horse should be considered in study designs, and that the biochemical response to the same disease is likely to vary as a function of joint location. Researchers should proceed with caution when using different types of joints for spectra comparisons either within subjects or between subjects. Further normal samples should be evaluated to better characterize the range and significance of IR spectral changes detected.

In Chapter 4 we examined the feasibility of using MIR spectroscopy of SF for the diagnosis of traumatic arthritis in racing horses based on the comparison of spectroscopic data derived from SF samples of the affected and control joints. Temporally this was the first experiment conducted due to reasons of sample availability. However, because traumatic arthritis represents a severe form of joint disease in which progressive degenerative changes are followed by catastrophic osteochondral failure, it was thought that this disease would be an appropriate first test of the feasibility of IR spectroscopy of SF for the diagnosis of equine joint disease. The MIR spectroscopic patterns of SF from joints with traumatic arthritis differed significantly from the corresponding patterns for controls. A classification model was developed based upon characteristics of 3 MIR regions that classified spectra from the calibration dataset with an overall accuracy of 97% (sensitivity 93%; specificity 100%). The same model with cost-adjusted prior probabilities of 0.60:0.40 produced an overall accuracy of 89% (sensitivity 83%; specificity 100%) for a validation sample dataset, and 100% correct classification for a second set consisting of independent normal control joints. This study confirmed the hypothesis that characteristic alterations in IR absorption patterns may be discovered and exploited via an appropriate feature selection and classification algorithm to differentiate the spectra of diseased joints from those of controls. The development of appropriate classification techniques proved difficult as it involved a level of modeling outside the experience of many veterinary researchers. Nevertheless this experiment (now published) clearly demonstrated the feasibility of this approach to diagnose joint

disease in the horse. Further recruitment of cases and normal control horses is anticipated to develop and expand the scope of applications, and is necessary to validate the clinical value and accuracy of the method for screening and diagnosing patients with joint disease in the larger equine population.

In Chapter 5 the feasibility of using MIR spectroscopy of SF for the diagnosis of tarsocrural osteochondrosis (OC) in horses was illustrated based on comparison of spectroscopic data derived from SF samples of the affected and control joints. Disease-associated characteristics within MIR spectroscopic patterns of SF were identified using a statistical approach and used for spectral classification purposes. By the use of linear discriminant analysis to classify the spectra, based on the characteristics of 6 MIR regions and leave-one-out cross validation, SF spectra derived from samples of joints with OC were differentiated from the control samples with an overall accuracy of 77% (81% specificity and 73% sensitivity). While confirming that IR-based diagnosis of OC is possible, this study further highlighted one of the major difficulties associated with the study of joint disease – its dynamic nature. That is to say that age, and the progression of the disease, affected the classification of OC spectra. In conclusion, this study demonstrated significant features in the FT-IR absorption pattern that were associated with OC, and hence that the differentiation of MIR spectra obtained from OC and control SF samples is feasible. Further study with a larger sample size including occult cases, and using matched controls, would further establish and validate the clinical value of IR-based diagnosis of equine OC, and complete the transition to clinical utility.

6.2 Significance and implications of the results

Changes in the composition of SF in concert with or as a response to the presence of disease, provides a basis for the diagnosis of joint diseases for both conventional SF analyses and novel molecular analyses of biomarkers (4-6). Various biochemical, immunological, and molecular methods have been employed to develop assays for specific biomarkers and various other SF constituents (7-12). In the current research, we proposed the use of FT-IR spectroscopy to detect characteristic diagnostic signatures in the IR absorption pattern of SF. Infrared absorption patterns for equine SF samples, measured using laboratory techniques developed in the course of the current research project, were comparable to SF spectra for human samples (3). Our study confirmed the reported advantages of MIR spectroscopy: with the exception of a simple aqueous diluent (4 g/L potassium thiocyanate in water), no reagents were required for spectroscopic analysis of SF because all infrared active constituents gave rise to absorption bands without any need for chemical or immunological modification; the laboratory techniques, once developed, were relatively simple and fast; only small amount of sample (8 μL) was required for spectroscopic analysis; and batch analyses of samples were performed at low cost.

We have pursued exploratory studies to determine the feasibility of using MIR spectroscopy and classification algorithms for diagnosis of equine joint diseases. Initially we had hoped to investigate a range of joint disorders, but challenges in the time required to develop expertise in this field, and difficulty in recruiting a large number of samples from clinical cases with the consent of owners led to a

rationalization of the initial project goals. As a consequence, two articular disorders, traumatic arthritis and osteochondrosis, were chosen to examine the diagnostic potential of this technique as an ex-vivo test. The preliminary results addressed our hypothesis that the IR spectra of SF can serve as biochemical fingerprints with sufficient latent information to permit the diagnosis of traumatic arthritis and osteochondrosis in horses by means of discriminant analysis. These findings favor the further development of this method in the diagnosis of joint diseases in horses. The lack of an affordable and accessible gold standard for diagnosing equine joint disease remains a significant challenge for the development of IR-based diagnostic technique, as does the recruitment of large numbers of well characterized samples. The extraction of genuine spectroscopic characteristics of traumatic arthritis and osteochondrosis may require the recruitment of large number of samples from both disease groups as well as other types of joint disease (e.g. septic arthritis) to develop an appropriate algorithm that capable of distinguishing among different types of joint disease. However, with future endeavors targeted towards its development, the ultimate goal of this type of research, to provide a rapid, economical, practical, and reliable means for objective evaluation of joint disease, as well as an unbiased monitoring of response to treatment can be accomplished.

6.3 Recommendations and direction for future research

In the initial phase, we have obtained evidence for the natural biochemical variability of SF composition among anatomically different types of joints (inter-

articular variation). Other possible sources of natural variation may include intra-subject and inter-subject variability associated with physiological, genetic, environmental factors, age, breed, sex, activity, occupation, and circadian rhythm (13). These possible sources of variation need to be characterized systematically and considered (as required) in future study design. The reproducibility of IR spectra may be affected by subtle instrumental and environmental variables. Considerable efforts were made to correct and to guard against possible biases from the instrumental and environmental sources of variation in the current research. We recommend minimizing such variability in the future by improving the design of the next generation of silicon plate and customization of the plate holder to correct for the imperfect positioning of modulated exiting beam onto the sample well situated on the silicon plate. To minimize environmental effects, the IR spectroscopic measurements should be conducted in appropriately controlled environment. The installation of a purging system on the multisampler compartment of the FT-IR spectrometer to reduce the effects of atmospheric water vapor and carbon dioxide on spectral noise on the instrument detector is suggested.

According to the current research laboratory protocol, after centrifugation, the cell portion was discarded. This portion may provide some useful information in diagnosis of joint disease either by studying IR absorption by the DNA content of the cells or the cytoplasmic contents. Future researchers may choose to focus on the IR spectroscopy of the cellular portion of SF. However, the development and

optimization of an optimal IR spectroscopic measurement protocol is required for the cell specimens, as are appropriate cell isolation and sample storage protocols.

The identification of IR spectral features suitable for the classification of disease often leads to questions regarding the constituent molecules contributing to those spectral features. Additional procedures could be added to the sample preparation process. The fractionation of the biological fluid composition using high performance liquid chromatography (HPLC) has been utilized prior to spectroscopic measurement in one study (14). A novel technology has also been reported using silicon nanoparticles as the substrate for immobilization of a particular protein of interest, followed by characterization of the protein attached to those particles by the use of FT-IR spectroscopy (15). The combination of nanobead-based technology and FT-IR spectroscopy may increase the sensitivity to detect cytokines, DNA or enzymes (15). This may open up the opportunity for development of advanced IR-based diagnosis in the near future. In addition, IR spectroscopy combined with other technologies such as nuclear magnetic resonance (NMR) and Raman spectroscopies, mass spectrometry and protein arrays may better serve for the structural identification and protein characterization purposes (15, 16). However, additional complex preparatory work prior to spectroscopic measurement and the use of other technologies may be conducted with the cost of increasing expense and time required to perform sample analysis. The latter disadvantages are undesirable when developing tests for clinical screening and diagnosis.

In future studies, the classification models may be improved and refined by the inclusion of more spectra. To our knowledge, firm recommendations for the calculation of sample size for multivariate spectral classification have not been reported. In fact, the development of IR-based diagnosis depends critically on the collection of a large number of spectra and their corresponding (true) disease status (17). Ideally, the search for genuine signature of disease in the spectra (optimal region selection procedure) requires a large number of spectra to encompass all possible spectral variations associated with the presence of particular disease of interest in the population at large (17). Sample size was a critical issue in all 3 experiments presented in this thesis. We support the use of the general guidelines for the design of diagnostic accuracy studies, and for justifying the sample size (1). According to these guidelines (1), the architecture of diagnostic accuracy research consists of three phases, the exploratory (n = 10-50), challenge (n = 10-100), and clinical phases (the number of subjects equivalent to several hundreds).

In order to expand the usefulness of IR spectroscopy in the field of arthrology, the application of this technique should not be confined to the uses based only upon qualitative analyses (i.e. to correlate spectroscopic data to the presence or absence of joint disease). Infrared-based analysis could be focused on the development of automated, reagent free analytical tools for routinely clinical use (2). The demonstrated potential of IR-based analysis in clinical chemistry to quantify several analytes in whole blood, serum, urine, and milk samples (18-23), suggests possibilities in quantifying some useful SF parameters (that could be passive

biomarkers or indicators for joint diseases) such as nucleated cell counts, protein, glucose, urea, and lipid concentrations within a single spectroscopic measurement (24-26). Concentrations of other important SF compositions such as hyaluronan and proteoglycan (e.g. chondroitin sulfate, keratan sulfate etc.) contents (that could be potential biomarkers for joint diseases) may be quantified by the use of IR spectroscopic measurement and appropriate algorithms (24, 27, 28). If the quantitative IR spectroscopic techniques for SF analysis could be successfully developed, this technique would complement the diagnostic fingerprinting approach developed within this thesis work. The implementation in arthrology of either quantitative or qualitative (IR pathology) analysis of IR spectra should be expanded to other species such as canine, feline and laboratory animals. The success in developing IR-based veterinary diagnostic tests may contribute benefits to both humans and animals by offering better disease detection and monitoring methods. These in turn would trigger more rapid and appropriate prevention strategies and treatment regimens, thus improving the quality of life for both human and animal patients.

Finally, once the satisfactory differentiation of the diseased from normal conditions can be achieved, future research should aim at disease staging. Joint disease staging, as it currently stands, is often based on subjective classification system that categorizes patients into homogenous clusters based on degrees of severity or clinical signs of a particular disease. Infrared analyses may offer objective classification of arthritis based upon discrete and objectively selected IR spectral

features. For instance, based upon spectroscopic features of SF spectra, traumatic arthritis horses may potentially be subcategorized into either acute or chronic stages accompanied by the presence of osteoarthritis. Osteochondritic horses may potentially be subcategorized as horses that have OC and are actively growing (young), horses that have OC and are undergoing adaptation to training, and horses that have chronic OC where the joints are also developing osteoarthritis as a consequence. The diagnostic results based on an IR-based disease staging system may provide more useful diagnostic information that best represents the pathophysiologic manifestation of joint disease. A disease staging system would further assist the decision making in medical or surgical treatment selection and expected treatment outcomes and would also provide an accurate prognosis of the joint disease. In addition, IR-based technique may serve as a screening tool for the detections of traumatic arthritis and osteochondrosis as well as other types of joint disorder in horse population followed by the use of other image modalities to confirm the final diagnosis. The improvement and refinement of the classification model to achieve as high as possible sensitivity and specificity are crucial for the development of the screening test for diagnosis of joint diseases. However, an appropriate study design by inclusion of more than one type of joint disease (e.g. traumatic arthritis, osteochondrosis, septic arthritis and normal controls etc.) with a large number of spectra in each disease category would be required to evaluate the clinical effectiveness in clinical settings and the prognostic impact on the population at large (1, 29).

References

(1) Zhou XH, Obuchowski NA, McClish DK. The design of diagnostic accuracy studies. In: Statistical methods in diagnostic medicine. New York: John Wiley & Sons, Inc., 2002:57-99.

(2) Shaw RA, Low-Ying S, Man A, Liu KZ. Reagent-free clinical analysis and diagnostics: laboratory medicine in a new light. IVD Technology 2003;9:43-49.

(3) Jackson M., Eysel HH, Shaw RA, Glen T.D., Mantsch H. Non-subjective Diagnosis of Arthritic disorders by multivaliate analysis of IR spectra of synovial fluid. In: Merlin J.C., eds. Sixth European conference on the spectroscopy of biological molecules. Dordrecht: Kluwer Academic Publishers, 1995:499-500.

(4) McIlwraith CW, Billinghurst RC, Frisbie DD. Current and future diagnosis means to better characterize osteoarthritis in the horse - routine synovial fluid analysis and synovial fluid and serum markers. In *proceedings*: 47th AAEP annual convention 2001;47:171-179.

(5) McIlwraith CW. Use of synovial fluid and serum biomarkers in equine bone and joint disease: a review. Equine Vet J 2005;37:473-482.

(6) Punzi L, Oliviero F, Plebani M. New biochemical insights into the pathogenesis of osteoarthritis and the role of laboratory investigations in clinical assessment. Crit Rev Clin Lab Sci 2005;42:279-309.

(7) Billinghurst RC, Buxton EM, Edwards MG, McGraw MS, McIlwraith CW. Use of an antineoepitope antibody for identification of type-II collagen degradation in equine articular cartilage. Am J Vet Res 2001;62:1031-1039.

(8) Chu Q, Lopez M, Hayashi K, Ionescu M, Billinghurst RC, Johnson KA et al. Elevation of a collagenase generated type II collagen neoepitope and proteoglycan epitopes in synovial fluid following induction of joint instability in the dog. Osteoarthritis Cartilage 2002;10:662-669.

(9) de Grauw JC, Brama PA, Wiemer P, Brommer H, van de Lest CH, van Weeren PR. Cartilage-derived biomarkers and lipid mediators of inflammation in horses with osteochondritis dissecans of the distal intermediate ridge of the tibia. Am J Vet Res 2006;67:1156-1162.

(10) Fujita Y, Hara Y, Nezu Y, Yamaguchi S, Schulz KS, Tagawa M. Direct and indirect markers of cartilage metabolism in synovial fluid obtained from dogs with hip dysplasia and correlation with clinical and radiographic variables. Am J Vet Res 2005;66:2028-2033.

(11) Matyas JR, Atley L, Ionescu M, Eyre DR, Poole AR. Analysis of cartilage biomarkers in the early phases of canine experimental osteoarthritis. Arthritis Rheum 2004;50:543-552.

(12) Skioldebrand E, Heinegard D, Eloranta ML, Nilsson G, Dudhia J, Sandgren B et al. Enhanced concentration of COMP (cartilage oligomeric matrix protein) in osteochondral fractures from racing Thoroughbreds. J Orthop Res 2005; 23:156-163.

(13) Poole AR. Biochemical/immunochemical biomarkers of osteoarthritis: utility for prediction of incident or progressive osteoarthritis. Rheum Dis Clin North Am 2003;29:803-818.

(14) Fabian H, Lasch P, Naumann D. Analysis of biofluids in aqueous environment based on mid-infrared spectroscopy. J Biomed Opt 2005;10:031103.

(15) Wang C, Zhang Y, Seng HS, Ngo LL. Nanoparticle-assisted micropatterning of active proteins on solid substrate. Biosens Bioelectron 2006; 21:1638-1643.

(16) Alkrad JA, Mrestani Y, Stroehl D, Wartewig S, Neubert R. Characterization of enzymatically digested hyaluronic acid using NMR, Raman, IR, and UV-Vis spectroscopies. J Pharm Biomed Anal 2003;31:545-550.

(17) Dubois J, Shaw RA. IR spectroscopy in clinical and diagnostic applications. Anal Chem 2004;76:360A-367A.

(18) Tsenkova R, Atanassova S, Kawano S, Toyoda K. Somatic cell count determination in cow's milk by near-infrared spectroscopy: a new diagnostic tool. J Anim Sci 2001;79:2550-2557.

(19) Liu KZ, Shaw RA, Man A, Dembinski TC, Mantsch HH. Reagent-free, simultaneous determination of serum cholesterol in HDL and LDL by infrared spectroscopy. Clin Chem 2002;48:499-506.

(20) Low-Ying S, Shaw RA, Leroux M, Mantsch HH. Quantitation of glucose and urea in whole blood by mid-infrared spectroscopy of dry films. Vib Spectrosc 2002;28:111-116.

(21) Shaw RA, Kotowich S, Leroux M, Mantsch HH. Multianalyte serum analysis using mid-infrared spectroscopy. Ann Clin Biochem 1998;35:624-632.

(22) Shaw RA, Mantsch H. Vibrational spectroscopy applications in clinical chemistry. In: Chalmers JM, Griffiths PR, eds. Handbook of vibrational spectroscopy. 2002:3295-3307.

(23) Shaw RA, Low-Ying S, Leroux M, Mantsch HH. Toward reagent-free clinical analysis: Quantitation of urine urea, creatinine, and total protein from the mid-infrared spectra of dried urine films. Clinical Chemistry 2000;46:1493-1495.

(24) Budsberg SC, Lenz ME, Thonar EJ. Serum and synovial fluid concentrations of keratan sulfate and hyaluronan in dogs with induced stifle joint osteoarthritis following cranial cruciate ligament transection. Am J Vet Res 2006; 67:429-432.

(25) Kraus VB, Huebner JL, Fink C, King JB, Brown S, Vail TP et al. Urea as a passive transport marker for arthritis biomarker studies. Arthritis Rheum 2002; 46:420-427.

(26) Pascual E, Jovani V. Synovial fluid analysis. Best Pract Res Clin Rheumatol 2005;19:371-386.

(27) Elsaid KA, Jay GD, Chichester CO. Detection of collagen type II and proteoglycans in the synovial fluids of patients diagnosed with non-infectious knee

joint synovitis indicates early damage to the articular cartilage matrix. Osteoarthritis Cartilage 2003;11:673-680.

(28) Sharif M, Osborne DJ, Meadows K, Woodhouse SM, Colvin EM, Shepstone L et al. The relevance of chondroitin and keratan sulphate markers in normal and arthritic synovial fluid. Br J Rheumatol 1996;35:951-957.

(29) Sackett DL, Haynes RB. The architecture of diagnostic research. In: Knottnerus JA, eds. The evidence base of clinical diagnosis. London: BMJ publishing group, 2002:19-38.

Appendix 1 Infrared spectra of 95 wells on a silicon plate without deposition of any sample (a set of flat lines) and the IR spectra derived from the deposition of a sample onto 95 wells

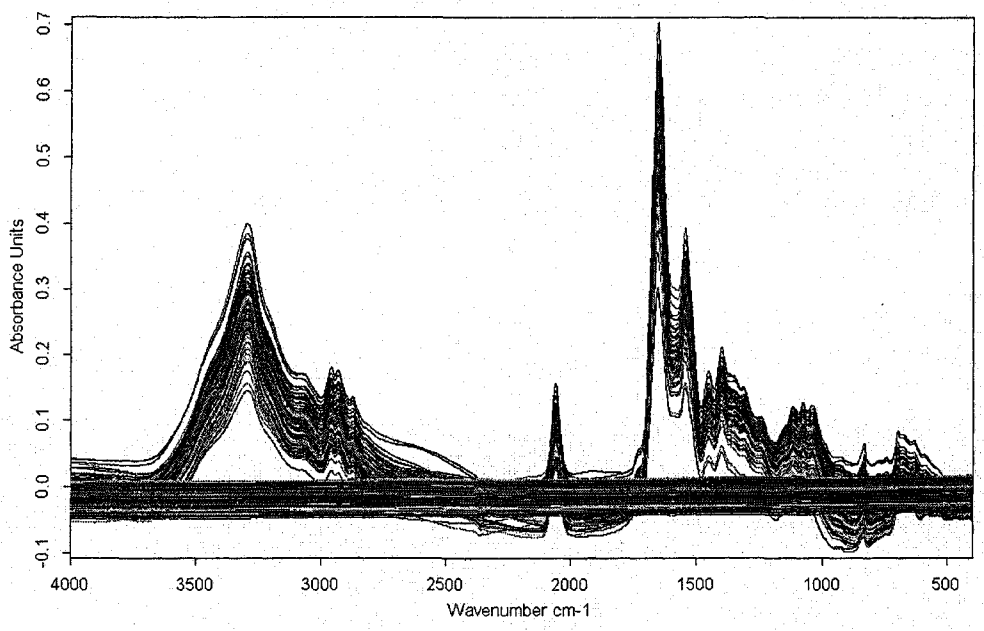

Note: The absorbance unit of spectra of a silicon plate without deposition of any samples are essentially situated below zero level.

Appendix 2 The plot of 2nd order differential intensity (absorb) at 1246 cm^{-1} for each of 95 wells in 3 different plates (well 1-95 corresponds to well order in plate 1, well 96-190 corresponds to well order in plate 2, and well 191- 285 corresponds to well order in plate 3)

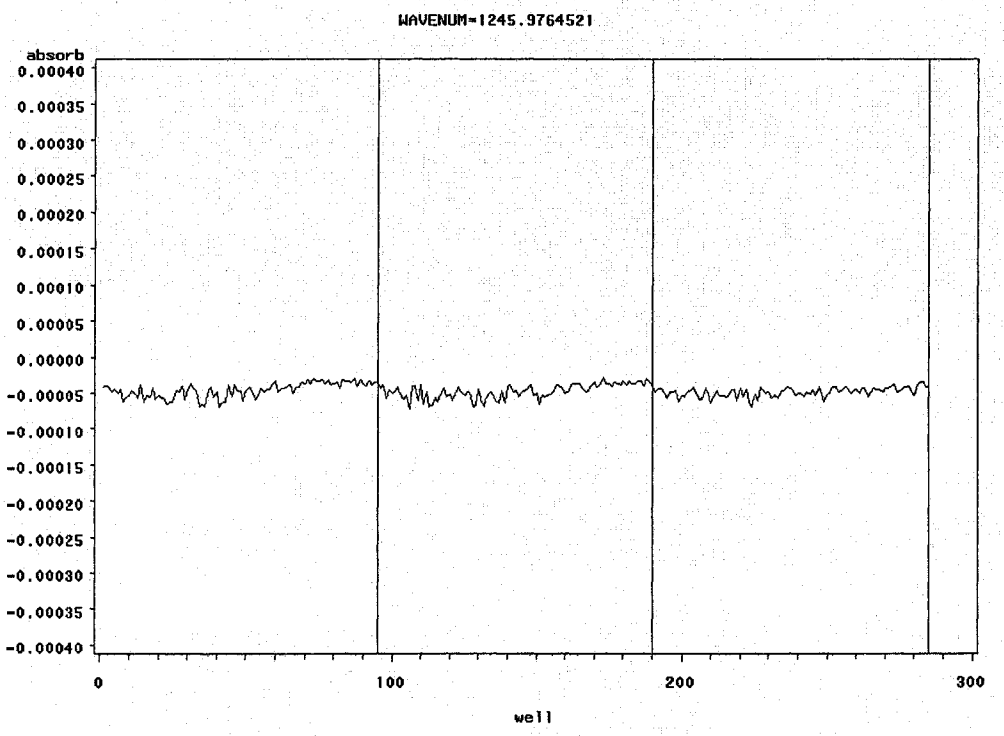

Note: the low within-plate variation with values distributed about the mean with no pattern. The vertical lines are to separate sets of wells of different plates.

Appendix 3 The plot of 2nd order differential intensity (absorb) at 2058 cm^{-1} for each of 95 wells in 3 different plates (well 1-95 corresponds to well order in plate 1, well 96-190 corresponds to well order in plate 2, and well 191- 285 corresponds to well order in plate 3)

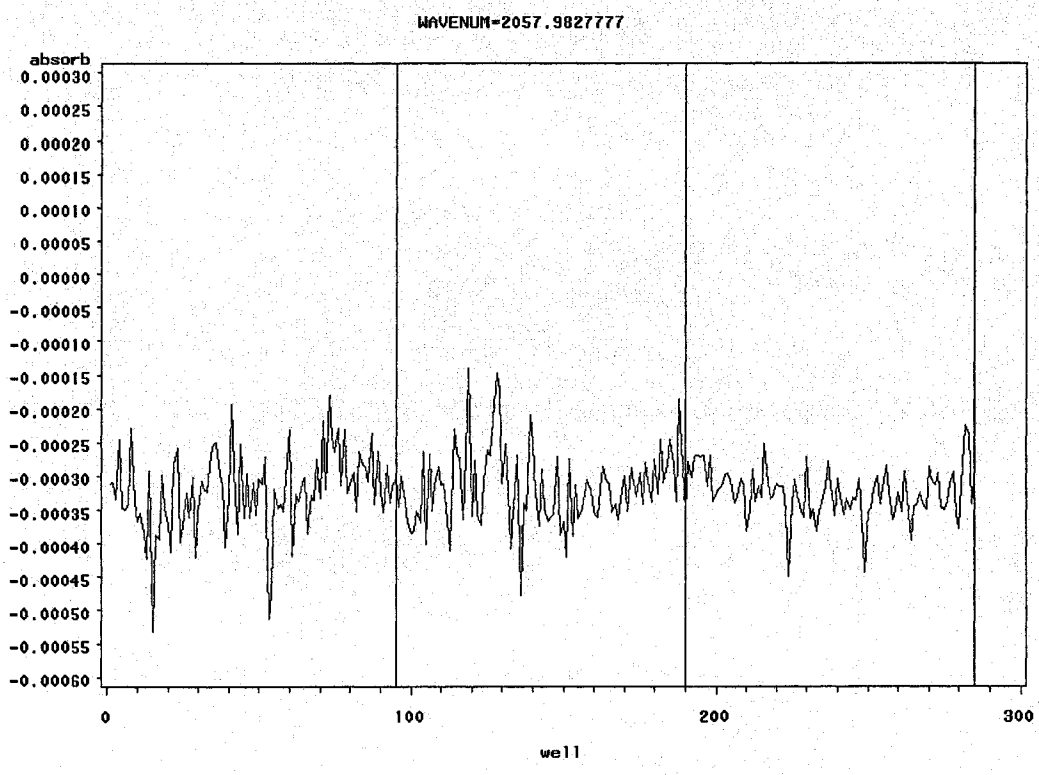

Note: The high within-plate variation and value distributed about the mean with no pattern. The vertical lines are to separate sets of wells of different plates.

Appendix 4 The plot of 2nd order differential intensity (absorb) at 3633 cm^{-1} for each of 95 wells in 3 different plates (well 1-95 corresponds to well order in plate 1, well 96-190 corresponds to well order in plate 2, and well 191- 285 corresponds to well order in plate 3)

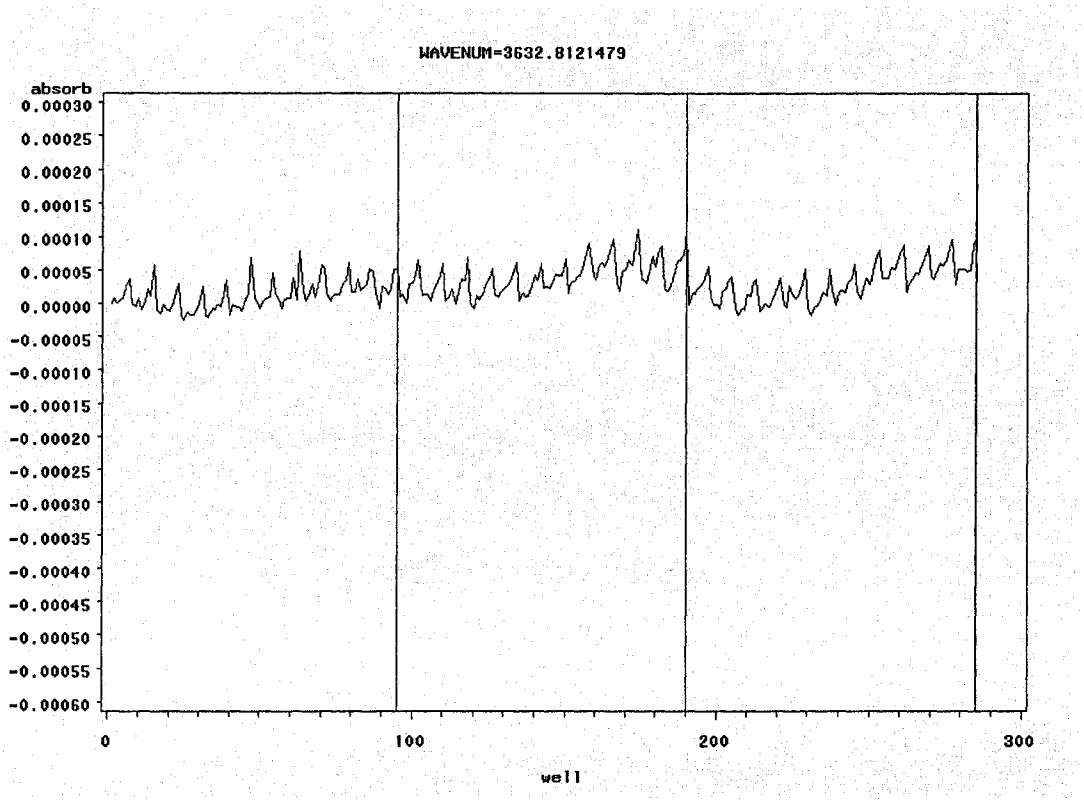

Note: Low within-plate variation, value distributed about the mean with some pattern, no differences among plates. The vertical lines are to separate sets of wells of different plates.

Appendix 5 The plot of 2nd order differential intensity (absorb) at 668 cm^{-1} for each of 95 wells in 3 different plates (well 1-95 corresponds to well order in plate 1, well 96-190 corresponds to well order in plate 2, and well 191- 285 corresponds to well order in plate 3)

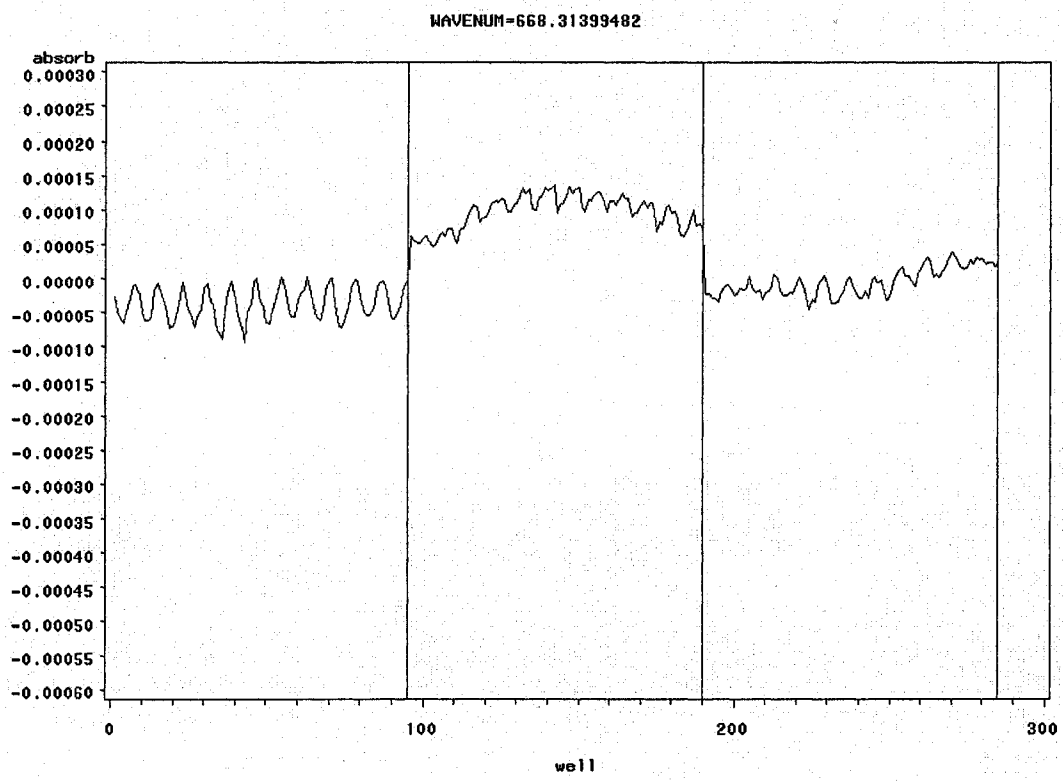

Note: Low within-plate variation, value distributed about the mean with some pattern and disparities among plates. The vertical lines are to separate sets of wells of different plates.

Appendix 6 The plot of 2nd order differential intensity (absorb) at 1658 cm^{-1} for each of 95 wells in 3 different plates (well 1-95 corresponds to well order in plate 1, well 96-190 corresponds to well order in plate 2, and well 191- 285 corresponds to well order in plate 3)

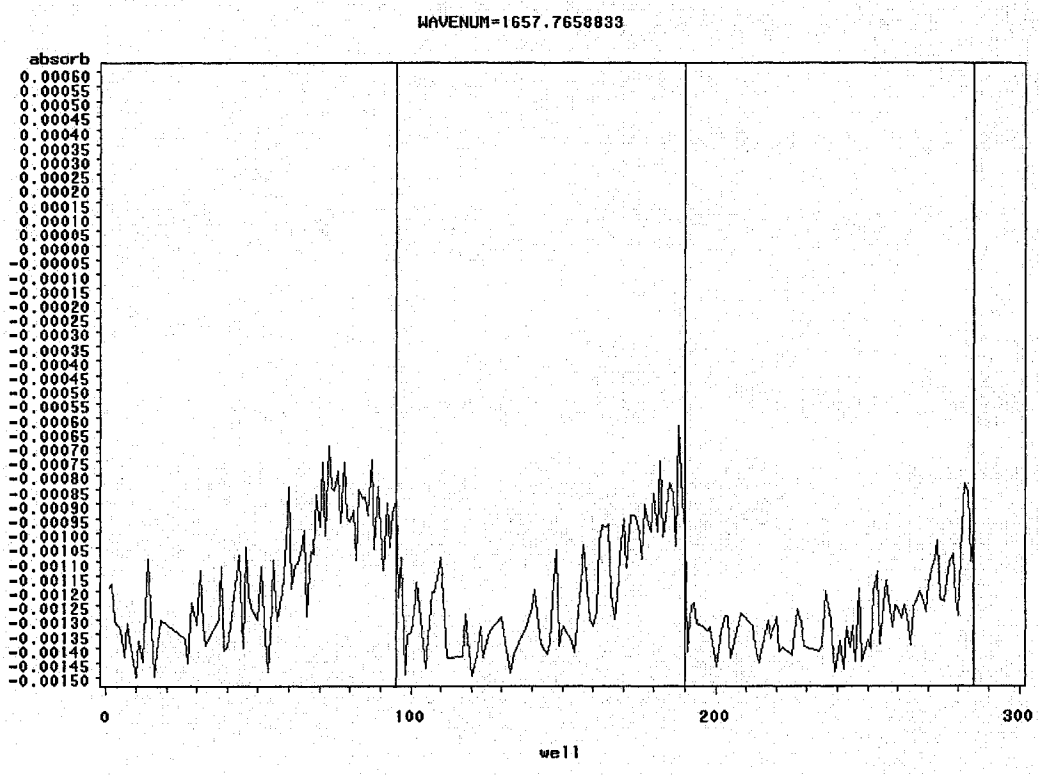

Note: High within-plate variation, value distributed about the mean with some pattern. The vertical lines are to separate sets of wells of different plates.

Appendix 7 The spectroscopic data preprocessing and classification strategies

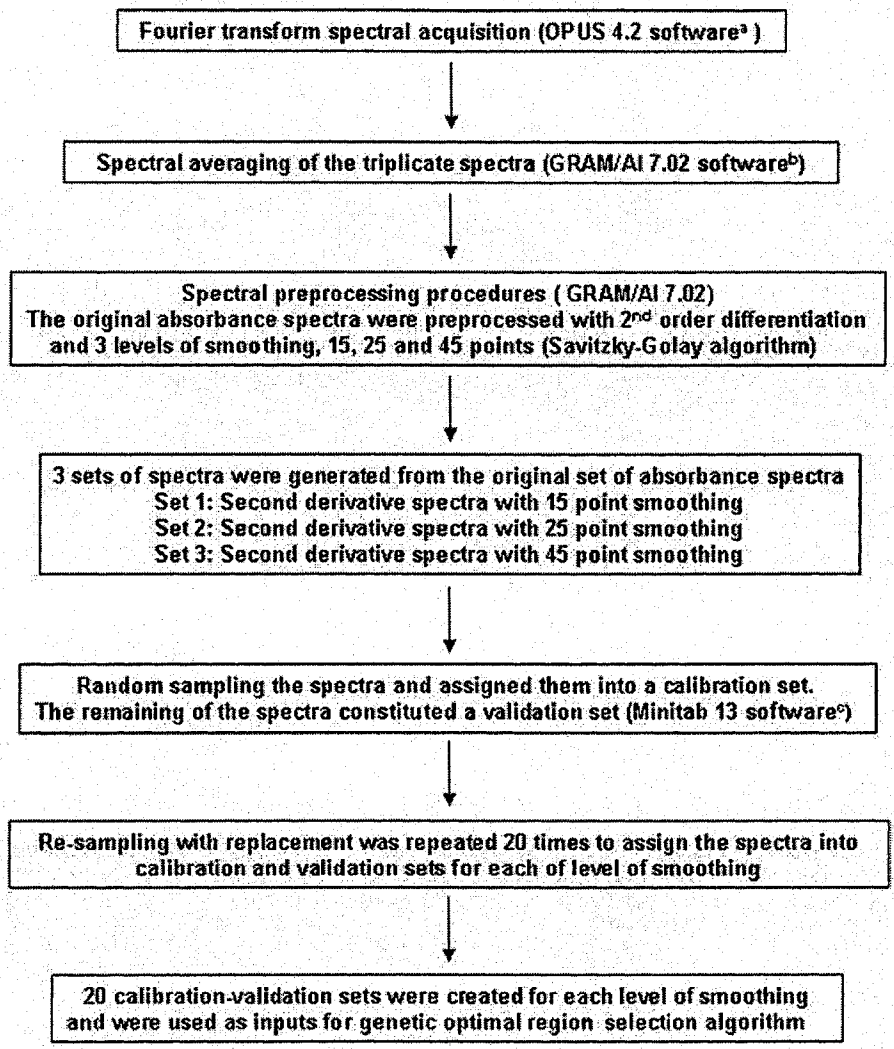

Note: [a] OPUS 4.2, Bruker Optik GmbH, Ettlingen, Germany

[b] GRAMS/AI 7.02, Thermo Galactic, Salem, NH, USA

[c] Minitab 13, Minitab Inc., College, PA, USA

Appendix 7 The spectroscopic data preprocessing and classification strategies

(continue from previous page)

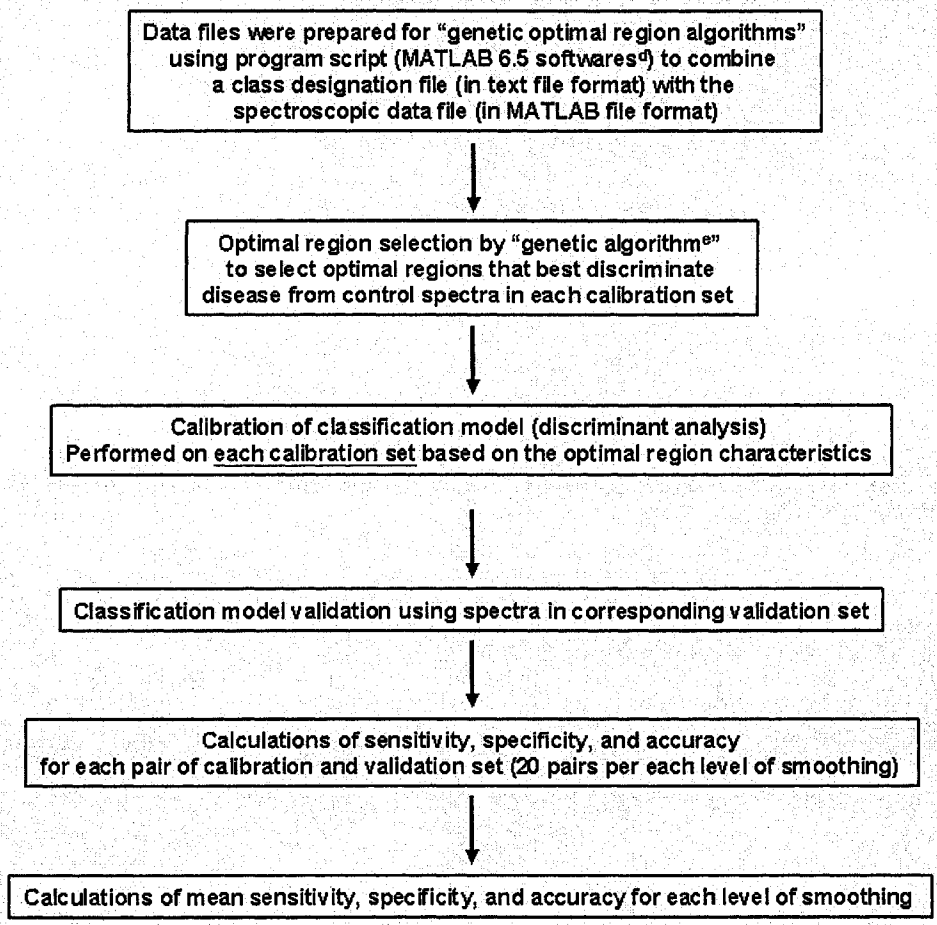

Note: [d] MATLAB, MathWorks, Natick, MA, USA

[e] The Institute for Biodiagnostics, National Research Council of Canada, Winnipeg, MB, Canada

Appendix 8 Number of samples with respect to anatomical location of joints in affected (traumatic arthritis) and control groups

Study Joints	Traumatic arthritic group	Control group
Fetlock	15	3
Antebrachiocarpal	10	16
Midcarpal	28	22
Total	**53**	**41**

Appendix 9.1 Three optimal regions selected by genetic algorithm for 20 pairs of calibration-validation sets of spectra in traumatic arthritis dataset (TT1-TT20) when preprocessing with 2nd order differentiation and 15 point smoothing technique (Savitzky-Golay algorithm)

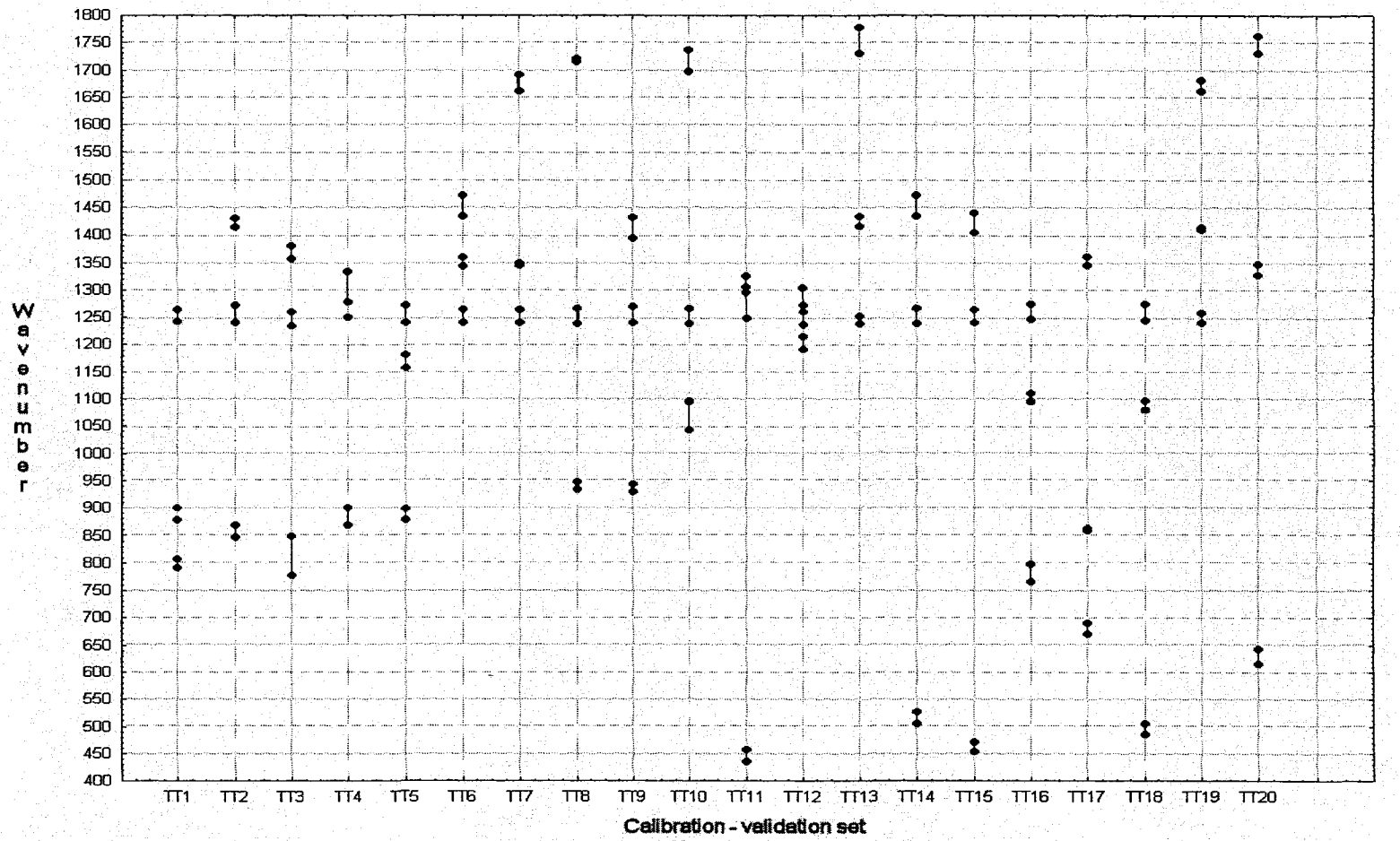

Appendix 9.2 Three optimal regions selected by genetic algorithm for 20 pairs of calibration-validation sets of spectra in traumatic arthritis dataset (TT1-TT20) when preprocessing with 2nd order differentiation and 25 point smoothing technique (Savitzky-Golay algorithm)

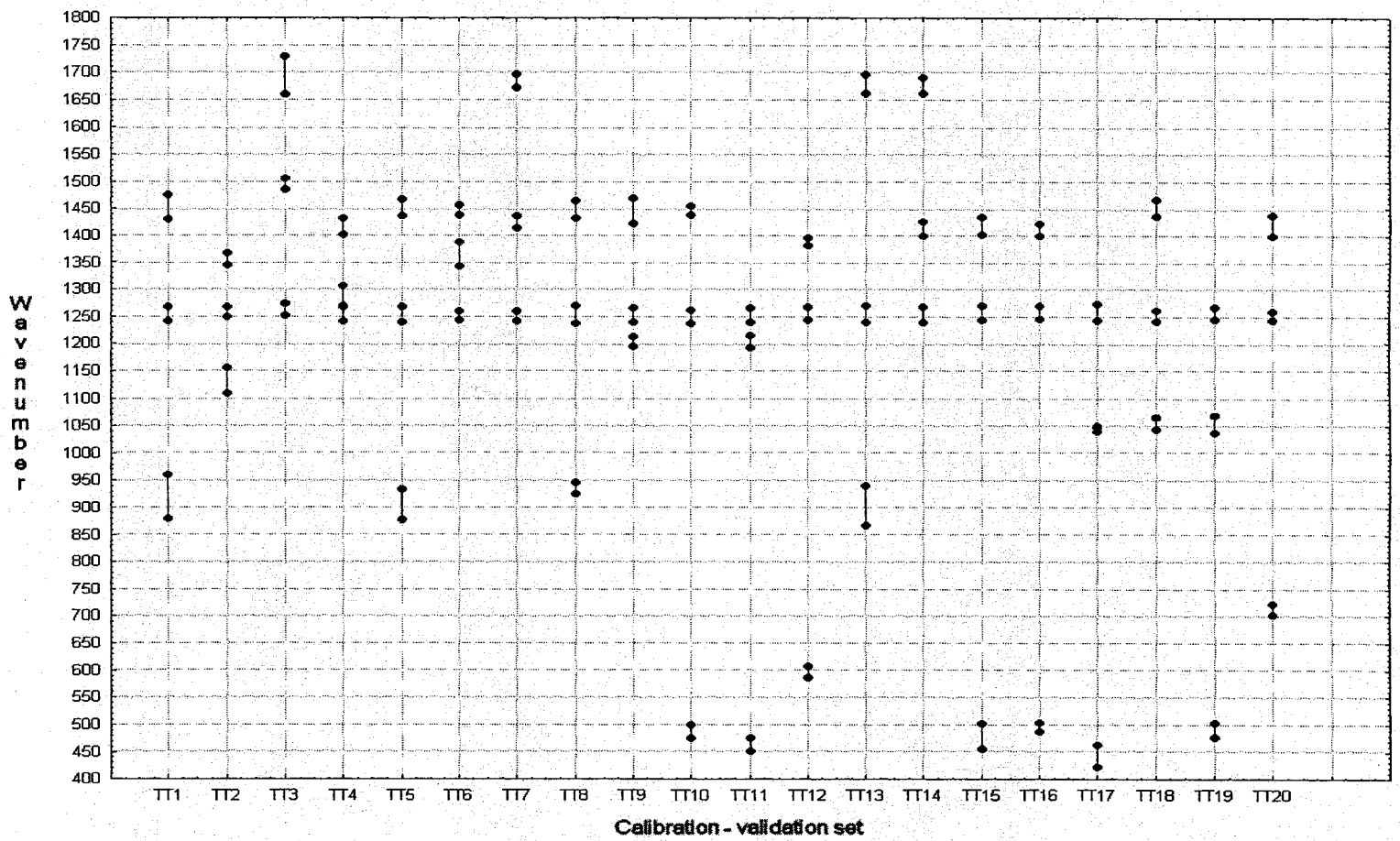

Appendix 9.3 Three optimal regions selected by genetic algorithm for 20 pairs of calibration-validation sets of spectra in traumatic arthritis dataset (TT1-TT20) when preprocessing with 2nd order differentiation and 45 point smoothing technique (Savitzky-Golay algorithm)

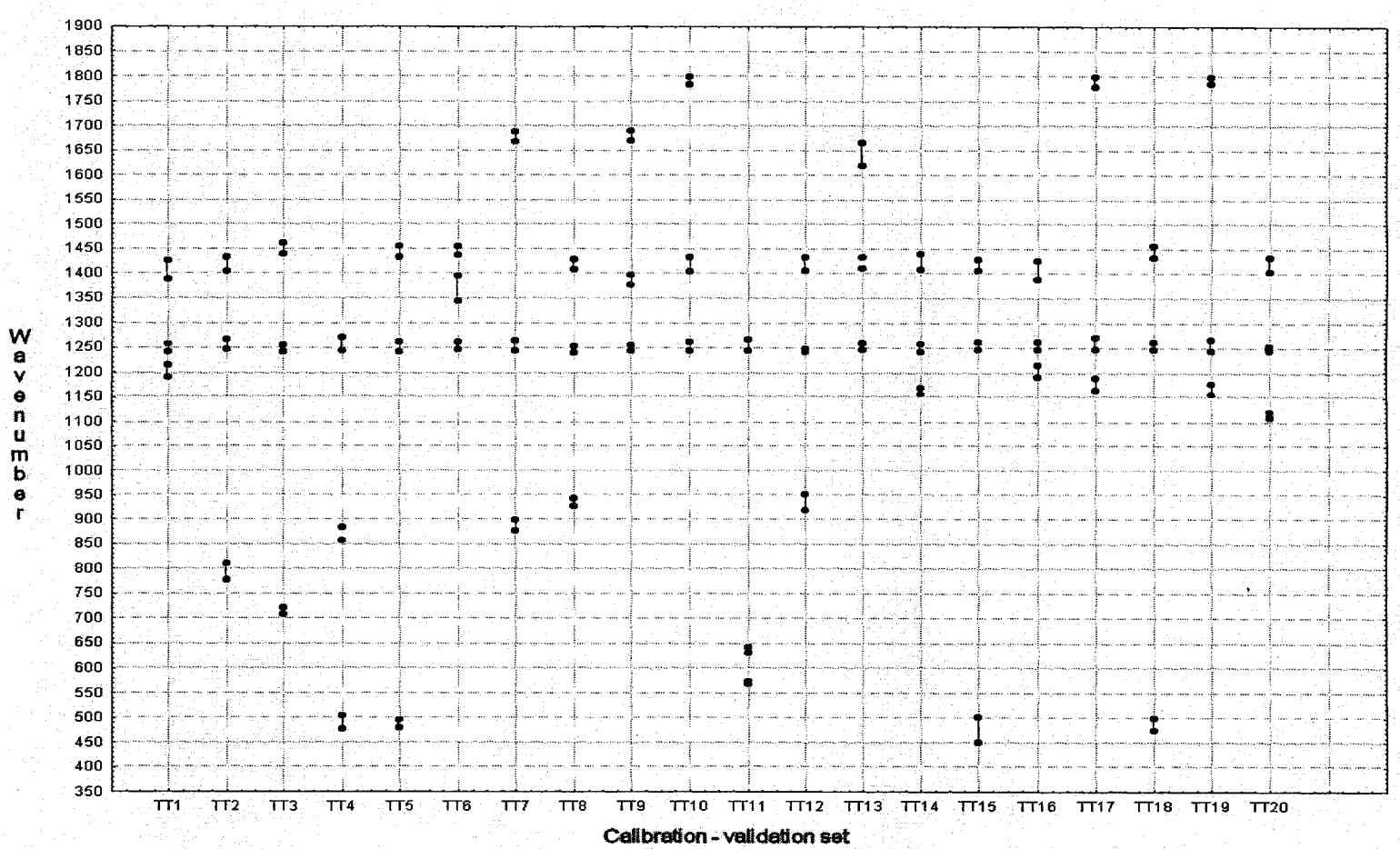

Appendix 10.1 Sensitivity, specificity and accuracy of all calibration and validation sets when preprocessing with 2nd order differentiation and 15 point smoothing

	Calibration			Validation		
Set	Sensitivity	Specificity	Accuracy	Sensitivity	Specificity	Accuracy
TT1	87.5	85.2	85.5	72.2	64.3	68.8
TT2	88.6	96.3	91.9	61.1	78.6	68.8
TT3	77.1	96.3	85.5	72.2	85.7	78.1
TT4	88.6	88.9	88.7	61.1	64.3	62.5
TT5	80	96.3	87.1	55.6	92.9	71.9
TT6	85.7	92.6	88.7	72.2	71.4	71.9
TT7	88.6	88.9	88.7	61.1	85.7	71.9
TT8	82.9	92.6	87.1	66.7	92.9	78.1
TT9	74.3	92.6	82.3	72.2	85.7	78.1
TT10	77.1	88.9	82.3	72.2	78.6	75
TT11	88.6	81.5	85.5	72.2	57.1	65.6
TT12	85.7	96.3	90.3	72.2	64.3	68.8
TT13	82.9	92.6	87.1	66.7	78.6	71.9
TT14	91.4	85.2	88.7	66.7	78.6	71.9
TT15	91.4	88.9	90.3	61.1	71.4	65.6
TT16	82.9	96.3	88.7	61.1	92.9	75
TT17	82.9	88.9	85.5	66.7	35.7	53.1
TT18	85.7	96.3	90.3	61.1	64.3	62.5
TT19	74.3	85.2	79	72.2	92.9	81.2
TT20	85.7	88.9	87.1	72.2	42.9	59.4

Note: TT1-TT20 correspond to calibration-validation set 1 - 20

Appendix 10.2 Sensitivity, specificity and accuracy of all calibration and validation sets when preprocessing with 2nd order differentiation and 25 point smoothing

	Calibration			Validation		
Set	Sensitivity	Specificity	Accuracy	Sensitivity	Specificity	Accuracy
TT1	82.9	100	90.3	61.1	78.6	68.8
TT2	82.9	96.3	88.7	55.6	78.6	65.6
TT3	85.7	81.5	83.9	61.1	92.9	75
TT4	85.7	88.9	87.1	72.2	64.3	68.8
TT5	80	92.6	85.5	72.2	85.7	78.1
TT6	85.7	96.3	90.3	77.8	71.4	75
TT7	82.9	92.6	87.1	55.6	78.6	65.6
TT8	88.6	88.9	88.7	61.1	92.9	75
TT9	80	81.5	80.6	83.3	85.7	84.4
TT10	82.9	88.9	85.5	72.2	78.6	75
TT11	85.7	92.6	88.7	77.8	42.9	62.5
TT12	88.6	81.5	85.5	72.2	57.1	65.6
TT13	85.7	88.9	87.1	77.8	64.3	71.9
TT14	94.3	81.5	88.7	72.2	92.9	81.2
TT15	85.7	96.3	90.3	55.6	78.6	65.6
TT16	85.7	92.6	88.7	72.2	71.4	71.9
TT17	80	74.1	77.4	77.8	50	65.6
TT18	80	100	88.7	55.6	85.7	68.8
TT19	77.1	88.9	82.3	77.8	100	87.5
TT20	80	100	88.7	88.9	42.9	68.8

Note: TT1-TT20 correspond to calibration-validation set 1 - 20

Appendix 10.3 Sensitivity, specificity and accuracy of all calibration and validation sets when preprocessing with 2nd order differentiation and 45 point smoothing

	Calibration			Validation		
Set	Sensitivity	Specificity	Accuracy	Sensitivity	Specificity	Accuracy
TT1	85.7	92.6	88.7	66.7	92.9	78.1
TT2	91.4	96.3	93.5	50	85.7	65.6
TT3	77.1	88.9	82.3	72.2	71.4	71.9
TT4	88.6	92.6	90.3	61.1	50	56.2
TT5	80	96.3	87.1	72.2	78.6	75
TT6	88.6	92.6	90.3	77.8	71.4	75
TT7	85.7	85.2	85.5	61.1	78.6	68.8
TT8	88.6	85.2	87.1	72.2	85.7	78.1
TT9	80	88.9	83.9	83.3	78.6	81.2
TT10	80	88.9	83.9	72.2	85.7	78.1
TT11	88.6	81.5	85.5	72.2	57.1	65.6
TT12	82.9	92.6	87.1	83.3	71.4	78.1
TT13	80	92.6	85.5	83.3	78.6	81.2
TT14	82.9	88.9	85.5	77.8	100	87.5
TT15	82.9	92.6	87.1	55.6	85.7	68.8
TT16	85.7	92.6	88.7	77.8	78.6	78.1
TT17	82.9	85.2	83.9	77.8	64.3	71.9
TT18	88.6	85.2	87.1	55.6	78.6	65.6
TT19	77.1	85.2	80.6	72.2	85.7	78.1
TT20	85.7	92.6	88.7	88.9	50	71.9

Note: TT1-TT20 correspond to calibration-validation set 1 - 20

Appendix 11.1 The 95% confidence interval of the mean sensitivity of the calibration and validation sets when preprocessing with 2nd order differentiation and 15, 25 and 45 point smoothing technique (Savitzky-Golay algorithm)

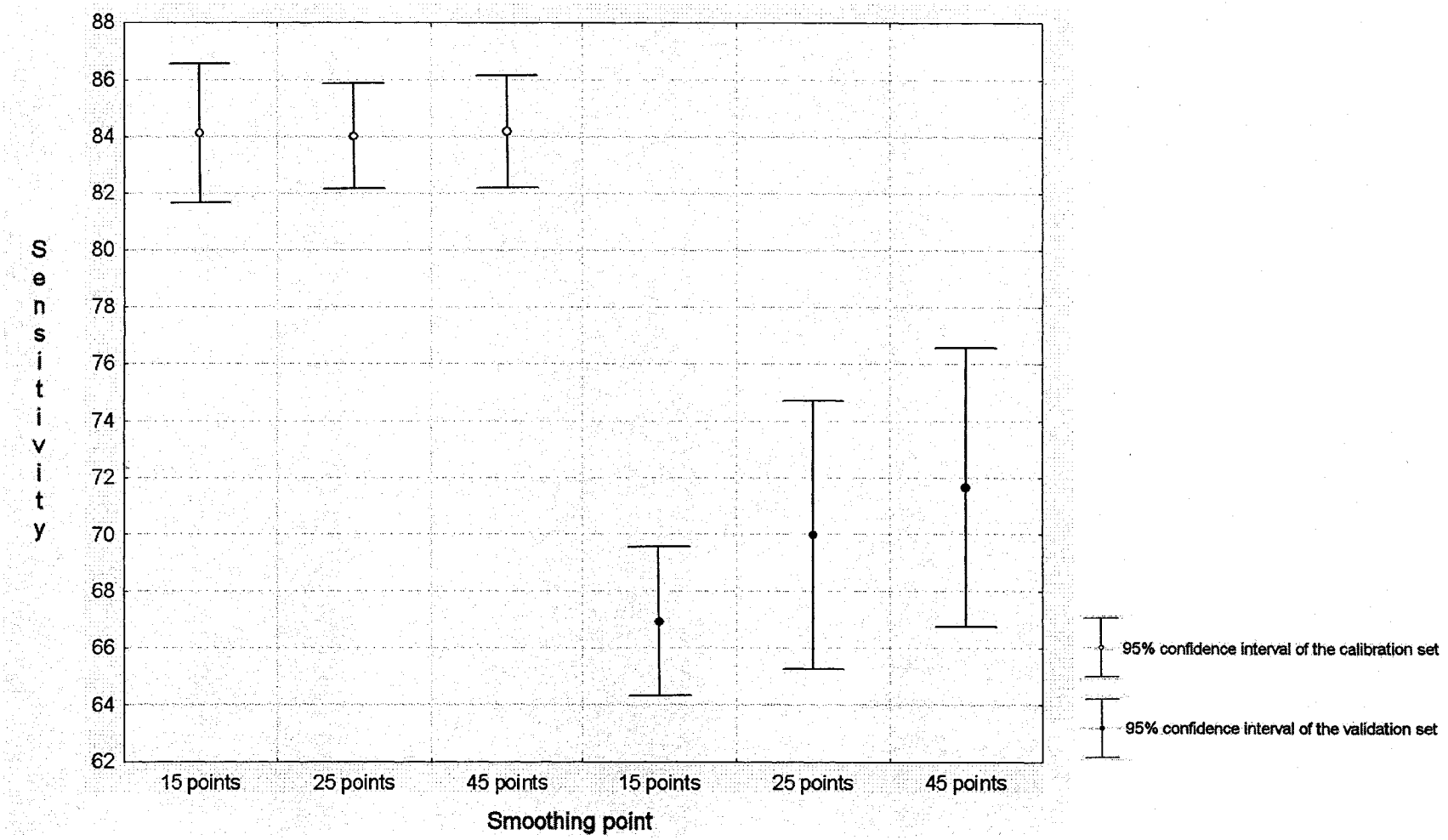

Appendix 11.2 The 95% confidence interval of the mean specificity of the calibration and validation sets when preprocessing with 2nd order differentiation and 15, 25 and 45 point smoothing technique (Savitzky-Golay algorithm)

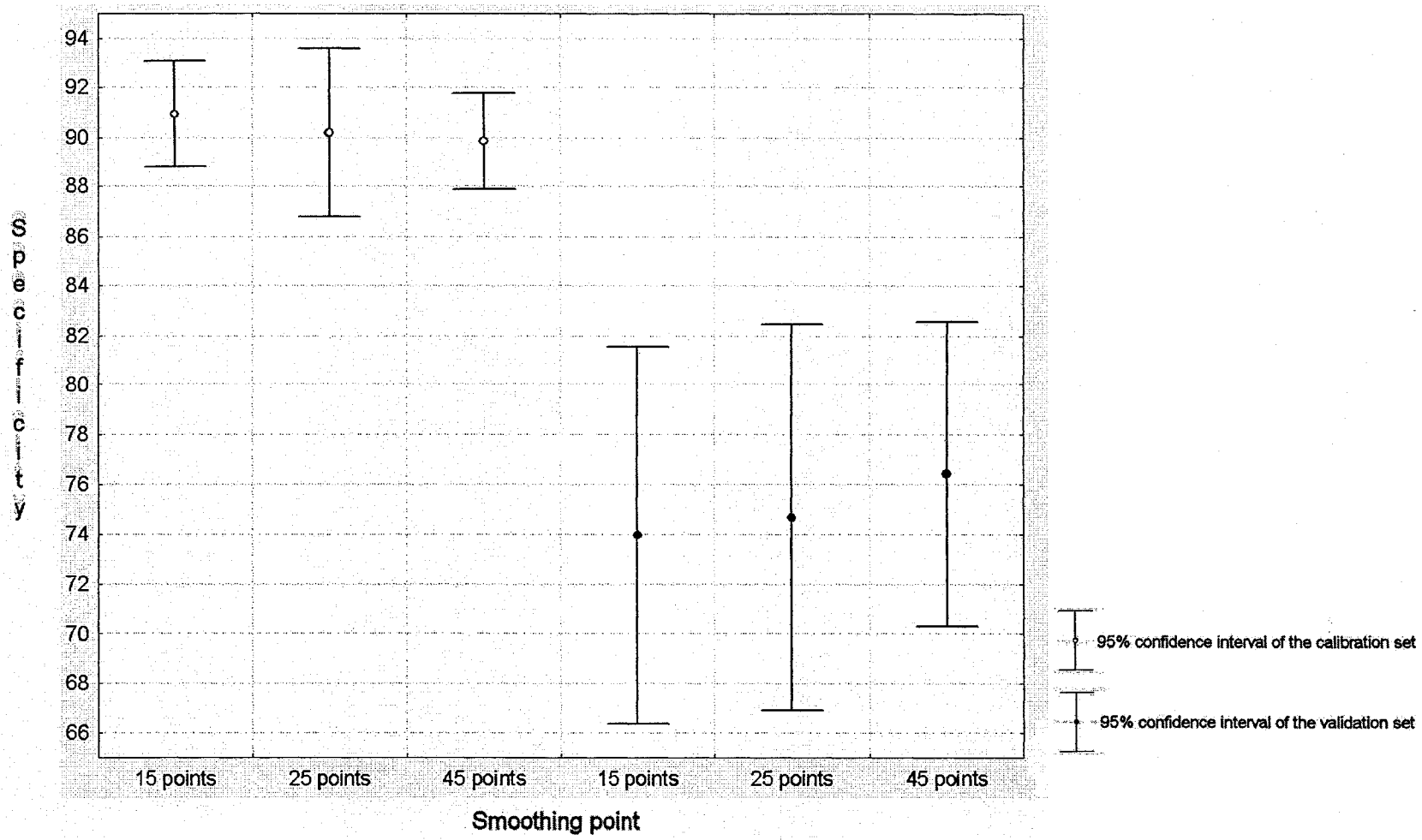

Appendix 11.3 The 95% confidence interval of the mean accuracy of the calibration and validation sets when preprocessing with 2nd order differentiation and 15, 25 and 45 point smoothing technique (Savitzky-Golay algorithm)

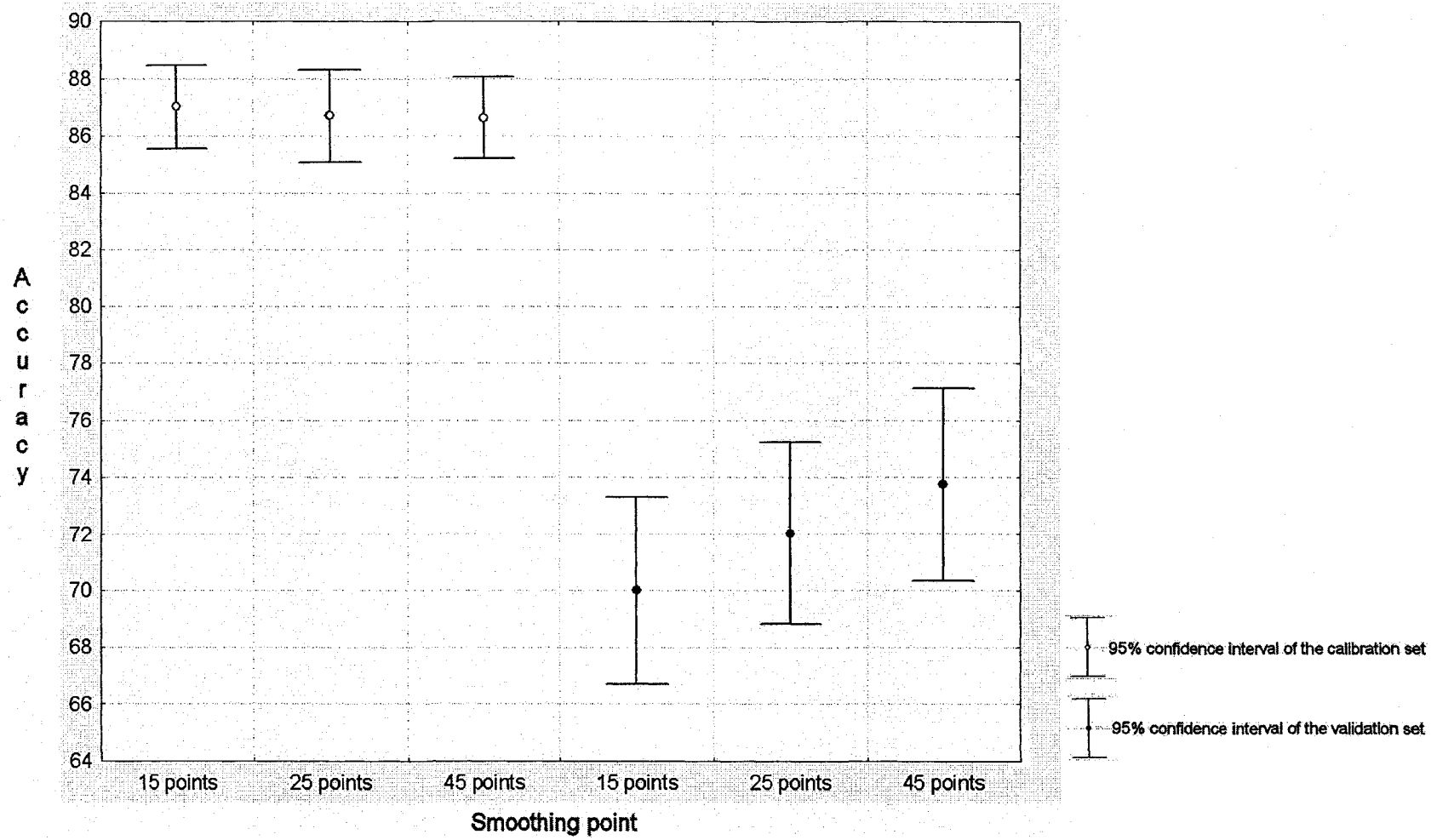

Appendix 12.1 The summary of spectral preprocessing and classification strategies of osteochondrosis dataset

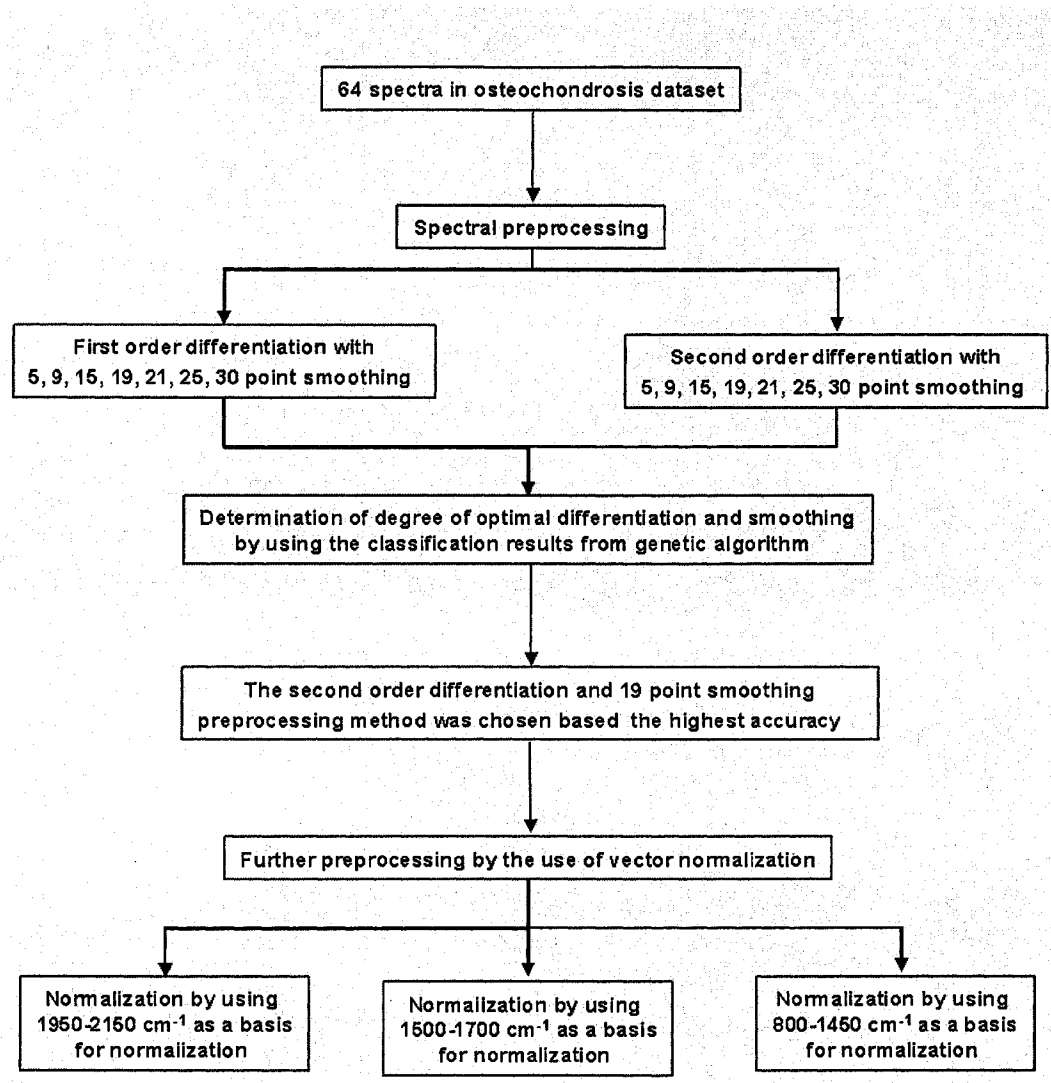

Appendix 12.2 The summary of spectral preprocessing and classification strategies of osteochondrosis (non-normalized) dataset

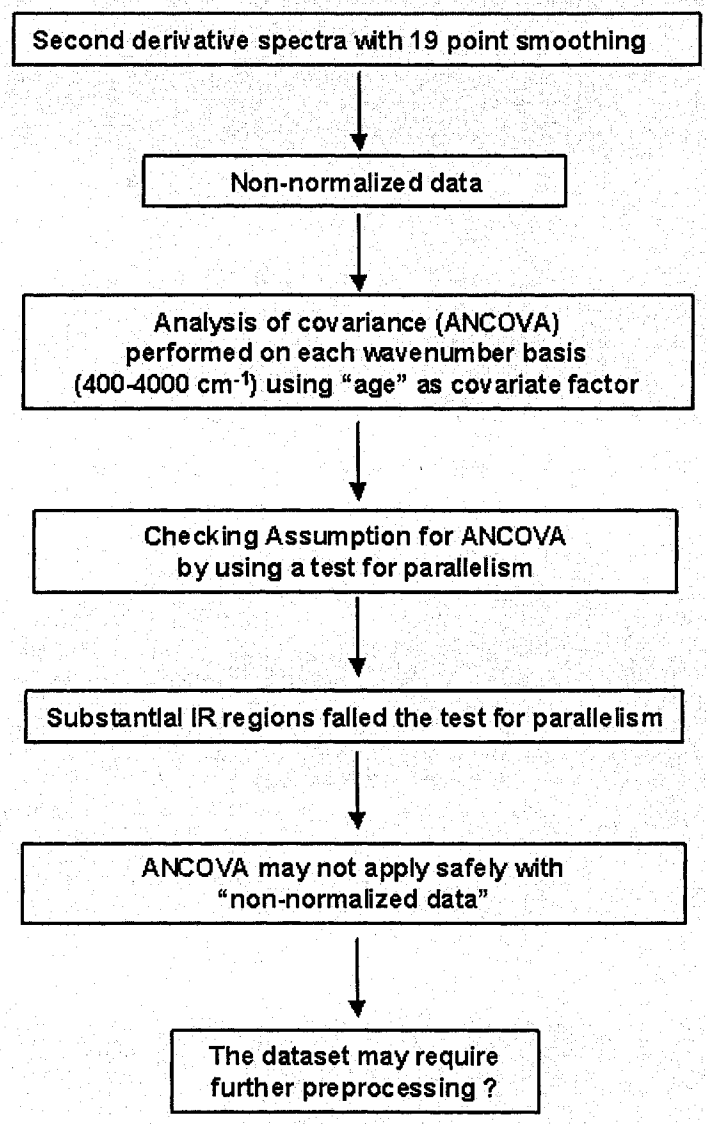

Appendix 12.3 The summary of spectral preprocessing and classification strategies of osteochondrosis (normalized) dataset

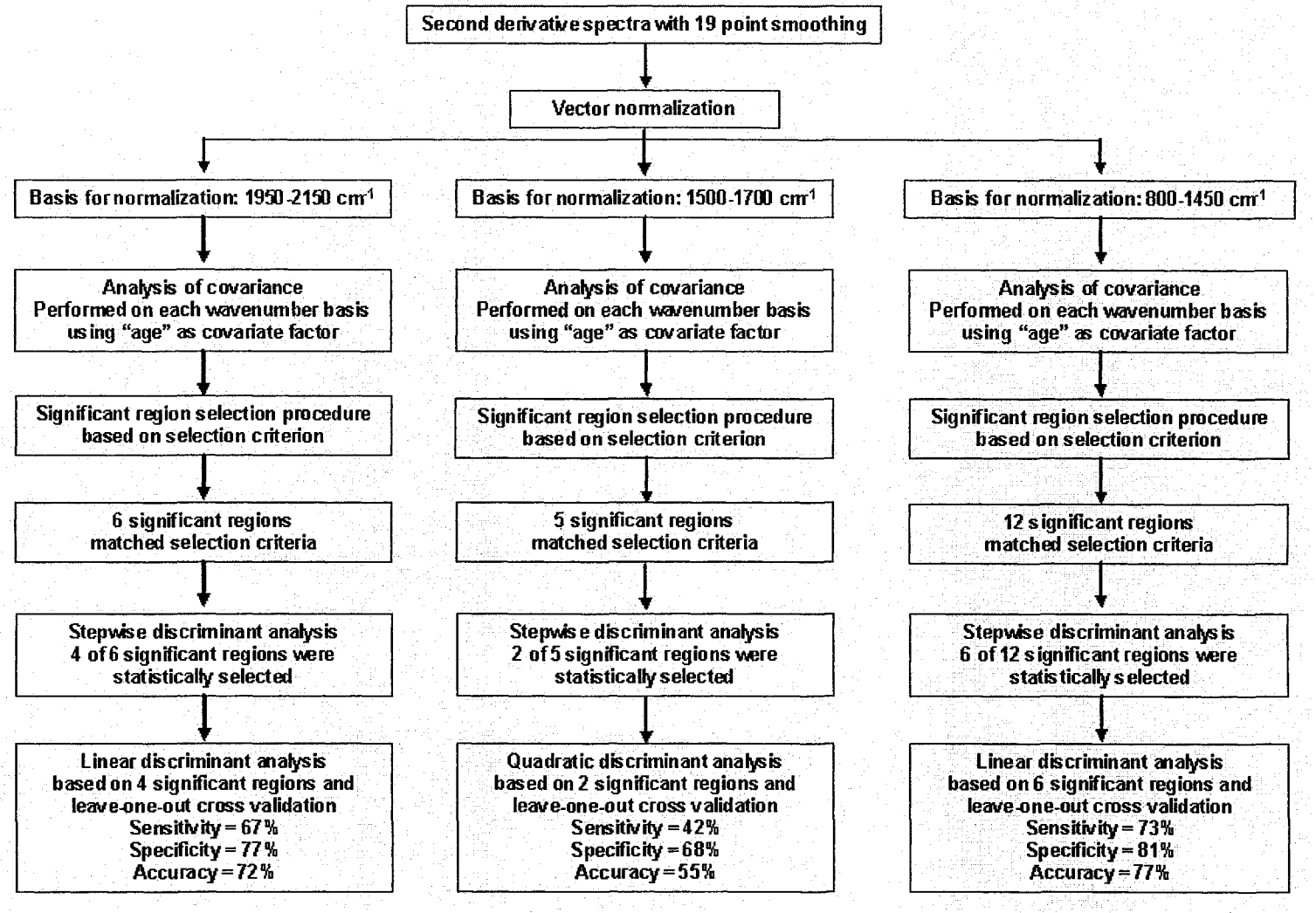

Appendix 13 The accuracy of the 1st and 2nd derivative spectra with varying degree of spectral smoothing based on 6 optimal regions selected by genetic algorithm

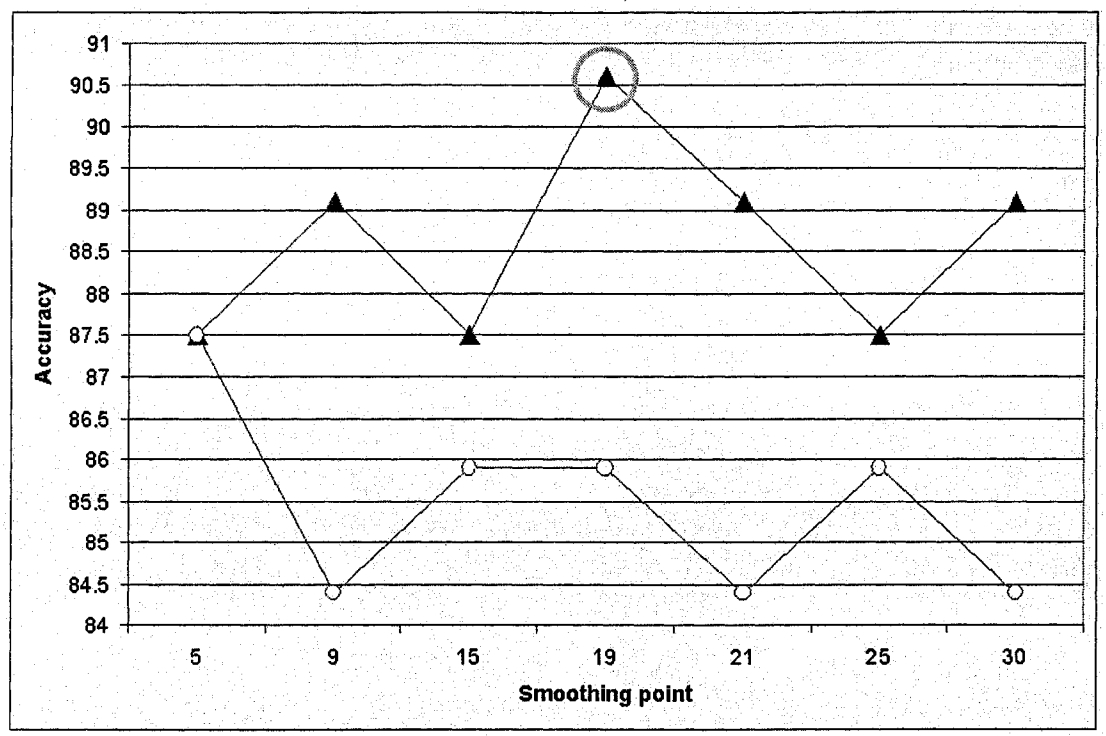

○ - First derivative spectra, ▲ - Second derivative spectra

Note: The second derivative spectra with 19 point smoothing yielded the highest accuracy of classification (marked by grey circle)